ADDITIVELY MANUFACTURED SPACECRAFT THERMAL CONTROL SYSTEM

THESIS

Daniel T. Lanzo, Capt, USAF

AFIT-ENY-MS-17-M-271

DEPARTMENT OF THE AIR FORCE
AIR UNIVERSITY

AIR FORCE INSTITUTE OF TECHNOLOGY

Wright-Patterson Air Force Base, Ohio

AFIT-ENY-MS-17-M-271

ADDITIVELY MANUFACTURED SPACECRAFT THERMAL CONTROL SYSTEM

THESIS

Presented to the Faculty

Department of Aeronatics and Astronautics

Graduate School of Engineering and Management

Air Force Institute of Technology

Air University

Air Education and Training Command

in Partial Fulfillment of the Requirements for the

Degree of Master of Science

Daniel T. Lanzo, BS

Capt, USAF

March 2017

AFIT-ENY-MS-17-M-271

ADDITIVELY MANUFACTURED SPACECRAFT THERMAL CONTROL SYSTEM

THESIS

Daniel T. Lanzo, BS
Capt, USAF

Committee Membership:

Carl R. Hartsfield, Ph.D.
Chair

Ryan P. O'Hara, Ph.D.
Member

James L. Rutledge, Ph.D.
Member

Abstract

Heat pipes offer a very effective thermal management solution when dealing with high powered spacecraft electronics. However, current technologies dictate that these solutions be manufactured via different processes with several integration steps. Additive manufacturing offers unique opportunities to manufacture integrated parts that cannot be realized via traditional means; heat pipes are no exception.

This thesis explores three key areas of additively manufacturing heat pipes for spacecraft thermal control. First, the ability to print different wick types is explored and test samples are printed and tested for wicking potential. Second, the functionality of an additively manufactured heat pipe design is tested by performing a side-by-side comparison between a heat pipe and conduction only setup. Lastly, the ability to create dual purpose components is explored by analyzing the structural capabilities of the heat pipe design and its impact on weight and complexity of spacecraft systems. Although conclusive test results were not obtained during this design revision, additive manufacturing offers viable and unique solutions for integrated heat management and structural solutions.

To my loving wife and beautiful daughters.

Acknowledgements

First and foremost, I would like to thank my wife and children for putting up with the late nights and long hours away from home. They provided the needed motivation throughout this process and kept me grounded. A special thanks goes to Dr. Hartsfield for his guidance and patience. Without a clear direction, this thesis would not have reached completion. I would also like to express my gratitude to Major O'Hara and Major Rutledge for their pointed expertise and suggestions. Thank you to Chris Sheffield and Sean Miller for their help in instrumenting my experiment and allowing me to perform my thesis in their space. I would also like to thank Phil Smith and Randall Sharp for their contributions to the design process and manufacturing assistance they provided. Last, but certainly not least, thank you the my fellow classmates in ENY4... "First in friendship, Fourth in ENY!"

Daniel T. Lanzo

Table of Contents

Page

Page

List of Figures

List of Tables

ADDITIVELY MANUFACTURED SPACECRAFT THERMAL CONTROL SYSTEM

1. Introduction

1.1 Background

The inception of heat pipes can be traced back to patents of A.M. Perkins and J. Perkins in the mid-1800's [1]. They developed and patented a device known as the Perkins tube which used either a single- or two-phase process to transfer heat from a furnace to a boiler. Without a wick, this design is currently referred to as a thermosyphon. In the 1940's P.S. Gaughler took this basic design and added a wick to patent the commonly known heat pipe. After the development of the heat pipe, applications were sparse until they re-surfaced in connection with the space program in 1962. A few years later, in 1964, George Grover published results of an independent investigation he conducted which studied heat pipe technology, confirming their usefulness and robustness. From this point forward, heat pipes have been included in many advanced technological triumphs from the earth-based Alaskan pipeline to spacecraft orbiting overhead [2].

A heat pipe is a closed-loop passive heat transfer device used to transfer heat between two solid interfaces. It uses a two-phase fluid-flow cycle to transport large quantities of heat from one location to another with very small temperature gradients. This ability is achieved by utilizing the working fluid's latent heat of vaporization. A schematic if this process is given in Figure 1.

NASA became increasingly interested in heat pipes after Grover published his

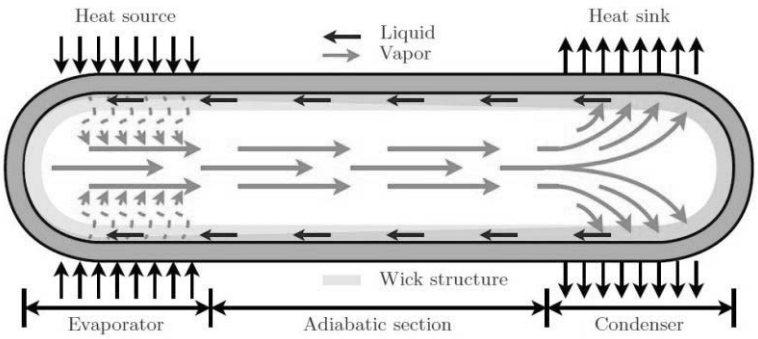

Figure 1. Basic concept of two phase heat pipe operation. [3]

findings and soon began to research and test heat pipe technologies for space applications due to the obvious benefits. These benefits include being relatively lightweight, having a high heat flux, being a passive system, and having the ability to work well in a zero-gravity environment. Spacecraft are perfect candidates for a heat pipe system for two reasons. First, solar radiation causes extreme temperature gradients during orbit. Second, their payloads are very power hungry which ultimately leads to large amounts of waste heat. As a result of this newly developed capability and increasing interest in putting more powerful electronics on orbit, numerous heat pipe experiments and flight hardware have been realized over the years attesting to the success of the heat pipe as a thermal management solution [4].

Switching gears to another significant technological breakthrough, additive manufacturing has garnered a significant amount of interest recently for its ability to manufacture customized parts that would otherwise be impossible to manufacture via traditional methods. Although using a layer-by-layer method to build an object is nothing new to a brick layer, a three-dimensional object created layer-by-layer from a CAD file is a more recent development that began in the 1980's for creating models and prototypes. [5] These products were mostly plastic and polymer representations of a prototype. The interest in AM for industry manufacturing applications did not take off until commercial systems utilizing lasers became available allowing for the

manufacturing of metal parts [6] [7]. This insertion of additive manufacturing into industry manufacturing techniques has been referred to as a "renaissance in manufacturing" [8].

1.2 Motivation

Closely examining the current industry in spacecraft design, it is clear to see that there is one constant trend – the need to decrease structure size while still increasing capability. This trend, however, poses a two-fold problem. Decreasing spacecraft size generally means there is less space for heat management solutions and/or excess structural components. Coincidentally, increasing capability, especially capabilities that utilize complex electronics, requires a substantial amount of power. This increased power is in turn, converted into waste heat that must be removed to ensure continued spacecraft operation. A common solution to this problem comes in the form of heat pipes.

Figure 2 depicts a radio thermal management solution concept that incorporates heat pipe technology into an additively manufactured containment box. It is designed to have a radio mounted inside and cooled through the utilization of heat pipes into the walls of the box which also acts as a structural component in the system. This design is the basis for this thesis and demonstrates the ability to additively create a thermal management solution that cannot be manufactured via traditional subtractive manufacturing processes. Additionally, the box design doubles as part of the structure allowing for weight savings while increasing the ability to manage the thermal loads induced by the enclosed electronics.

The first benefit to additively manufacturing a heat pipe is the decrease in thermal resistance compared to traditional heat pipe designs. By manufacturing the heat pipe as one structure, unnecessary junctions and material discrepancies are eliminated

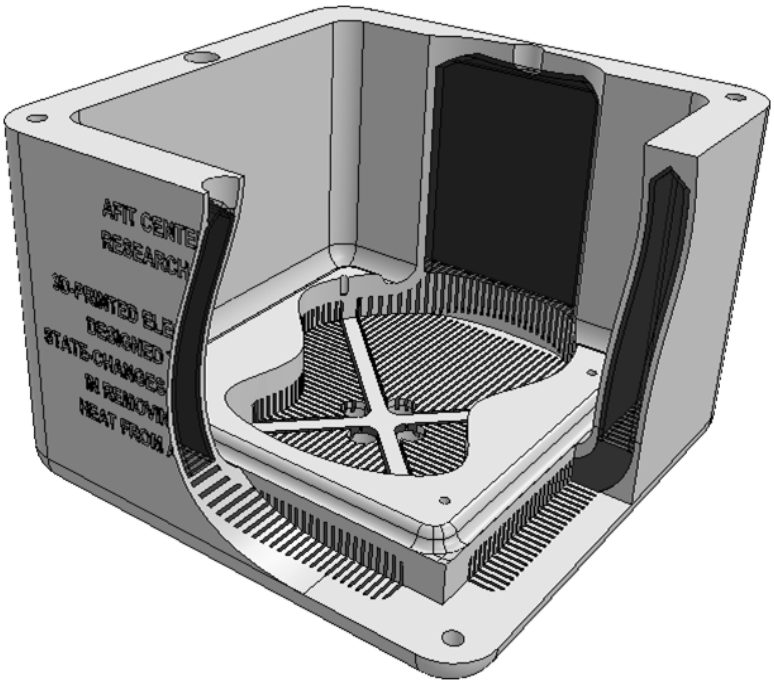

Figure 2. Radio cooler concept combining heat pipe and additive manufacturing technology for thermal management and structural subsystems. (Courtesy of Phil Smith.)

allowing for a heat pipe design that could cut the temperature difference between heat source and radiator.

Furthermore, heat pipes have a fairly high operating pressure which necessitates thick walls. This added stiffness can be beneficial in its ability to add rigidity to the overall system. By integrating the heat pipe into the structure itself, the weight of the entire structural and thermal systems can be reduced. Lastly, integrating components in a spacecraft system is beneficial as it streamlines the construction process making integration easier and cheaper as well as simplifying the overall design.

Each of these benefits combine to reduce overall system costs while allowing for a more capable spacecraft. For small satellites, such as CubeSats, this heat pipe design promotes expansion of the mission profile and the deliverance of a more robust orbiting solution.

1.3 Research Objectives

With an understanding of the research problem, specific action items can be itemized to ensure the problem is investigated thoroughly. This is done by breaking the problem up into three main focus areas: additively manufactured heat pipe wick manufacturing envelope, the ability to additively manufacture a functioning heat pipe, and the integration of thermal management and structural functions.

The first focus area outlined above is specifically aimed at determining the current additive manufacturing abilities in printing viable wick designs. This will focus on three designs and determine their potential to be integrated into an additively manufactured heat pipe. The second focus area specifically looks at the ability to additively manufacture a functioning heat pipe while deliberately using a design that could not be manufactured via traditional techniques. Lastly, the heat pipe design and overall ability to additively manufacture one will be analyzed for structural integration viability.

The specific objectives to achieve the aforementioned focus area are:

- Evaluate the ability of the Direct Metal Laser Sintering Additive Manufacturing process to manufacture metal wicks to include: porous metal wicks, structured lattice wicks, and axial groove wick designs.
- Design and manufacture a heat pipe that mimics Figure 2 in its design within the envelope of available additive manufacturing techniques while producing a part that cannot be manufactured with traditional techniques.
- Inspect additively manufactured products for adherence to design specifications.
- Test manufactured heat pipe designs to determine performance over a conduction only scenario of the same test articles.

- Perform structural testing to ensure the current design can be used as a structural member in addition to a thermal management solution.

2. Background

2.1 Spacecraft Thermal Management

Before talking about heat pipes and their applicability, it is important to understand basic spacecraft thermal control approaches. The first concept to understand is that conventional terrestrial based thermal solutions rely heavily on convection as an external heat dissipation method. This heat transfer mode does not exist in these terms when discussing spacecraft thermal control because there is no fluid to convect heat away from the external surfaces of the spacecraft. This leaves two forms of heat transfer to control spacecraft temperatures: conduction and radiation. In most spacecraft systems, conduction is the main mechanism to move heat through the spacecraft while radiation is used to remove that heat from the spacecraft.

2.1.1 Conduction

First, look at Fourier's Law:

$$q_x = -kA\frac{\partial T}{\partial x} \tag{1}$$

This is the defining conduction equation and several important conclusions can be made that apply directly to thermal control constraints. First, if ∂T and ∂x are held constant (i.e. - constant temperature drop and constant length), q_x will be directly proportional to A. In a practical sense, this means for a larger heat transport capability, a larger cross-sectional area will be needed. In addition, if A and ∂x are fixed, q_x will be directly proportional to ∂T [9].

Typical spacecraft requirements usually desire large heat removal to drive lower overall temperatures which requires a relatively high thermal conductivity. For ex-

ample, a radio with significant power requirements will generate significant amounts of heat which needs to be removed as efficiently as possible for optimum operation. If this radio is mounted directly to a conductive heat strap, there will need to be some length that the heat will need to travel before it can be radiated out. In this case, the cross-sectional area will be constant (barring any exotic heat strap designs) and the length will be fixed. However, referring to the above paragraph, this leaves only heat flux or temperature difference to be varied which is not an ideal solution. This leaves the option of increasing the thermal conductivity which can be by using different materials or a different solution.

2.1.2 Radiation

As mentioned, the second active heat transfer mechanism prevalent in spacecraft is radiation. Radiation is the only way to remove heat from a spacecraft and can only do that when heat is effectively and efficiently transported to the surface of the spacecraft through conduction. Once at the surface, the amount of heat emitted by the surface is given by the Stefan-Boltzmann law

$$E_b = A\sigma T_s^4 \tag{2}$$

and for a real surface (i.e. - not a blackbody)

$$E = A\sigma\epsilon T_s^4 \tag{3}$$

where ϵ is defined as the *emissivity* and is a measure of how efficiently a surface emits its energy relative to a blackbody.

Assuming a gray body that is at a higher temperature than its surroundings, the net radiative heat exchange can be derived as:

$$q_{rad} = A\sigma\epsilon(T_s^4 - T_{surr}^4) \tag{4}$$

2.1.3 Heat Paths

Since spacecraft typically house their electronics inside the bus, a combination of conduction and radiation is needed to remove waste heat from the spacecraft resulting in a heat path. When discussing heat paths, there are two distinct resistances observed: thermal resistance and contact resistance.

Every heat transfer mode has some effective thermal resistance [9]. For conduction and radiation they are:

$$R_{t,cond} = \frac{L}{kA} \tag{5}$$

$$R_{t,rad} = \frac{1}{h_r A} \tag{6}$$

In addition to these heat transfer resistances, the contact resistances between surfaces is a major source of resistance in a spacecraft system. This resistance compounds in systems where several metal to metal connections are made to transfer heat from one point to another. In CubeSats, this resistance becomes a limiting factor due to the limited heat paths from the electronic stacks. That is, many thermal solutions want to route heat through the stack stand-offs which are threaded rods. This is less than ideal since getting good contact in these regions is difficult and introduces significant contact resistance. In addition, going from the component to the stack stand-offs forces a longer heat path where additional resistances will be encountered. These issues combine into an inefficient thermal management solution. A more ideal solution would be to go directly from the component that needs thermal control to

the outer faces of the spacecraft but not every component can be installed near the spacecraft's external surfaces.

When discussing heat pipes, there are also thermal resistances associated with this heat transfer mechanism. If liquid/vapor interface resistance is ignored (a common assumption that will be discussed in Section 2.2) and the evaporator and condenser sections are physically identical, the effective thermal resistance can be written as:

$$R_{hp} = 2\left(R_{p,e} + R_{w,e}\right) \tag{7}$$

where $R_{p,e}$ is the radial resistance of the heat pipe wall at the evaporator (and condenser for physically identical evaporators/condensers) and $R_{w,e}$ is the resistance of the liquid/wick combination [2]. $R_{p,e}$ is essentially a conduction resistance through the heat pipe wall and $R_{w,e}$ is a resistance that is based on working fluid and wick type.

Despite the inability to completely escape thermal and contact resistance, heat pipes are advantageous in this aspect for several reasons. First, the wall thickness drives $R_{p,e}$. By using the thinnest walls possible, this resistance can be driven down to a fairly low level. Additionally, when looking at the overall implementation system, heat pipe solutions would have significantly lower contact resistances. For example, assume there is a hot radio that needs to be cooled. With a traditional heat strap, there would be contact resistance at the thermal strap connection point, a conduction resistance along the length of the heat strap, and a contact resistance where the thermal strap connects to the radiator. If instead, a heat pipe is used, there would only be the contact resistance at the radio connection interface and then the heat pipe effective thermal resistance. The contact resistance at the radiator interface can be excluded since the outside casing of the heat pipe at the condenser end is the radiator. Additionally, looking at the thermal conductivities observed between

heat pipe and conduction solutions, heat pipe thermal conductivities are orders of magnitude greater. This points to a resistance that is significantly lower for the overall system.

2.2 Heat Pipes

2.2.1 Overview

A heat pipe is a closed-loop passive heat transfer device used to transfer heat between two solid interfaces. It uses a two-phase fluid-flow cycle to transport large quantities of heat from one location to another with very small temperature gradients. This ability is achieved by utilizing the working fluid's latent heat of vaporization.

Physically, heat pipes are generally a sealed metal container with a working fluid operating at some specified pressure. When one end of the heat pipe is heated (becoming the evaporator section) the working fluid is heated until it vaporizes. When this happens, the high(er) temperature and pressure force the vapor into the cooler condenser section where is condenses back into a liquid, giving up its latent heat of vaporization. The fluid is then transported back to the evaporator section due to capillary forces exerted on the fluid by a wicking structure. Figure 1 provides a basic concept overview of a heat pipe operating at a steady state condition.

2.2.2 Benefits

A significant advantage of heat pipe use is the greater heat transfer capacity as compared to solid conductors due to effective heat pipe thermal conductivities that are several orders of magnitude greater than solid metal heat sinks. This results in a minimal temperature difference occurring over the axial length of a heat pipe. This is not true for a solid conductor where the temperature difference would be greater over a certain length when compared to a heat pipe with a similar cross section and length.

This comparison can be seen in Figure 3 where several commercial copper-water heat pipes were tested and compared to a cooper rod with the same dimensions [10]. A lower temperature difference indicates a system with that has a lower thermal resistance. As discussed in Section 2.1, lower thermal resistances are advantageous which make heat pipes even better for transporting heat around a spacecraft. In addition, the thermal response time of heat pipes is much quicker than other heat management solutions (Figure 4) making them more ideal for electronic cooling since it reaches its operating capacity much quicker than conduction-based approaches [2].

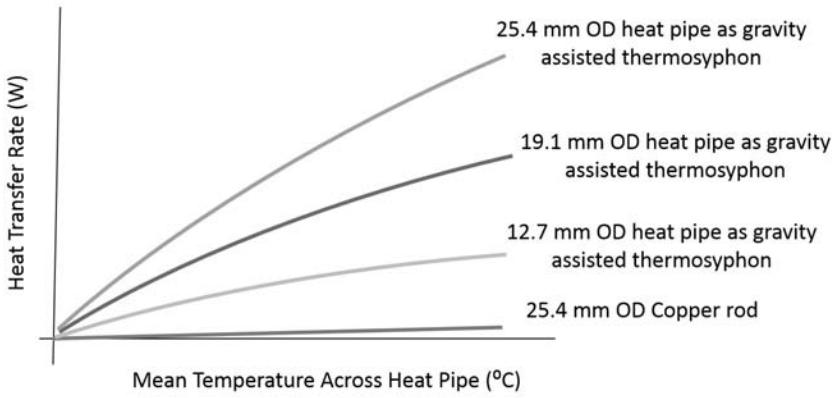

Figure 3. Heat transfer testing comparison among copper-water heat pipes and solid copper rod. [10]

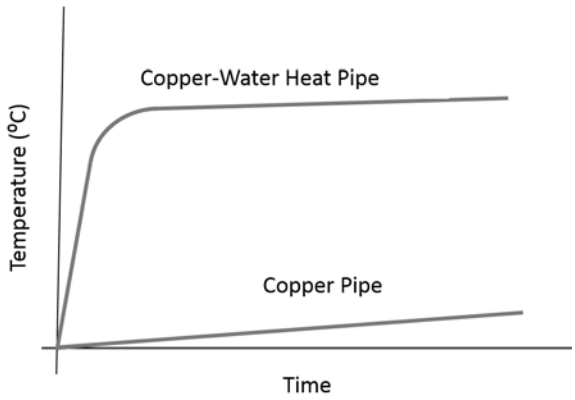

Figure 4. Transient response of copper-water heat pipe compared to copper pipe with the same dimensions [10]

Specific to spacecraft design, heat pipes also allow for significant reductions in

weight. Looking at Fourier's Law, in order to minimize the temperature difference along the axial length of a solid conductor for a given length, the area would have to increase proportionally. This translates to a solid conductor that gets bulkier as you decrease $\triangle$T. In terms of weight, this is not ideal considering heat pipes offer a solution that has a better system thermal conductivity while being hollow with nearly constant cross section, therefore much lighter.

2.2.3 Manufacturing Techniques

To date, most heat pipes are manufactured via traditional techniques that use multiple steps and parts. This multi-step process exists because of the difficulty in producing a case that can withstand the structural requirements of the heat pipe while also integrating a wick whose dimensions are several orders of magnitude smaller than that of the case. This limitation forces the manufacturing process to revolve around the integration of a wicking structure after the case has been manufactured. This leads to the following techniques being implemented to integrate the wicking structures:

- Mesh Screen Wick: Mesh screens are inserted into an appropriately shaped case.
- Axial Grooved Wick: Extruded sections of pipe with integrated axial grooves.
- Porous Metal Wick: Copper particles are sintered onto an existing flat plate which is subsequently wrapped and sealed into a tube.

For each of the above techniques, the wick integration is followed by ensuring that the vessel is filled with a working fluid and sealed to create a closed system. This process has a few challenges but the most prominent is thermal resistance associated with poor wick/case bonding. If the wick is not installed in good contact with the case, the overall heat pipe thermal resistance increases. In fact, the contact resistance

between the wick and case usually accounts for a significant portion of the overall heat pipe thermal resistance [10].

2.2.4 Wick Characteristics

The wick used in a heat pipe drives the operating abilities of that heat pipe. Its main purpose is to provide a vehicle to return the working fluid from the condenser to evaporator after the working fluid condenses. Additionally, the wick helps keep the working fluid uniformly distributed around the evaporator surface ensuring the maximum amount of heat transport [2]. This is usually a desirable feature but can cause problems in a CubeSat design that requires getting heat removal from an internal box to a radiator surface. However, designs decisions, such as condenser shape and wick presence, can help alleviate this issue.

There are three broad categories that wicks can be classified: homogeneous, composite, and advanced. Homogenous wicks are usually composed of a single design that does not consist of multiple materials or vary axially in the heat pipe. Figure 5 shows three of the most common homogeneous wick designs. Composite wicks usually employ a combination of the homogeneous wicks and can include multiple material or differing porosities and geometry axially. The last category builds upon composite wicks and generally tries to refine certain features such as circumferential distribution or maximizing heat transfer in the condenser and evaporator sections.

Again, wick design becomes a balancing act of heat pipe function, manufacturing ability, and needed application. It is generally desirable to have low fluid resistance when traveling from the condenser to evaporator which points to a wick with a high permeability. In direct contrast to this, a smaller effective radius points to greater capillary ability. This increased capillary pumping ability means a greater heat transport capability. The solution to this problem usually results in composite

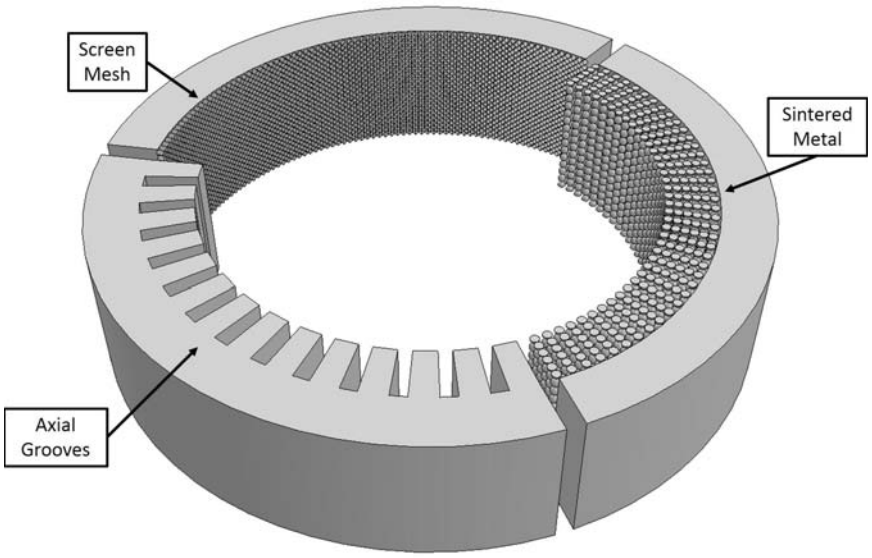

Figure 5. Typical homogeneous heat pipe wick designs. (Courtesy of Phil Smith.)

Wick Type	Capillary Pumping Ability	Thermal Conductivity	Permability
Wrapped Screen	High	High	Low/Average
Sintered Metal	High	Average	Low/Average
Axial Grooves	Low	High	Average/High
Open Annulus	Low	Low	High
Open Artery	Low	High	High
Integral Artery	High	High	Average/High

Table 1. Typical homogeneous wick designs and their associated attributes. [11]

or advanced wick designs; however, many successful heat pipe applications use simple homogeneous wick design. This includes space based applications, due to the lower pumping capacity needed in the absence of gravity to achieve the same heat transport capability.

2.2.5 Working Fluid

Many different working fluids can be used in heat pipes based on their intended operating ranges. Table 2 shows some common working fluids and their associated ranges in which they can be used. Clearly, insight into the intended operating conditions is required as Table 2 contains entries that can be used in a wide range of applications from cryogenic to liquid metal heat pipes [2].

When selecting a working fluid, the main factor that needs to be taken into account is the fluids thermophysical properties. However, with advances in manufacturing techniques introducing a wide range of case and wick materials, care must be taken to ensure compatibility with the case and wick material. Additionally, the wettability of the working fluid plays an important role in the ability of the wick to create capillary action for a given fluid [2].

Working Fluid	**Boiling Point (K) (@ 1 atm)**	**Useful Range (°C)**	
		Low	**High**
Helium	4.21	-271	-269
Nitrogen	77.35	-263	-170
Oxygen	90.18	-200	-154
Freon 22	232.2	-80	24
Ammonia	239.9	-60	100
Acetone	329.4	0	120
Ethanol	351.5	0	130
Water	373.1	30	200
Mercury	630.1	250	650
Lithium	1615	1000	1800
Silver	2485	1800	2300

Table 2. Selected heat pipe working fluids and their useful temperature ranges. [10]

2.2.6 Capillary Pressure Balance

The Young-LaPlace equation (Equation 8) defines the capillary pressure difference occurring across the meniscus separating the liquid and vapor regions as a function of the two principal radii of curvature (r_1 and r_2) and the surface tension, σ [2].

$$P_v - P_l = \sigma \left(\frac{1}{r_1} + \frac{1}{r_2} \right) \tag{8}$$

Taking into account that the pressure difference is between the liquid and vapor interface (P_l & P_v, respectively), the left side of the equation becomes $\triangle P_c$. Additionally, taking into account common heat pipe wicking structure designs, the two radii are expressed in terms of a single radius of curvature, r_c. In this manner, the maximum capillary pressure between the wet and dry points can be expressed as the difference between the capillary pressure across the meniscus at the wet and dry points. The dry point refers to the point where the meniscus has a minimum radius of curvature and contrarily, the wet point refers to where the meniscus has the maximum radius of curvature [2].

$$\triangle P_c = \frac{2\sigma}{r_{c,e}} + \frac{2\sigma}{r_{c,c}} \tag{9}$$

At this point, it is important to note that vaporization occurring in the evaporator causes the liquid meniscus to recede into the wick. Contrarily, condensation in the condenser causes the wick to become flooded. The effect of these actions causes similar effects on the local meniscus radius of curvature. In the evaporator the local capillary radius, $r_{c,e}$, is reduced and in the condenser section there is an increase in the local capillary radius, $r_{c,c}$. The difference between these two radii causes a pressure difference resulting in a pumping action from the condenser to evaporator. During typical steady state operation, it is assumed that the local capillary radius

in the condenser approaches infinity. This results in an expression for maximum capillary pressure for a heat pipe operating under stead-state conditions thats is solely a function of the effective capillary radius of the evaporator, $r_{c,e}$, and surface tension, σ.

$$\triangle P_{c,m} = \frac{2\sigma}{r_{c,e}} \tag{10}$$

In order to use Equation 10 for an axial groove wick design, the effective radius for a grooved wick needs to be determined. Luckily, this has been investigated thoroughly and for axial grooves the effective radius is the width of the channel, W [12] [2].

2.2.7 Capillary Limitation

When designing a heat pipe, the factors discussed thus far (i.e. - wick design, working fluid, dimensionality) all contribute to the functionality of the device but the physical phenomenon enabling a heat pipe to function is the capillary pressure difference that exists across the liquid-vapor interface in the evaporator and condenser regions. As discussed earlier, vaporization in the evaporator causes a recession in the wick whereas there is a flooding of the wick in the condenser due to condensation. This results in a meniscus radius of curvature that varies along the length of the heat pipe and the "dry" and "wet" sections of a heat pipe refer to the local meniscus radii of curvature. The location where the meniscus radius of curvature is at a minimum is the "dry" section and is usually the evaporator. Contrarily, the "wet" section is the condenser region and is characterized by having a maximum meniscus radius of curvature since the vapor and liquid pressures are approximately equal.

Since the capillary pressure difference between the wet and dry points is the only source of pressure gains, to attain the maximum heat transfer capability from the heat pipe, the capillary pressure must be greater than the losses resulting from in the

vapor-liquid path. This relationship is referred to as the capillary limitation of a heat pipe. Mathematically, this can written as [2]:

$$\triangle P_{c,m} \geq \int_{L_{eff}} \frac{\partial P_v}{\partial x} dx + \int_{L_{eff}} \frac{\partial P_l}{\partial x} dx + \triangle P_{ph,e} + \triangle P_{ph,c} + \triangle P_g \tag{11}$$

Where:

$\triangle P_{c,m}$ = maximum capillary pressure

$\int_{L_{eff}} \frac{\partial P_v}{\partial x} dx$ = pressure drops in vapor phase

$\int_{L_{eff}} \frac{\partial P_l}{\partial x} dx$ = pressure drop in liquid phase

$\triangle P_{ph,e}$ = pressure gradient across phase transition in evaporator

$\triangle P_{ph,c}$ = pressure gradient across phase transition in condenser

$\triangle P_g$ = pressure drop due to gravity

As discussed in the previous section, the maximum capillary pressure head is given as

$$\triangle P_{c,m} = \frac{2\sigma}{r_{c,e}} = \frac{2\sigma}{W} \tag{12}$$

for a rectangular grooved design. The pressure drop due to gravity is given as

$$\triangle P_g = \rho_l g L_t sin\phi \tag{13}$$

where ϕ is the angle of inclination of the heat pipe from horizontal. Typical handling of $\triangle P_{ph,e}$ and $\triangle P_{ph,c}$ allow for them to be neglected since the pressure drop from phase transitions is relatively small.

The remaining two pressure drop terms, can be simplified by [12]

$$\int_{L_{eff}} \frac{\partial P_v}{\partial x} dx = \triangle P_v = F_v Q L_{eff} \tag{14}$$

$$\int_{L_{eff}} \frac{\partial P_l}{\partial x} dx = \triangle P_l = F_l Q L_{eff} \tag{15}$$

In these equations L_{eff} is given as

$$L_{eff} = 0.5L_c + L_a + 0.5 + 0.5L_e \tag{16}$$

Now, the only values left to be defined are F_v and F_l, the frictional coefficients for the vapor and liquid flows respectively. These values are dependent on the working fluid chosen as well as the wick design. The derivation for the liquid frictional coefficient for a rectangular grooved wick design is shown in Equations 17 to 23 and was derived by Wang et al [12].

$$F_l = \frac{\mu_l}{K A_w \lambda \rho_l} \tag{17}$$

$$K = \frac{2\epsilon r_{h,l}^2}{(f_l Re_l)} \tag{18}$$

$$A_w = NSL \tag{19}$$

$$\epsilon = \frac{W}{S} \tag{20}$$

$$r_{h,l} = \frac{2LW}{2L + W} \tag{21}$$

$$f_l Re_l = 24(1 - 1.3553a + 1.9467a^2 - 1.7012a^3 + 0.95654a^4 - 0.2537a^5) \tag{22}$$

$$a = \frac{W}{L} \tag{23}$$

Where:

μ_l = liquid viscosity

K = wick permeability

A_w = wick cross-sectional area

λ = latent heat of vaporization

ρ_l = liquid density

ϵ = wick porosity

$r_{h,l}$ = hydraulic radius

$f_l Re_l$ = coefficient of drag

N = number of grooves

The vapor frictional coefficient is a more involved calculation and can be expressed as [2]

$$F_l = \frac{C(f_v Re_v)\mu_v}{2r_{h,v}^2 A_v \rho_v \lambda} \tag{24}$$

When a heat pipe is at a steady-state condition, the mass flow of the vapor and liquid must be equal, however, depite a laminar liquid flow, the vapor flow can be laminar or turbulent. The local axial Reynolds number provides insight to this problem and determines what flow regime the vapor is in as a function of heat flux. This is given by

$$Re_v = \frac{2r_{h,v}q}{A_v \mu_v \lambda} \tag{25}$$

In addition, it is important to determine if the flow should be treated as com-

pressible or incompressible using the local Mach number.

$$Ma_v = \frac{q}{A_v \rho_v \lambda (R_v T_v \gamma_v)^{1/2}} \tag{26}$$

Using Equations 25 to 26, previous investigations have demonstrated that an approximation for $(f_v Re_v)$ and C can be used with reasonable accuracy. This approximation is based on determining flow conditions and using the Reynolds and Mach number and using given values for each value [2]. These approximations are given in the conditional as:

If $Re_v < 2300$ and $Ma_v < 0.2$:

$$(f_v Re_v) = 16 \qquad\qquad C = 1.00 \tag{27}$$

If $Re_v < 2300$ and $Ma_v > 0.2$:

$$(f_v Re_v) = 16 \qquad\qquad C = \left[1 + \left(\frac{\gamma - 1}{2}\right) Ma^2\right]^{-1/2} \tag{28}$$

If $Re_v > 2300$ and $Ma_v < 0.2$:

$$(f_v Re_v) = 0.038 \left(\frac{2 r_{h,v} q}{A_v \mu_v \lambda}\right)^{3/4} \qquad\qquad C = 1.00 \tag{29}$$

2.2.8 1G vs 0G Operation

Once the model for the heat pipe is analyzed, its specific uses can be determined. In the case of space applications, it is important to note that the required pumping capacity of the heat pipe wick is greatly reduced when operating in a zero-gravity environment. It is clear that without the adverse effects of gravity on the capillary action of the wick, the total necessary capillary pressure difference to overcome is significantly less. This results in heat pipe operation that is much easier to realize

in zero gravity environments. This is reflected in the difference in minimum wick designs between terrestrial and zero gravity environments. As discussed in Section 2.2.4, the lower pumping capacity of grooved wick designs makes them less than ideal in terrestrial applications since they have a lower capillarity pumping capacity. However, they are easier to design into a system making them ideal for integrated structures.

Testing products designed for space applications also becomes an issue when testing can only realistically be performed in a 1G environment. Luckily, there is a subset of heat pipes known as thermosyphons that do not require a wick to operate. Thermosyphons operate under the presumption that the condenser is oriented above the evaporator. This ensures the liquid can be returned to the evaporator not by capillary action but by gravitational effects. Due to this, most wick designs suitable for space use can be tested in terrestrial environments in certain orientations, but this limits attitude for testing.

2.3 Additive Manufacturing (AM)

Additive manufacturing (AM), commonly referred to as 3D printing, has recently gained significant traction as an area of interest from industry to academia. Additive manufacturing is the process of manufacturing a part by successively "printing" cross-sectional layers of an object. This unique "additive" approach provides an opportunity for many industries to reinvent their manufacturing and realization processes to include many ideas that could not be realized several years ago. This, in part, can be attributed to decreased cost of printer parts to include: programmable controllers, lasers and CAD software. This has allowed a drastic increase in printer proliferation from home-built garage-scale plastic printers to million dollar metal printers [13].

On the hobbyist end of the spectrum, AM provides an opportunity for individuals

to design a part, tinker with the design, and ultimately rapidly manufacture it. Many forums and resources are available online for hobbyists ranging from design databases to DIY printer support. Most individuals in this category use plastic-based printing technologies. As a result, the market for these low-medium fidelity and relatively low cost AM options have allowed a niche market of hobbyist designers and manufacturers to create customized and innovative parts with a very quick turnaround.

On the opposite end of the spectrum, industry is also seeing a significant boom in AM printing capabilities and needs. Although AM will not completely replace traditional manufacturing processes, it can provide unique opportunities for design and integration advances that would otherwise be unattainable by traditional manufacturing techniques.

There are many benefits to additive manufacturing technologies. The first advantage is the ability to manufacture a part layer by layer rather than subtracting material from raw material. This allows for very complex and optimized solutions to be manufactured that cannot be realized by traditional subtractive techniques. As a result of only using material where it is needed in each layer, AM allows for extremely complex designs to be manufactured at minimal costs as compared to subtractive techniques, in addition to the opportunity for weight savings by printing structurally sound but significantly lighter lattice sections integrated into the part. An example of this is seen in Figure 6 where the part shown has been optimized to reduce weight while keeping its structural integrity. Additionally, additive processes allow for integration of components that would otherwise be unattainable by traditional manufacturing techniques. An example of this can be seen in Figure 7 where the part shown would require more parts and integration steps than the same part which has been optimized for the AM process. Lastly, the ability to modify whatever is being printed next without changing the tooling or process allows for time and

cost effective low-quantity production runs. That is, although manufacturing time is generally slower for additively manufactured parts, they can go from the drawing part to realization significantly faster than using traditional approaches. This is the reason AM has a hold on prototyping and low quantity builds [13].

Figure 6. Comparison of traditionally manufactured (rear) and AM (front) parts and size and weight savings possibilities. [14]

A real world example of the using the advantages of AM to create an integrated single part can be seen in the fuel nozzle for the GE9X engine. The current design utilizes AM to create a nozzle design that could not be manufactured otherwise. By using AM, the part count for the fuel injector went from 18 to just one. In redesigning the nozzle into just one part, GE was also able to increase fuel efficiency for the entire engine resulting in a 1 percent reduction in fuel costs [15]. Figure 8 shows the redesigned fuel nozzle as it will be installed in the LEAP engine.

(a) Traditional Manufacturing Techniques (b) Additively Manufatured Part

Figure 7. Comparison between traditional and AM manufacturing techniques and their impact on part count and integration efforts. (Courtesy of Phil Smith.)

Figure 8. An additively manufactured jet engine fuel nozzle developed by GE for the LEAP. [16]

2.3.1 Process

Regardless of application, all additive manufacturing processes begin with a CAD based design. Once a working design is finalized, the model is sliced into hundreds to thousands (depending on print resolution) of cross-sectional slices by AM preparation software. This software also allows for control of numerous print setting adjustments to many aspects of the printing process. Later in this section several different types of AM will be presented and with each, comes its own set of variables that change how the print job finishes. Additionally, the prep software also contains algorithms to determine proper print orientation and support material locations to ensure the best print quality. Once these steps are complete, the job is sent to the printer and it starts creating the object layer by layer [13].

2.3.2 Types of Additive Manufacturing

As mentioned, there are several types of additive manufacturing technologies that each provide unique abilities but come with inherent downsides. Recently, the American Society for Testing Materials (ASTM) categorized AM process into seven categories [17]. These categories and associated attributes are outlined in Figure 9.

Each of these classifications of AM technology has a plethora of information on its technology, operating concept, uses, pros/cons, etc. but this paper will focus on Direct Metal Laser Sintering (DMLS) due to its applicability to this thesis.

2.3.3 Direct Metal Laser Sintering

Direct metal laser sintering is one of the powder bed fusion AM technologies that has gained attention in industry due to its ability to create parts that rival traditionally manufactured parts. DMLS uses a high energy laser to fuse certain x-y points of a very thin metal powder bed based on the current layer being sintered.

CATEGORIES	TECHNOLOGIES	PRINTED "INK"	POWER SOURCE	STRENGTHS / DOWNSIDES
Material Extrusion	Fused Deposition Modeling (FDM)	Thermoplastics, Ceramic slurries, Metal pastes	Thermal Energy	• Inexpensive extrusion machine • Multi-material printing • Limited part resolution • Poor surface finish
	Contour Crafting			
Powder Bed Fusion	Selective Laser Sintering (SLS)	Polyamides /Polymer	High-powered Laser Beam	• High Accuracy and Details • Fully dense parts • High specific strength & stiffness • Powder handling & recycling • Support and anchor structure
	Direct Metal Laser Sintering (DMLS)	Atomized metal powder (17-4 PH stainless steel, cobalt chromium, titanium Ti6Al-4V), ceramic powder		
	Selective Laser Melting (SLM)			
	Electron Beam Melting (EBM)		Electron Beam	
Vat Photopolymerization	Stereolithography (SLA)	Photopolymer, Ceramics (alumina, zirconia, PZT)	Ultraviolet Laser	• High building speed • Good part resolution • Overcuring, scanned line shape • High cost for supplies and materials
Material Jetting	Polyjet / Inkjet Printing	Photopolymer, Wax	Thermal Energy / Photocuring	• Multi-material printing • High surface finish • Low-strength material

Figure 9. AM classification by ASTM International [13]

After one layer is complete, the build platform is lowered and a successive layer of metal powder is applied over the print area creating the z-dimension. The laser once again fuses the powder to both the previous layer (z-dimension) and the other in-plane (x-y dimension) points. This process continues until the whole part is realized at which point post-processing of the printed part can take place. This process is visualized in Figure 10.

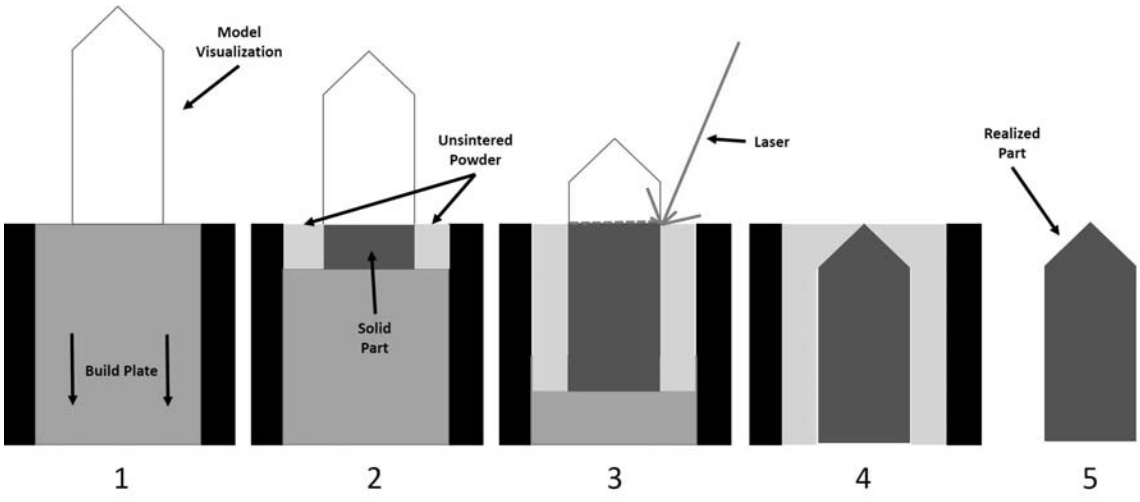

Figure 10. Depiction of DMLS process from concept to realization.

2.4 Structural Requirements

Since structural verification is important to ensure an additively manufactured heat pipe can be manufactured and used as a structural component, typical structural requirements are applicable to this experimental setup. In designing spacecraft systems, the prominent structural limiting loads are experienced during takeoff. This is a result of the massive engines used by launch vehicles and the resulting airflow over the skin of the launch vehicle addition to a severe vibroacoustic environment. This means that the launch environment is a prominent design consideration when designing spacecraft and components [18].

In terms of testing a system's ability to survive launch, a common practice is to consider both the acoustic and random vibration environments. This vibroacoustic environment ranges from 20 Hz to 20 kHz and is applied in accordance with NASA-STD-7001 [19]. Figure 11 shows the vibration testing profile as defined by NASA's General Environmental Verification Standard (GEVS). This profile is the simplest way to envelope the entirety of the launch event (engine ignition to deployment) in one testing profile and encompasses numerous test cases and launch vehicle vibration profiles to ensure the worst case scenarios are covered.

When running vibration testing, two important aspects of the vibratory response are being determined. First, the natural frequencies of the system are measured to ensure they align with the launch provider structural requirements. In addition, the ability to survive the launch environment is being tested. This is done by running a series of alternating sine sweep and random vibration profiles. The first sine sweep run acts as a baseline for subsequent testing. After the first sine sweep test is performed, a random vibe test at reduced input, usually -6 dB, is run. After this test another sine sweep test is performed to determine if the natural frequencies of the system changed which would indicate a structural issue. This process continues for random vibe levels

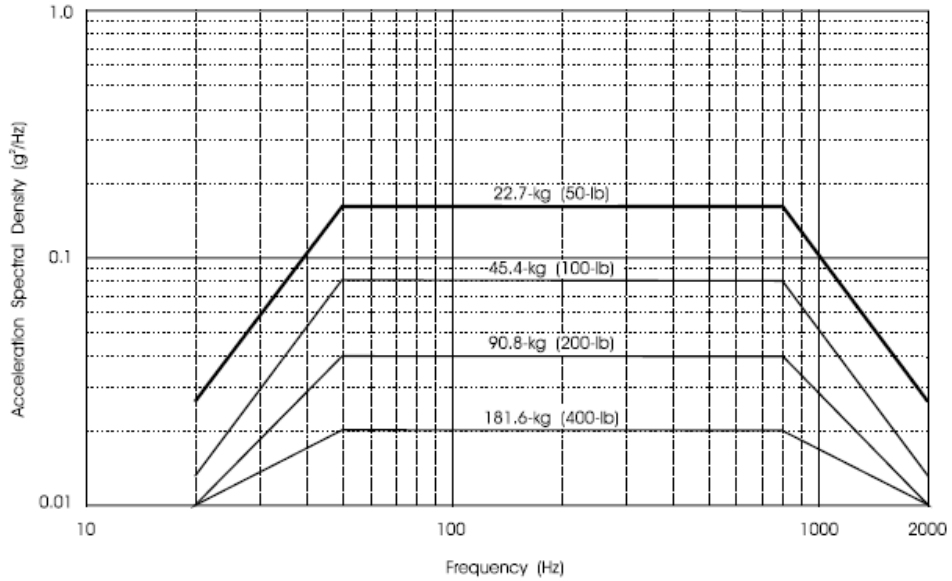

Figure 11. Random vibration profile defined by NASA GEVS. [18]

at -3 and 0 dB until the final sine sweep is performed. After this is performed, the natural frequencies observed are compared between the baseline and final sine sweep sets. If there is significant discrepancies between the two, inspections are performed to determine where the system encountered structural issues during the vibration test.

3. Methodology & Experimental Setup

This chapter will focus on the steps taken to achieve the research objectives outlined in Chapter 1. First, the methods and design considerations for certain aspects of this thesis will be described. After that, the experimental setup will be defined to ensure the reader understands what data was collected and how it will be utilized in the next chapter.

3.1 Additively Manufactured Porous Wick

As discussed in Section 2.2 the wick that transports the working fluid back to the evaporator section of the heat pipe is very important to a functioning heat pipe. The capillary pressure ability is directly proportional to the porosity of the wick and typically, a mesh screen is used to get a high pumping potential. In the case of an additively manufactured heat pipe, the opportunity arises to print this wick directly. In theory, this can be achieved in one of two ways. The first would be to print a structured mesh to dictate how porous the wick would be after manufacturing. The second would be to scale the print settings to achieve a porous part due to pockets of powder not being sintered. In the following two sections, a method in realizing these two methods will be discussed.

3.1.1 The Printer

To fully understand the constraints of the problem, an understanding of the additive manufactured technology used is essential. There are many additive manufacturing businesses that provide metal based AM services but i3DMFG was the provider chosen. They house 3 different metal 3D printers all supplied by EOS. Specifically, they use 1x EOS M280 and 2x EOS M290 DMLS 3D printers (Figure 12) [20]. These

machines provide a very versatile and well known platform for metal 3D printing.

Figure 12. EOS M290 metal DMLS machine. [21]

Spec	EOS 280	EOS 290
Building volume	250 x 250 x 325 mm (9.85 x 9.85 x 12.8 in)	250 x 250 x 325 mm (9.85 x 9.85 x 12.8 in)
Laser Type	Yb-fibre laser 200 or 400 W	Yb-fibre laser 400 W
Precision optics	F-theta-lens, high-speed scanner	F-theta-lens; high-speed scanner
Scan Speed	up to 7.0 m/s (23 ft/s)	up to 7.0 m/s (23 ft./sec)
Focus Diameter	100 μm - 500 μm (0.004 in - 0.02 in)	100 μm (0.004 in)

Table 3. Printer Specifications for the EOS M280 & M290 systems [21]

.

Since i3DMFG uses these printers exclusively, they have a very good understanding of their abilities and provided a guide that outlines their printing capabilities. Since this thesis is aimed at a new use for additive manufacturing, the limits of 3D printing were tested and the printer limitations were a major concern. Specifically, for Aluminum Alloy (AlSi10Mg) parts a minimum wall thickness of 0.308 - 0.406

mm (0.012 - 0.016 in) is recommended. This variable is very dependent on the part geometry. That is, shorter walls can be built at these specified thicknesses but taller walls may need additional supports to ensure minimal distortion. This limitation is a function of the printing process and the powder re-coater. Additionally, i3DMFG cites that tolerances for AlSi10MG are ± 0.004 in (± 0.102 mm) [20].

3.1.2 Wick Achieved by "Scaled" Print Setting

The first wick type that will be investigated is the porous wick. This design should yield a large capillary head resulting in a very robust heat pipe in terms of heat transport capability. Despite the obvious attractiveness of this design, its ability to be integrated into an atypical heat pipe design via additive manufacturing has yet to be demonstrated.

There are many methods to create porous metal samples. In a study aimed at characterizing different hybrid heat pipes, 4 different porous wick designs were manufactured and tested as the wick in a heat pipe. These wicks ranged from having pore sizes of 10 μm to 25 μm with solid features on the same scale. Although AM techniques have seen advances in print capabilities, there would be no way to print porous material by actually modeling each pore and sending that geometry to the printer. The printing restrictions on size and tolerances do not allow for an approach like this. Additionally, the preparation software could not handle porous geometry since the pores would be on the micrometer scale while the overall heat pipe would be on the centimeter scale leading to unacceptable levels of part complexity in the design space.

Despite the aforementioned issues with printing a porous part, additive manufacturing still uses a layer by layer approach to building a part which allows for a possible technique to overcome this issue. This technique uses adjustments to the

laser settings to drive variations in the finished part. Specifically, if the scan spacing or speed is altered, there is the potential that not all the powdered will be sintered for each laser pass. Ideally, a combination of setting adjustments could allow for pores of unsintered powder to form within the part creating continuous pores.

This idea was presented to i3DMFG and they had experience with manufacturing techniques such as this and proposed a set of print runs to vary different print settings. This resulted in printing 4 "batches" of 3 bars with each bar having a different print setting. At the time, the print setting limits that i3DMFG were comfortable with are outlined in Table 4. In addition, Figure 13 shows four selected samples from the final manufactured 12 bar set.

Sample	Printer Settings					
	Spacing (mm)	Speed (mm/s)	Layer Thickness (mm)	Max Power (Watts)	Energy Input	Power (J/mm^3)
Standard	0.19	1300	0.03	370	100%	49.93
A1	0.19	2600	0.03	370	50%	24.97
A2	0.2375	2080	0.03	370	50%	24.97
A3	0.285	1734.2	0.03	370	50%	24.95
A4	0.19	1950	0.04	370	50%	24.97
A5	0.2375	1560	0.04	370	50%	24.97
A6	0.285	1300	0.04	370	50%	24.97
A7	0.19	1560	0.05	370	50%	24.97
A8	0.2375	1248	0.05	370	50%	24.97
A9	0.285	1040	0.05	370	50%	24.97
A10	0.19	1300	0.06	370	50%	24.97
A11	0.2375	1040	0.06	370	50%	24.97
A12	0.285	867.1	0.06	370	50%	24.95

Table 4. i3DMFG print settings for 12 bar porous manufacturing test.

Several analysis techniques will be performed on the printed bars to estimate their porosity and wicking ability. The first of these is a simple porosity estimation from the measured density of the printed parts. This will be done by weighing and measuring each bar and calculating the bulk density. From this data, the simple density method of estimating porosity can be used as outlined in the equation below.

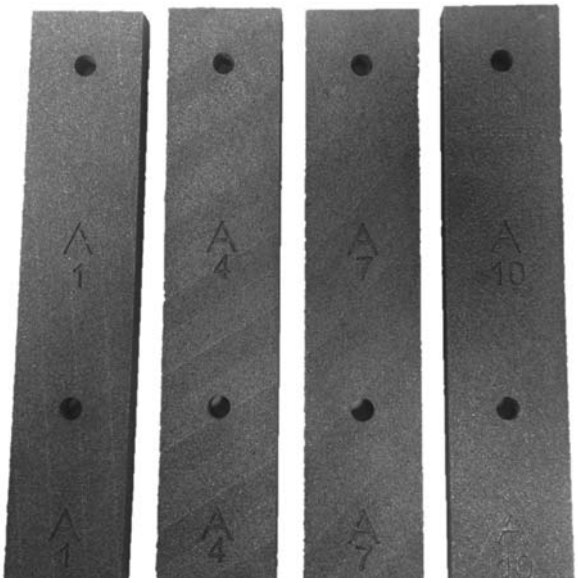

Figure 13. Selected bars from AM job to try and achieve porosity from print setting manipulation. Each bar is the first one of its print run.

$$\phi = (1 - (\rho_b/\rho_s)) \times 100 \tag{30}$$

In this equation ρ_b refers to the bulk density whereas ρ_s refers to the sample density [22].

The next inspection technique was to image the samples with a scanning electron microscope to get an understanding of the resulting structure. This will only be performed on the surface since additively manufactured parts are created layer by layer and the surface layer is representative of the entire part. This will provide information on actual pore size and connectivity can be estimated from surface images.

Once the visual inspection is complete a simple wicking test was constructed that would allow for documentation of each bar's wicking ability. This setup is pictured in Figure 14.

In this setup, an acrylic support was made which allows each bar to have one end suspended in a dyed liquid. Once the structure was placed in the liquid, the height of the wicked liquid was recorded. This test allowed for an understanding of the wicking

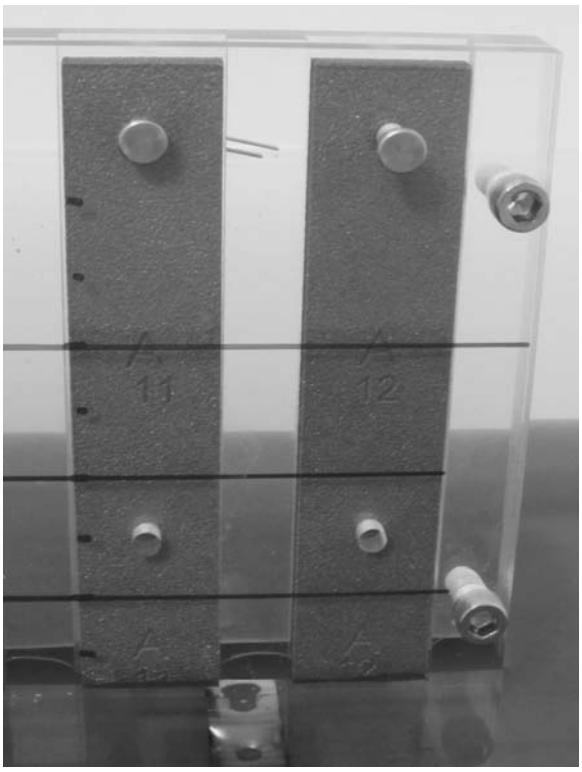

Figure 14. Experimental Setup for simple wicking ability test for additively manufactured "porous bars".

ability of each bar and their potential use as a wick in a heat pipe. The results of these tests are in Section 4.1

3.1.3 Structured Lattice Wick

Another wick type is a screen mesh that is inserted into the heat pipe. Mesh size refers to the number of openings in one square inch of a screen. Typical mesh sizes that are used in heat pipes range from mesh size 100 to 200 openings per square inch [2] [10]. Table 5 shows this range of mesh number sizes. The dimensions cited in Table 5 are the thickness values of the wire used to manufacture the mesh. [23]

Mesh Size (opening/in^2)	**Feature Size (μm)**
100	149
120	125
140	105
150	89
170	88
180	76
200	75

Table 5. US screen mesh sizes and their associated dimensions. [23]

Using this info, a method to create a structured lattice that would mimic a 3D screen was devised for use as a heat pipe wick. This design would be beneficial because the mesh size would dictate the wick characteristics. However, based upon the typical mesh sizes used in heat pipe wicks and i3DMFG's best practices guide, this could not be additively manufactured due to wall thickness and tolerance constraints.

3.2 Grooved Wick Heat Pipe Design

Both of the techniques presented in the previous section provide a significant capillary pumping capability (See Table 1); however, they both have significant additive manufacturing obstacles. That is, the structured pore and lattice designs have

features that are too small to be explicitly modeled and imported into the AM preparation software. Therefore, a grooved wick design was chosen as the way-forward for use in an additively manufactured heat pipe despite the printing issues that limit the heat pipe function to microgravity or condenser-above-evaporator limitations. This choice was made for several reasons; all of which would allow for the successful execution of the research objectives of this thesis. First, grooved wick designs are used frequently in space applications since the heat pipe operates in a microgravity environment. As mentioned in Section 2.2, this means that there are significantly fewer pressure losses as a result of both the wick design and operating environment. Second, despite axial grooves being less than ideal in a terrestrial environment, the heat pipe can still function even if the axial grooves cannot provide enough capillary pumping capacity.

In order to get as much capillary pressure draw as possible, the grooves were designed according to i3DMFG's best practices guide. A minimum wall thickness for AlSi10Mg is 0.308 to 0.408 mm. [20] Using this as a guide, a heat pipe was designed utilizing 0.5 mm axial grooves with 0.5 mm spacing. Smaller walls and spacing were not chosen due to the distance vertically that the grooves were printed in the hopes that this would help keep any deformation to a minimum. This is a significant limitation in being able to manufacture the most effective heat pipe but this research was aimed and determining the ability to additively manufacture a functioning heat pipe and this was one concession in doing this. Additionally, based on heat pipe theory, axial grooves with these dimensions will not allow for a functioning heat pipe if the evaporator is above the condenser in a 1G environment. However, the design was built so that the condenser would be above the evaporator which allows for gravity assistance in getting the working fluid back to the evaporator rather than relying solely on capillary action. That is, what was actually built will function as

a thermosyphon. Figures 15 & 16 show the model and internal wick structure while Figure 17 shows the printed product.

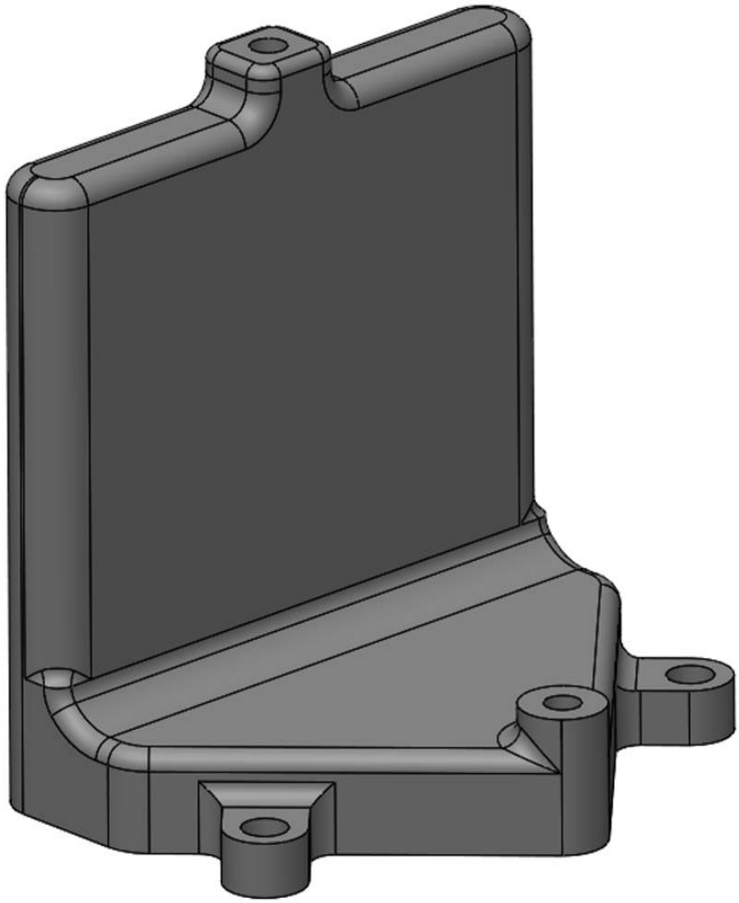

Figure 15. Full model of designed heat pipe.

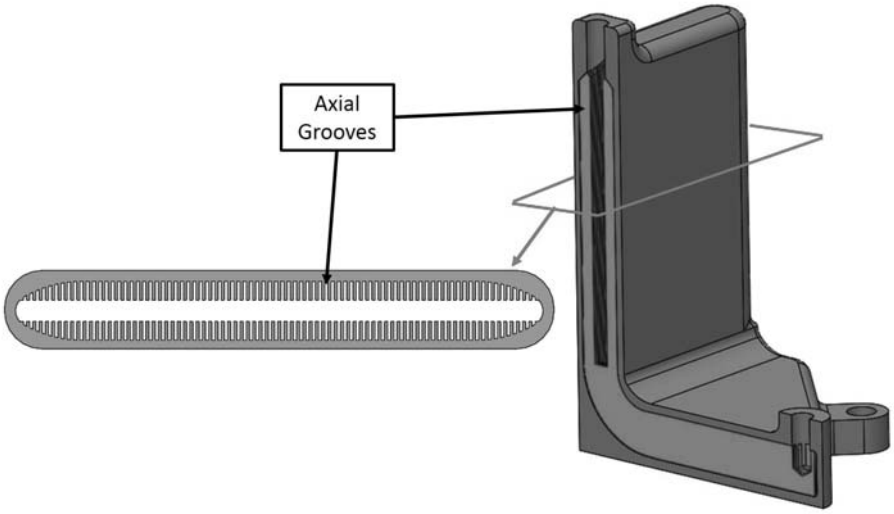

Figure 16. Sectioned model of desgned heat pipe showing internal axial grooves.

Figure 17. Additively manufactured heat pipes.

3.3 Non-destructive Inspection

Since additively manufactured parts usually have features that are not easily accessible via visual inspection, non-destructive inspection methods are very beneficial in determining the manufacturing integrity of AM parts. 3D Computed Tomography (CT) is one of these technologies that allows a user to view and inspect the external and internal structures of an object. CT functions by taking hundreds to thousands of 2D digital radiography (DR) projections. These 2D "slices" of the part can be used to reconstruct a digital 3D rendering of the scanned object. For the purposes of this thesis, the 2D DR "slices" were used so a side-by-side comparison could be made between the designed and printed geometries [24].

For this effort AFRL/RX offered up the use of their X-Ray CT scanner to determine internal feature print quality. This was very important since there are many small internal axial grooves that have thin wall thicknesses. In addition, even though access holes were included in the design, NDI offered an opportunity to ensure that all the remaining powder was cleared from the interior of the part during post-processing.

The machine used was the North Star Imaging X50 CT scanner. It is one of NSI's most popular models and can handle products with a nominal size of 8" x 8" x 12". It has a geometric magnification of up to 4000x. The overall system is pictured in Figure 18.

As mentioned, the wick print quality is crucial for an additively manufactured heat pipe. In addition, getting the unsintered powder out of the heat pipe design is very important so that there are no unintended obstructions or material present in the heat pipe internals. This led to several key cut planes being identified that will be represented by digital radiography projections. These cut planes are identified and shown in Figure 19.

Figure 18. North Star Imaging X-50 CT Scanner

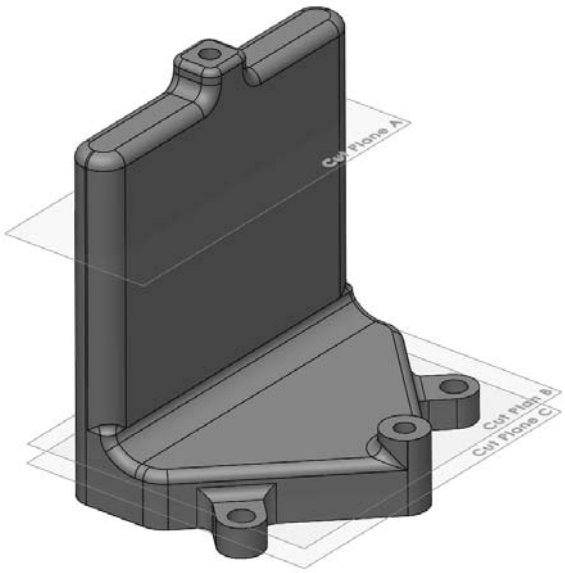

Figure 19. Depiction of cut planes used for model and CT scan comparison.

3.4 Thermal Testing Setup

The main focus of testing in this research is verifying that an additively manufactured heat pipe can, in fact, function as a heat pipe. In general, the test setup is fairly simple. Simply put, the tests consisted of heating the heat pipe and recording the temperatures at several locations along the length to determine heat pipe functionality and performance.

3.4.1 Heating

Since several different input powers need to be tested to verify heat pipe performance, an electric resistance heater was used to apply a specific input power to the system. Minco HK5417R36.1 polymide thermal resistance heaters were used due to their wide range of applications and frequent use. These heaters provided 36.1 $\Omega \pm 10\%$ of resistance and have a temperature range of -200 °C to +200 °C. The heaters came without adhesions so 3M thermally conductive adhesive was used to attach the heaters to the bottom of the heat pipes to ensure very good thermal conduction from the heater to test article. Figure 20 shows the attached heater location and orientation. Additionally, Table 6 shows the input power, in Watts, as a function of input voltage.

Input Voltage	Heater Power (W)
10	2.77
15	6.23
20	11.08
25	17.3

Table 6. Heater output power from input voltages.

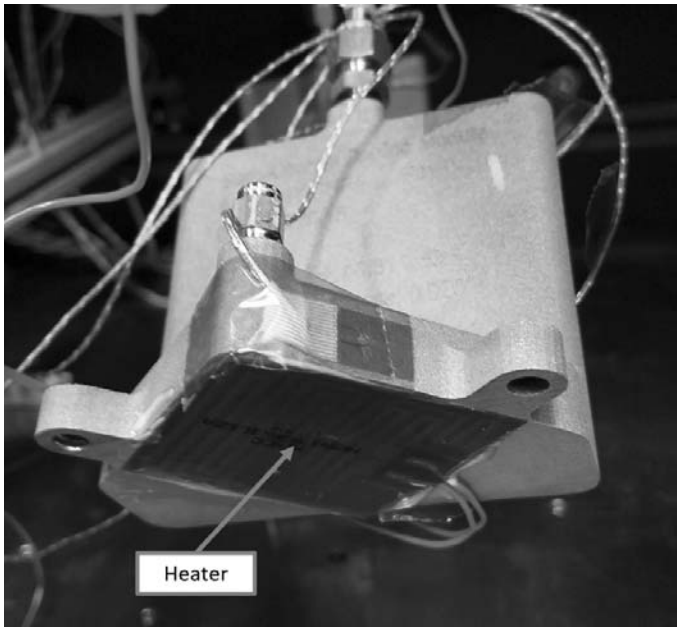

Figure 20. Location of patch heaters on heat pipes.

3.4.2 Working Fluid and Pressure

As discussed in Section 2.2 many working fluids can be used in heat pipes depending on the application and desired heat transport capability. Acetone was chosen as the working fluid of choice due to its fairly high latent heat of vaporization (518 kJ/kg), low boiling point, and ease of use as compared to working fluids such as ammonia.

When deciding upon a working fluid, it is also important to ensure that the expected temperatures in the heat pipe align with the working fluid boiling point. Figure 21 shows the boiling point of acetone as a function of temperature. Luckily, acetone has a low boiling point at standard atmospheric pressure and at the expected temperature ranges for the experimental setup, standard atmospheric pressure would allow for boiling at 60 °C. If this had to be adjusted the curve shown in Figure 21 would be used to determine what operating pressure would be needed for higher temperatures.

Although a high pressure heat pipe is not needed for this application, the ability to keep the heat pipe at a consistent pressure is crucial. To ensure this was the case,

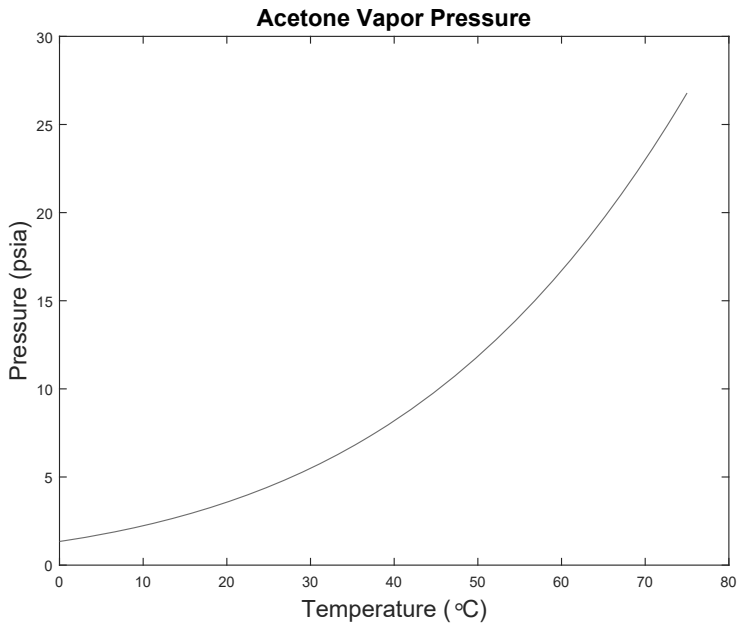

Figure 21. Vaporization pressure of acetone as a function of temperature. [25]

the access holes needed to clean the heat pipe post manufacturing and to fill it with a working fluid were designed small so they could be tapped. Unfortunately, even after care was taken to ensure the holes were threaded correctly and using Teflon thread sealing tape, leaks were still present in the system (See Figure 22). This led to the use of a two part sealant to ensure there were no leaks in the system (see Figure 23).

3.4.3 Heat Pipe Filling

Another important aspect of manufacturing and testing a heat pipe is getting the heat pipe filled with its working fluid and sealed. Since this test setup only needed atmospheric pressure inside, this process was a bit easier but care still had to be taken to ensure the proper amount of working fluid was put into the system. Since this heat pipe design was more atypical than most systems, the amount of working fluid was estimated based on the evaporator volume. To ensure dryout did not occur, 2/3 of the volume of the evaporator volume was used. This equated to 10.65 mL of acetone.

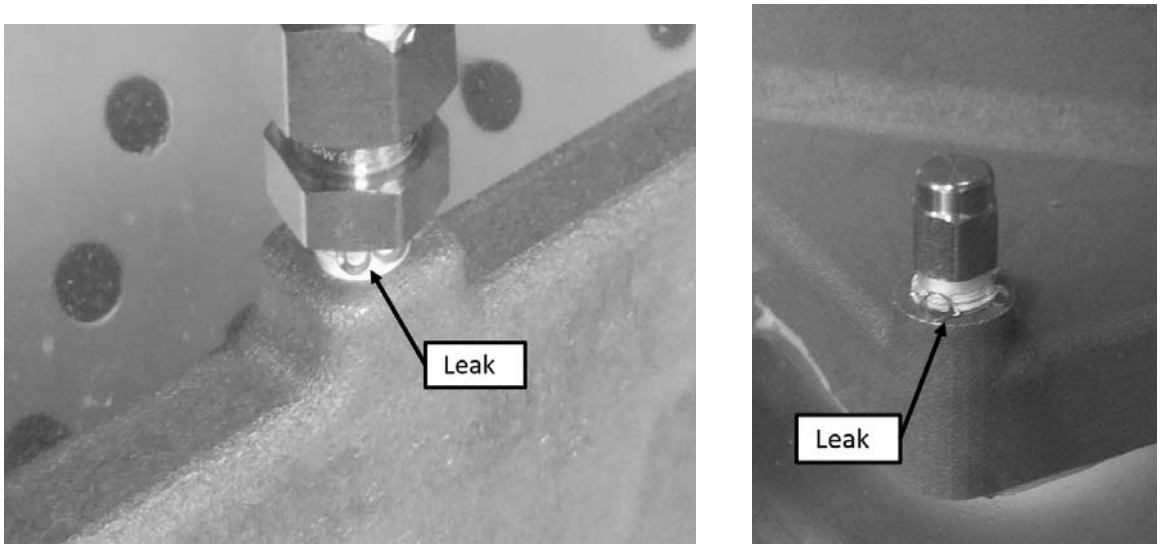

(a) Upper Leak (b) Lower Leak

Figure 22. Locations of pressure leaks prior to epoxying fittings into place.

Figure 23. Method used to ensure heat pipe held pressure without leaking.

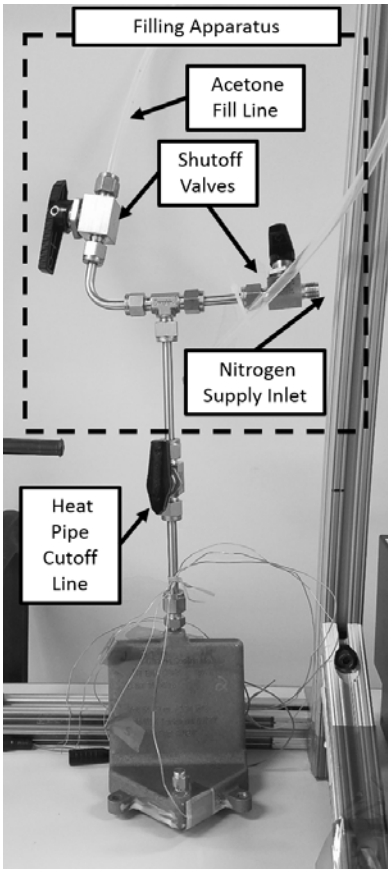

Figure 24. Setup used to fill heat pipe.

An additional item considered when charging the heat pipe was the amount of oxygen in the heat pipe. Since this design operates ∼60 - 70 °C a method was needed to purge as much oxygen as possible to minimize ignition probability. The steps to accomplish filling and purging the system were executed in the following manner. First, a nitrogen supply was attached to the nitrogen supply inlet. The system was pressurized to 100 psi, detached from the supply, and then vented. This sequence was carried out 6 times to ensure as much air was purged form the system as possible. next, the nitrogen supply valve was closed and the acetone filling valve was opened. Since the tubing ID is fairly small the heat pipe was rotated and angled to allow the acetone to flow into the heat pipe. This configuration was left to sit for several hours to allow the acetone to settle into the heat pipe evaporator section. Once this was complete the acetone supply valve was closed and the nitrogen source was attached and the system was pressurized to 10 psig to clear the lines. The heat pipe shutoff valve was then closed and the filling apparatus was removed. The heat pipe valve was then opened after one hour of settling time to return the heat pipe pressure to the desired atmospheric conditions. Once this was all complete, the open end after the valve was capped to ensure no pressure was lost thru the valve.

3.4.4 Instrumentation

The main data collected for this thesis was the temperature at a specific location along the length of the heat pipe. To do this, OMEGA surface mounted fast response thermocouples were used at specific locations to measure temperatures as the heat pipe tests were run. Figure 25 shows the thermocouples used and the differences between the two used was a function of what was readily available. From a measurement perspective, the data taken was exactly the same and the only difference is the calibration used. This difference was resolved by the data logging program

which automatically applied calibration curves to the incoming temperature data. The specifications for these thermocouples are given in Table 7.

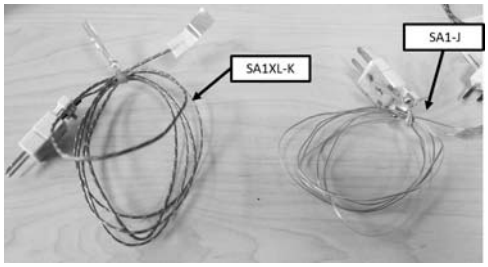

Figure 25. Thermocouples used to take temperature data.

Spec	SA1XL-K	SA1-J
Temperature Range (°C)	-73 to 260	-60 to 175
Calibration	K	J
Error (°C)	2.2	2.2

Table 7. Specifications for thermocouples used.

The number of thermocouples that could be used was limited to three per test article due to recording program limitations. Therefore, the placement of these thermocouples was crucial in order to ensure the data needed was collected. Since an electric resistance patch heater was used, the actual temperature of the base was unknown so one recording location had to be as close to the heater as possible. This value was important to know what the input temperature was to allow for adjustments of the operating pressure ensuring the actual function of the heat pipe. The two remaining thermocouples had to be separated along the length of the heat pipe to ensure that $\triangle$T's were obtained. Without these values, the heat transport capacity of the system as a heat pipe and conductor could not be determined. The specific locations of the thermocouples are pictured in Figures 26 & 27.

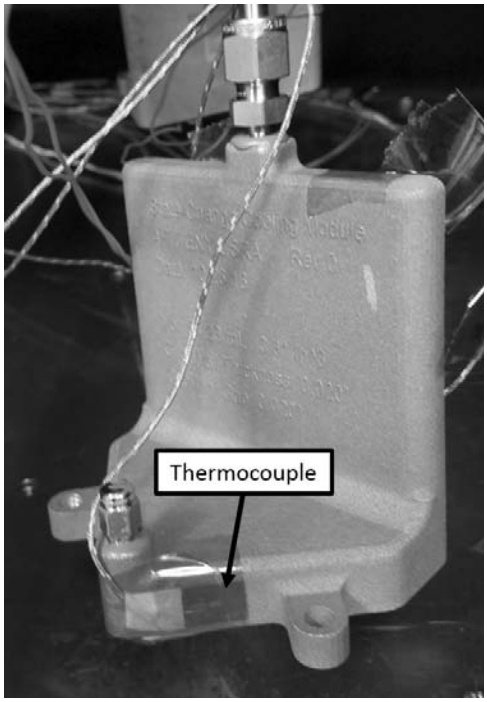

Figure 26. Location of control thermocouple measuring heat input temperature.

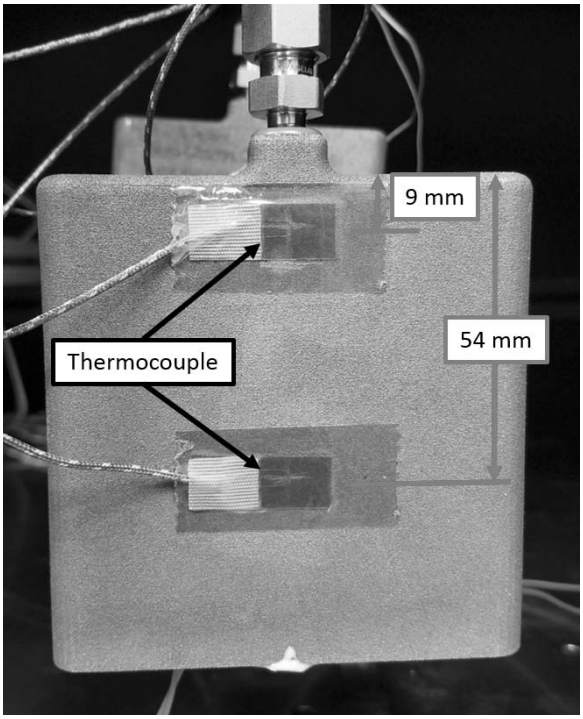

Figure 27. Locations of thermocouples on back face of test articles.

3.4.5 Data Acquisition

As mentioned, the main data that was needed were the temperatures at specific locations along the length of the heat pipe. Thermocouples were used to get these temperatures and this data was passed through LabVIEW. LabVIEW performed the necessary calibration curve adjustments to the data and plotted it in real time and generated a data log for each of the thermocouples.

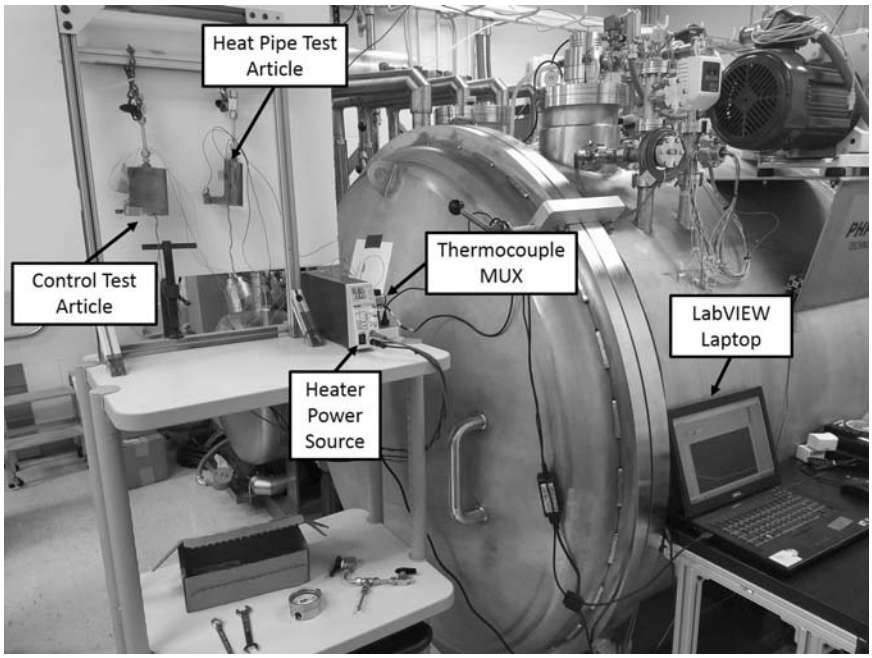

Figure 28. Picture showing overall test setup.

There were some other considerations when setting up this experiment. First, the test articles were suspended to a fixed bar via a chain to minimize any heat conduction through the base as compared to a setup that had the heat pipes bolted at their base to a support structure. This ensured that natural convection was the only other significant heat transfer method that the test articles were exposed to. Additionally, the upper valves were left on both heat pipes to ensure there were minimal differences between the test article geometry. Lastly, the ends of the valves were capped to ensure that there was no acetone leakage from the filled heat pipe test article.

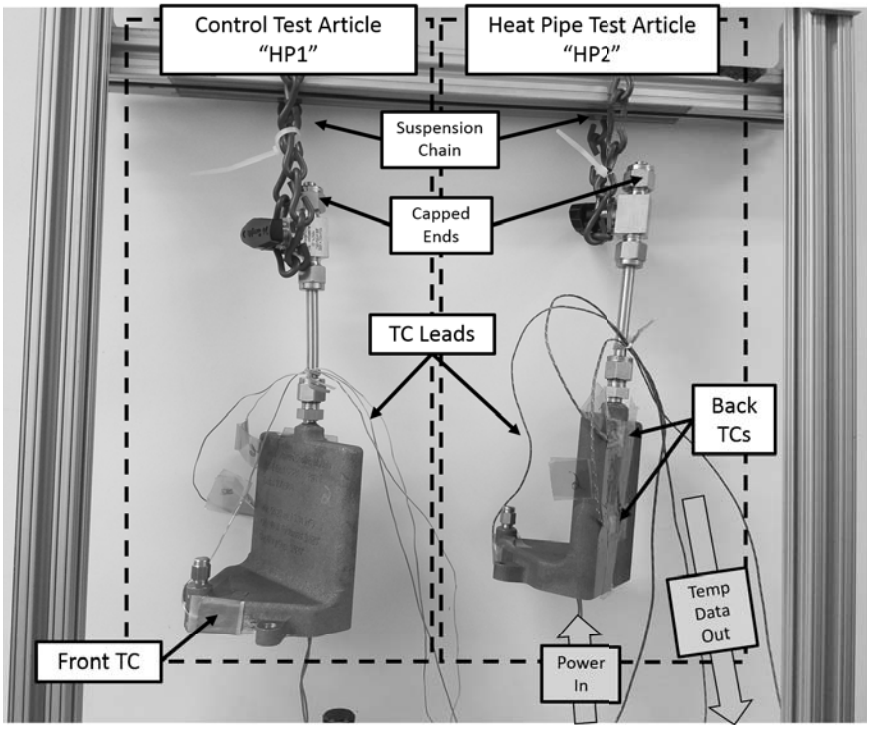

Figure 29. Test setup showing control and heat pipe test article configurations.

3.4.6 Conduction Test

The first test cases that were executed were the conduction test cases. This was performed by running a set tests each at a different input voltages. The input provides in the conduction test cases are outlined in Table 8. This variation in input voltage translates to different power inputs which will be reflected in the temperature distributions.

Test Case	Input Voltage	Input Power (Watts)
1	10	2.77
2	15	6.23
3	20	11.08
4	25	17.31

Table 8. Conduction test case heater inputs.

As discussed in the heat pipe filling and pressurization sections, a good under-

standing of the temperatures that could be expected in this system was needed to accurately predict the internal pressure required. This temperature profile was obtained using conduction tests of purged test articles. In these tests, both printed heat pipes were used to ensure accurate results and to verify that performing a one to one comparison in the heat pipe tests would be valid. Performing these conduction tests allowed for temperature measurements to be taken near the heater and at the end of the heat pipe to see what temperature ranges could be expected at various heating input levels.

From these results, it was expected that an operating temperature range could be determined based on heater input levels which would correlate to a range of operating pressures.

Expected conduction test result are shown in Figure 30. Although this is nominal data it should follow these general trends since the system in these test cases are only a function of input power, conduction through the test article, and convection of heat out of the test article from all free surfaces. Since the only variable in this case will be input power, the curves remain consistent with the only changes being the equilibrium temperatures.

Another important metric on Figure 30 is the temperature difference ($\triangle$T) that is measured between the upper and lower thermocouples on the back face of the test article. These values will be compared to the temperature values observed during the actual heat pipe test.

Additionally, the maximum temperatures recorded at each power input level is very important data since it will be used as the control case when determining if the system was functioning as a heat pipe. Theoretically the constant convection boundary condition will result in a max temperature vs input power function that is linearly dependent on the input power.

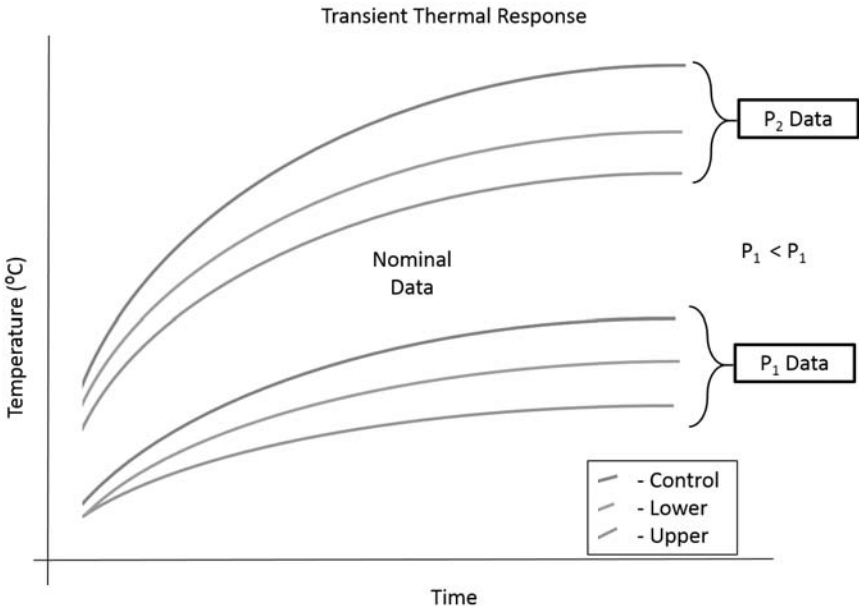

Figure 30. Expected transient temperature results from conduction testing.

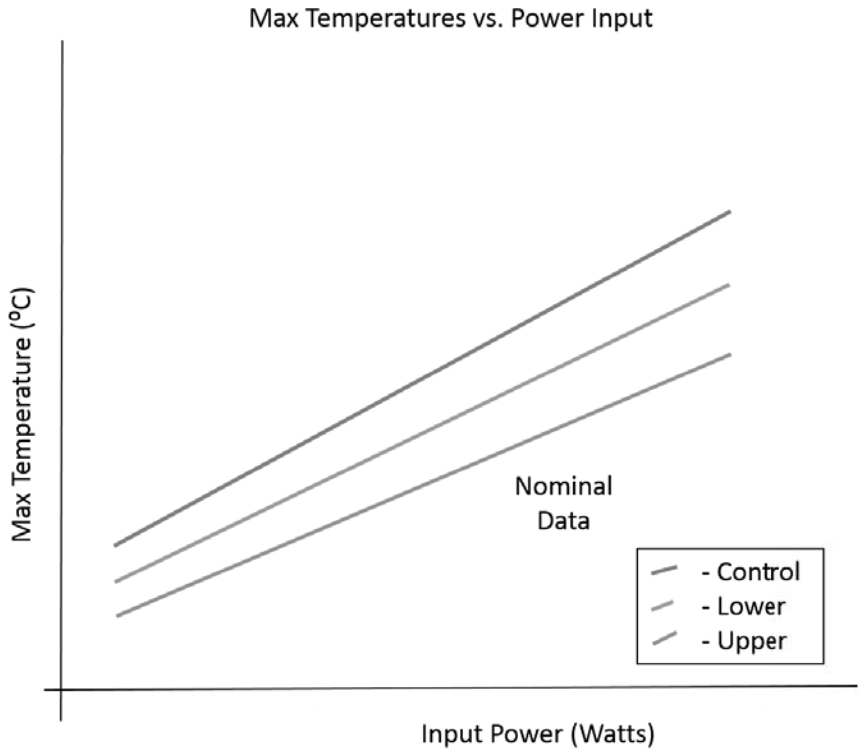

Figure 31. Conduction testing expected maximum temperatures as a function of input power.

Test Case	Input Voltages	Input Powers	Comments
1	10.0	2.77	- Working Fluid Leak - Multiple Test Profiles
	15.0	6.23	
	16.0	7.09	
	17.0	8.01	
	18.0	8.98	
	19.0	10.00	
	20.0	11.08	
	21.5	12.80	
	23.0	14.65	
2	17.5	8.48	- Refilled and retest of Test Case 1 - Single Test Profile
	19.0	10.00	
	20.0	11.08	
	21.0	12.22	
	22.0	13.41	
	23.0	14.65	
3	18.0	8.98	- Increased Convective Environment - Single Test Profile
	20.0	11.08	
	27.5	20.95	
	29.0	23.30	
	30.5	25.77	
	31.5	27.49	
	32.5	29.26	

Table 9. Inputs and comments on the 3 heat pipe tests cases that were run.

3.4.7 Heat Pipe Tests

Once the conduction tests were completed, one of the heat pipes was filled and prepared as discussed in Sections 3.4.2 & 3.4.3. Then, testing of the test articles was repeated in much the same manner as the conduction tests. Several tests were run in order to definitively conclude the functioning of the heat pipe. Additionally, several modifications needed to made between tests. An outline of the test modifications and inputs of each test case are outlined in Table 9.

In these tests, there should be several key differences in the temperature data that is collected as compared to the conduction tests. First, the $\triangle$T between the upper and lower portions of the heat pipe should be less than that of the conduction test article.

This goes back to heat pipe theory discussed in Section 2.2. Second, the maximum temperature recorded should be lower than that of the conduction only case. This, again, is due to heat pipe theory in that heat pipes have a thermal conductivity that is orders of magnitude greater than that of conduction only thermal management solutions.

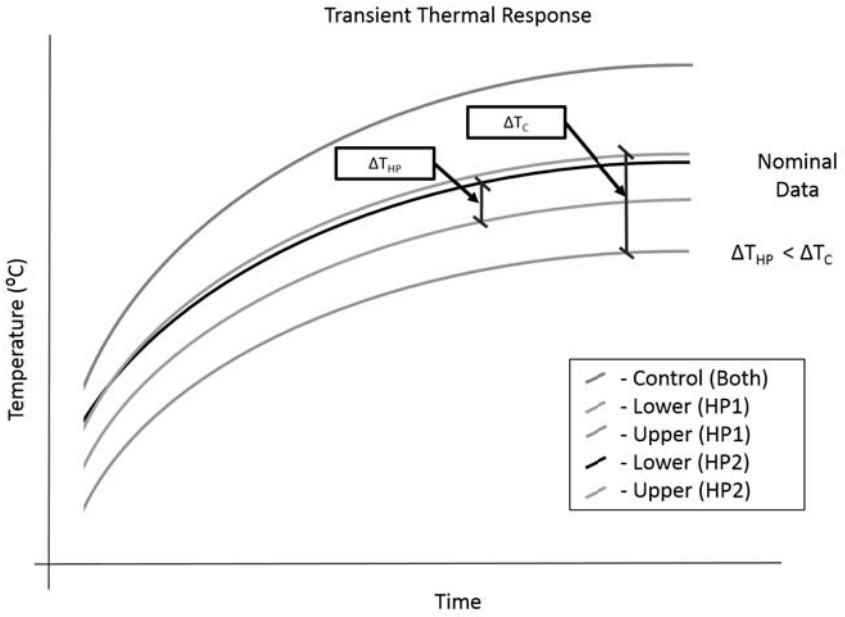

Figure 32. Transient response expected during heat pipe testing.

3.5 Structural Testing

Structural testing was performed on the printed heat pipe test articles to determine their ability to be categorized as a structural member in addition to thermal control system. Since vibrational testing was planned for this project, Finite Element Analysis (FEA) was performed in conjunction with testing to support the obtained results.

For the FE model, data was taken from the EOS material data sheet for AlSi10Mg [21] to ensure the most accurate material properties were being used for the finite el-

ement model; however, the material was assumed to be homogeneous and anisotropic material properties were not taken into account. The FE model can be seen in Figure 33 and shows the general mesh density used for the modal analysis. The boundary conditions imposed on the system were simple displacement/rotation constraints on the bottom face of the heat pipe.

Figure 33. FE model for vibration testing.

With the FE model complete, an actual vibrational test was the next test to be performed. This test would give natural frequencies as well as structural integrity data. This was done by running a series of sinusoidal and random vibration testing as outlined in Table 10.

Event #	Description
1	Sine Sweep
2	-6 dB Random Vibe
3	Sine Sweep
4	-3 dB Random Vibe
5	Sine Sweep
6	0 dB Random Vibe
7	Sine Sweep

Table 10. Vibe testing outline.

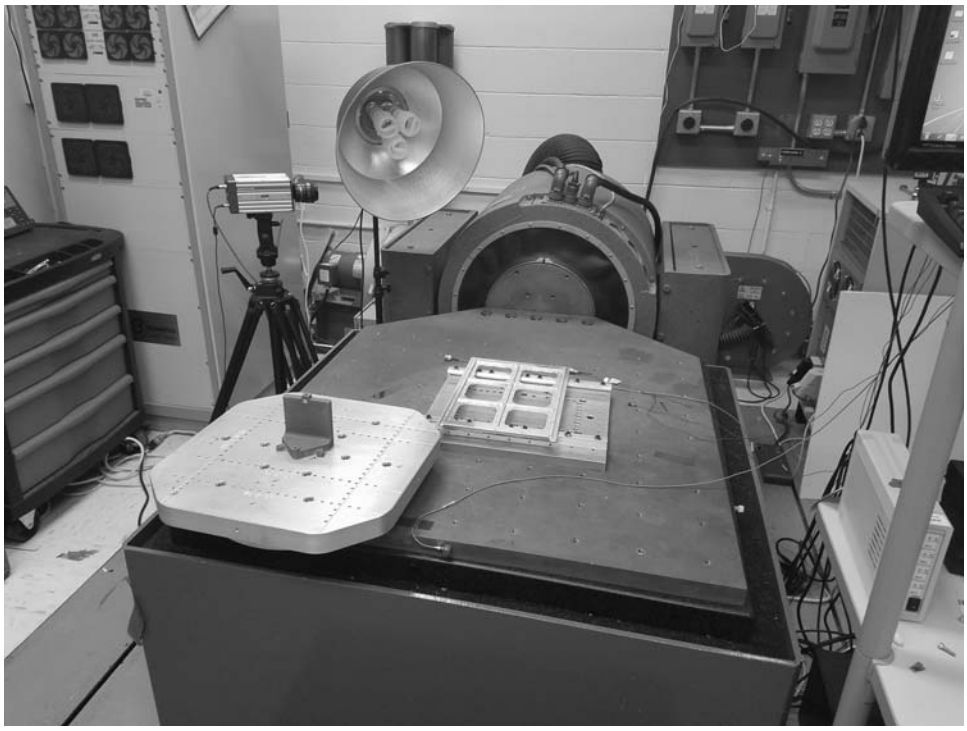

Figure 34. Vibration testing test setup.

4. Results and Analysis

4.1 Testing of Porous Wicks by Altered Print Settings

The first step in evaluating the porosity and wicking potential of the additively manufactured bars was to get an understanding of what was actually produced in the printing process. As mentioned, this was an attempt to create porosity by altering the 3D printer settings so actual correlations to porosity and wicking ability was unknown.

4.1.1 Porosity Estimation

This process began with measuring and weighing the samples to compare the densities of the printed parts with a nominal solid aluminum bar printed with same material. Additionally, the density method of estimating porosity, Equation 30, was used to estimate each bars porosity. The results of this analysis are shown in Table 11. The results presented in this table give the first clear evidence that altering the print settings may not be a viable option for additively manufacturing heat pipe wicks. Looking specifically at the range of estimated porosities, it is clear that the achieved porosity levels are too low to have any wicking potential. Typical minimum wick porosities for sintered metal wicks are 30% and the samples created by this technique are all less than a 25% of this minimum porosity [26] [27].

4.1.2 SEM Imaging

SEM imaging was the next step in analyzing the test bars for wicking potential. Although SEM imaging does not give an understanding of internal features, it provides very useful insight into the surface features for each print setting. Since these bars were additively manufactured (i.e. - layer by layer), the surface feature structure can

Sample	Mass (g)	Density Change	Estimated Porosity
A1	46.451	-9.07 %	8.31 %
A2	46.762	-7.62 %	7.08 %
A3	46.916	-6.68 %	6.26 %
A4	47.975	-5.21 %	4.95 %
A5	47.837	-5.78 %	5.47 %
A6	47.481	-5.52 %	5.23 %
A7	47.888	-3.92 %	3.77 %
A8	47.921	-3.97 %	3.82 %
A9	47.842	-4.10 %	3.94 %
A10	48.176	-3.04 %	2.95 %
A11	48.019	-3.59 %	3.47 %
A12	47.738	-4.06 %	3.90 %

Table 11. Results of calculating AM test bar densities compared to solid AlSi10Mg bar. Values based on EOS material data sheet. [28]

be applied to each successive layer giving insight into the overall sample structure. Figure 35 shows the first print batch that was printed with the thinnest layer thickness at 0.03 mm but fastest print speed. Figures 36 & 36 show the two middle batches with layer thicknesses of 0.04 and 0.05 mm, respectively. Lastly, Figure 38 shows the last print batch which had the thickest print layer at 0.06 mm but slowest overall print speed.

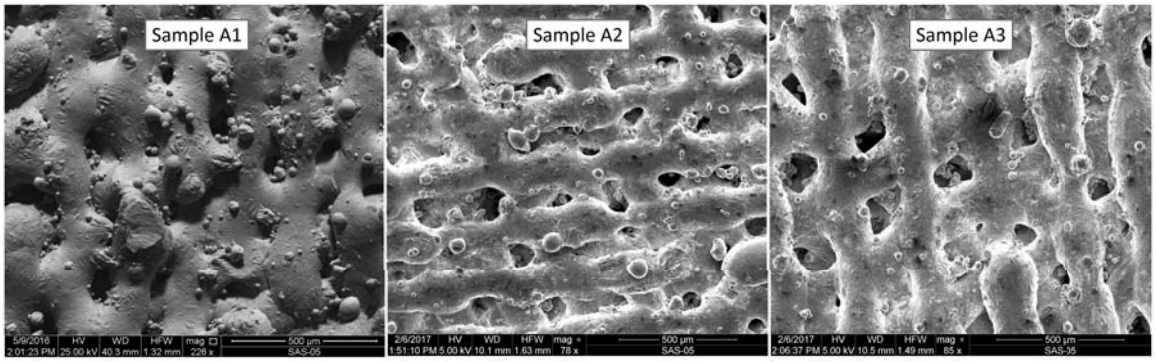

Figure 35. SEM surface images of the first set of 3D printed bars.

Looking at the SEM image grouping it is clear that there are several distinct trends in terms of print batches and achieved porosity levels. First, as the layer thickness increases, the ability to generate voids through this method is greatly reduced. Sam-

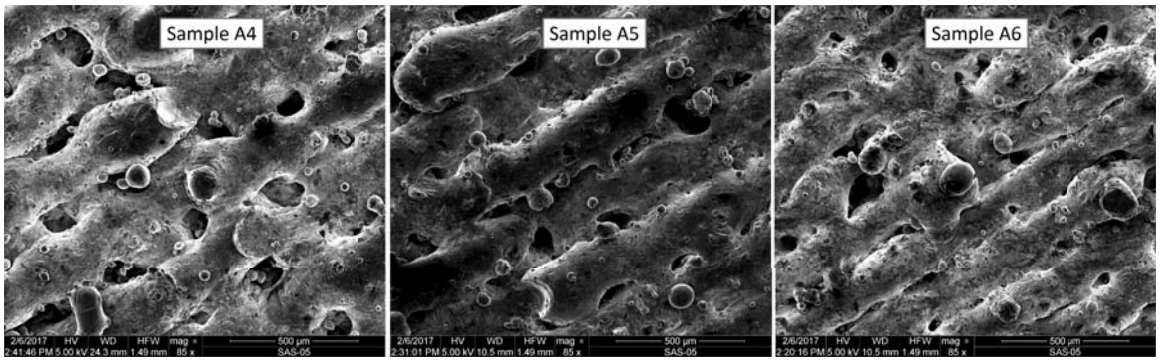

Figure 36. SEM surface images of the second set of 3D printed bars.

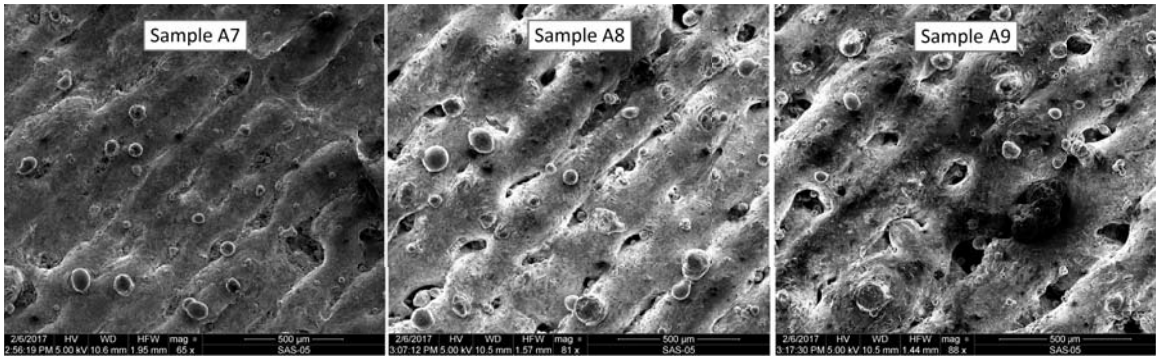

Figure 37. SEM surface images of the third set of 3D printed bars.

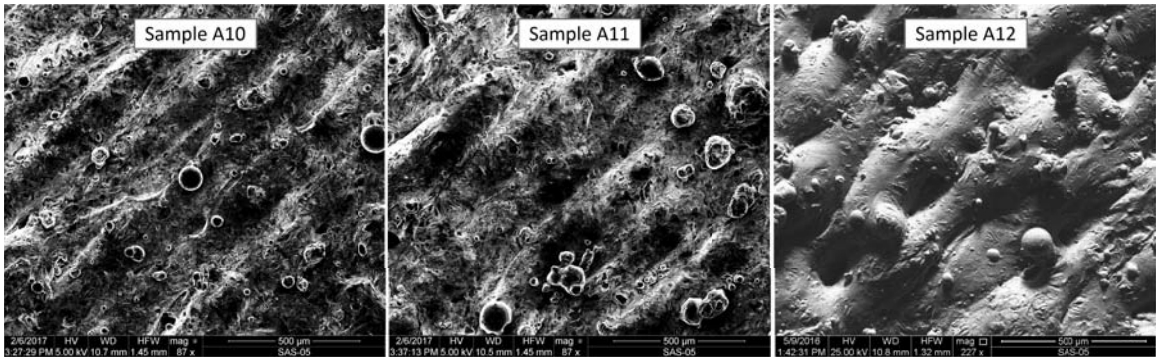

Figure 38. SEM surface images of the fourth set of 3D printed bars.

ples A1-A3 have the thinnest print layer and show the most potential in achieving a porous part. Conversely, samples A7-A12 have the two thickest layers settings and both sets of samples show very few voids on the surface. The other evident trend that is observed is that as print speed increases the resulting realization is less porous. This trend is observed in the individual print batches but is very consistent across all four batches.

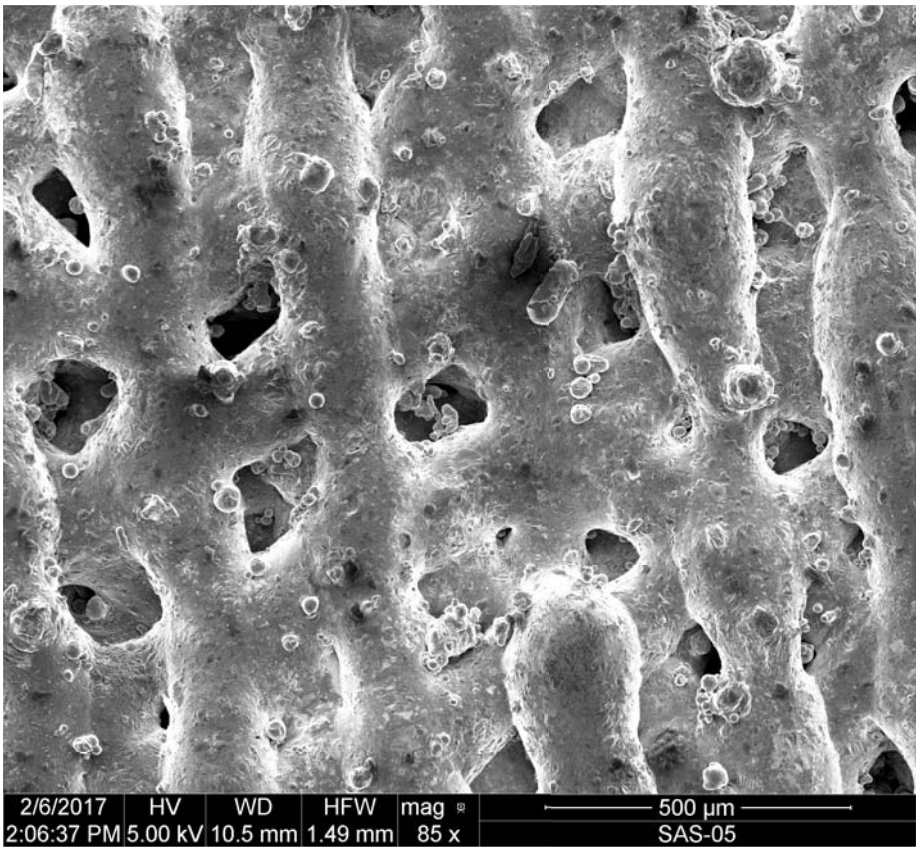

Figure 39. SEM surface images of the most successful porous print sample; Bar A3.

With the above results, it is clear that the most porous sample was sample A3. A close-up of this bar is seen in Figure 39. This sample contains the most "pores" per imaged area and the ratio of pore to solid is the largest amongst the printed samples. By taking this image and estimating the surface porosity, an extrapolation can be made as to the overall bar porosity assuming that the surface layer can act as a model

for the successive layers. When this is done, sample bar A3 is estimated to have a porosity of 8.5%. This agrees in an absolute sense with the estimated porosity of this sample using the density method in that both methods estimate a porosity <10%. Although this agreement is desirable, the estimated porosity that this bar was printed with is still well below a useful bulk porosity value for a wick and still contains no continuous channels for fluid flow.

Additional information can be extracted from these images in the form of achieved pore size. Looking at the A1 bar sample SEM image, 50-75 μm circular voids can be seen on the first printed layer. Bar A2 has slightly larger surface voids at 75-100 μm. As mentioned, bar A3 had the most potential of being a porous metal and had pores averaging 100×150 μm. Sample A4 was similar to A3 but all samples after that decreased in their potential to be a wicking material.

These results by themselves would not disprove the ability to additively manufacture a heat pipe wick. Voids on this magnitude would be perfectly viable for a functioning porous heat pipe wick; however, the ratio of void space to solid material is too low for a wicking structure. In the additively manufactured samples, there is much more solid material with very few voids. If this was a structured pore system, those voids could be stacked resulting in a continuous channel but in the case of these bars, the pores are at random intervals throughout the bar resulting in encapsulated pores and noncontinuous channels. This results in a material that has trapped pores but no channels for a working fluid to travel which supports the previous conclusion that these samples have no wicking potential.

Lastly, the performance of the print setting used (as outlined in Table 4) can be summarized based on the SEM images taken. From each SEM image, the centerline distance between laser scan passes was measured. The results are summarized in Table 12.

Sample	Desired Spacing (mm)	Observed Spacing (mm)	Difference
A1	0.19	0.20	7.2%
A2	0.2375	0.2500	5.3%
A3	0.285	0.292	2.3%
A4	0.19	0.21	9.6%
A5	0.2375	0.2500	5.3%
A6	0.285	0.333	17.0%
A7	0.19	0.22	17.0%
A8	0.2375	0.2391	0.7%
A9	0.285	0.327	14.6%
A10	0.19	0.24	28.9%
A11	0.2375	0.2041	-14.1%
A12	0.285	0.222	-22.0%

Table 12. Comparison of intended vs realized spacing determined by SEM image analysis.

From the results shown, it can be observed that the realized spacing at smaller layer thicknesses is desirable. Luckily, this also occurs in the samples with the greatest porosity, bars A1-A4.

4.1.3 Wick Test

The last test to verify previous conclusions about the sample bars was to test the wicking ability of the samples. The wick test was carried out for a duration of 4 hours and there was no active fluid wicking observed during this test. This result was not a surprise since the visual inspections indicated that there would be no pores or channels to actively pull the liquid up the bars.

4.1.4 Summary

After performing the three tests outlined above it is clear that a suitable metal porous wick cannot be additively manufactured by altering the 3D printer settings as outlined in Section 3.1.2. Despite the results from this research, there is still the potential for additive manufacturing to be used in creating a heat pipe with

integrated porous wick. Based on the results observed in the SEM imaging, it is plausible that by altering the print settings to mimic bar A3 settings and force the laser to a specific beam pattern, a porous wick could be achieved. In addition, if alterations to this research were to be performed, using smaller laser spacing will result in a more accurate printed object.

4.2 Additive Manufacturing of Structured Screen/Lattice Wicks

After obtaining the results outlined in the previous section, plans to move forward with two full scale heat pipe with different wick types began with designing the heat pipes and associated wicks. The two types of wicks that were planned to be used were a grooved and mesh wick design. However, during the design process it was determined that current additive manufacturing capabilities are not precise enough to manufacture a screen/lattice design.

Using Table 5 and i3DMFG's Best Practices Guide as the manufacturing envelope, the ability of the EOS M280 printer to print the required mesh/lattice dimensions does not exist. To additively manufacture a mesh size 100 mesh (or equivalent lattice) the printer would need to have the capability of printing features on the 150 μm scale. However, the EOS printer is limited to printing, at an absolute minimum, 308 μm wall thicknesses. In addition, the tolerances of i3DMFG's manufacturing techniques are $\pm$102 μm. With minimal wall thicknesses double and tolerances at the level of the required features, using additive manufacturing to make a heat pipe with integrated mesh wick is not feasible with current AM capabilities.

4.3 CT Scan Results

Regardless of the wick design chosen, NDI was to be carried out on the manufactured design to ensure the design was manufactured properly and to evaluate the

wick structure. Since an axially grooved wick design was used and the dimensions were well within i3DMFG's size guidance, no distorted features or print anomalies were expected in the manufactured parts.

4.3.1 Wick

Figure 40 shows a SolidWorks rendering of the designed wick and a digital radiography cross section of the actual wick that was printed in the vertical section of the heat pipe. There are numerous images along the axial length where the wick was inspected but all images show the same result. Visually, the axial grooves were printed as designed with no discernible print distortions. This proves that an integrated wick structure can be successfully printed, integral to a heat pipe. Albeit, one that cannot fully function in a terrestrial 1G environment but one that should theoretically function in a micro gravity spacecraft application.

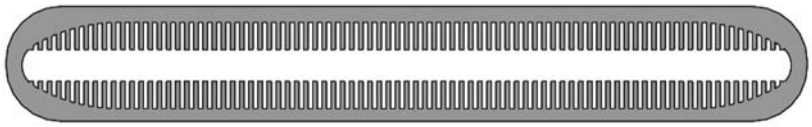

(a) Cut Plane A Expectations

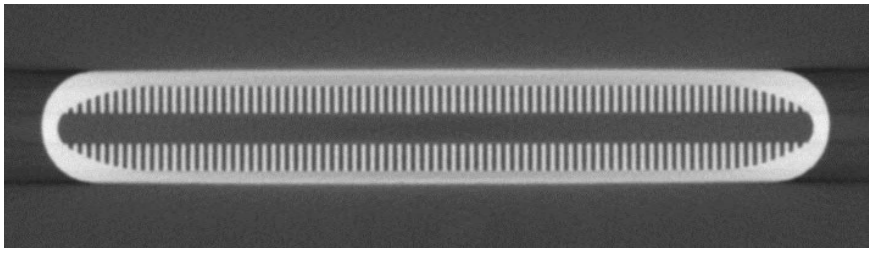

(b) Cut Plane A CT Scan

Figure 40. Solidworks vs. CT comparison of axial grooves

4.3.2 Other Heat Pipe Features

Although the actual wick was printed without issue, a few areas in the part suffered print distortions during the print process. Both of these issues occurred in the evaporator "triangle" section. First, Figure 42 shows a cross section of the printed heat pipe in the evaporator section. The fins in these figures are an extension of the grooved wick and were included to support the top face of the evaporator section. Unfortunately, the grooves are fairly thin and long at this point and started getting distorted due to an aspect ratio issue. Specifically, the width to length aspect ratio for this feature is what is causing print distortion issues due to the consistency in the height of the fins but warping in length away from a wall support. In addition, Figure 41 shows a significant amount of trapped powder near the top of the evaporator. This should have been extracted during post-processing through the access holes included in the design for this exact purpose. Alternatively, this print distortion could be fully sintered powder and be a permanent mass of unintended aluminum.

4.3.3 Conclusions

In the wick section, the width vs length aspect ratio of the groove cross-section was much lower than that of the grooves in the evaporator section. This difference allowed for the axial grooved wick to be printed as designed. Additionally, the orientation of the print procedure was perpendicular to the figures shown. This allowed for a anchoring point when printing each successive layer of the wick. This is in direct contrast to the vertical grooves in the evaporator. They had very high aspect ratios and one end that was not attached to the wall. These features combined to create long, tall, very thin walls that were distorted by almost 100% during the printing process. The walls may have also been distorted from the spreader introducing unintended sideways forces when applying another layer of powder for the successive print layer.

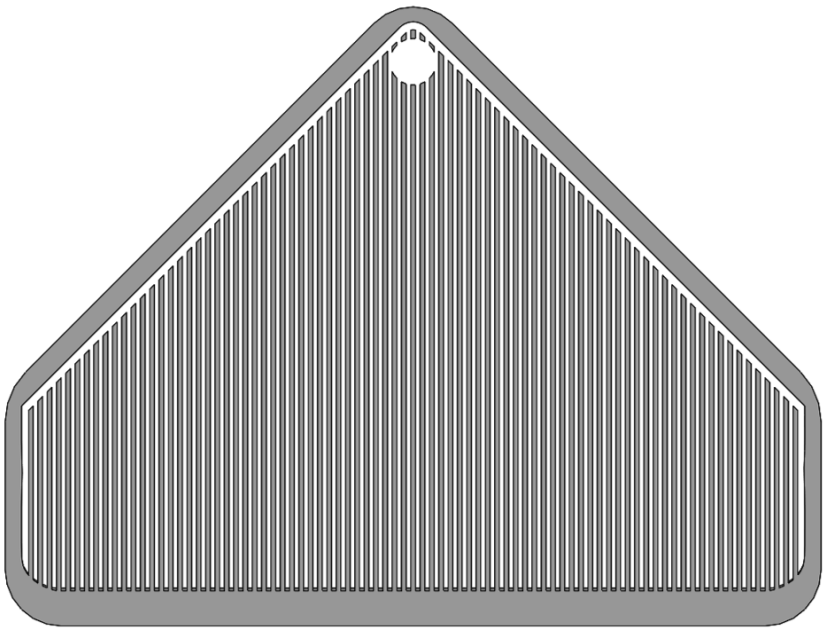

(a) Cut Plane B Expectations

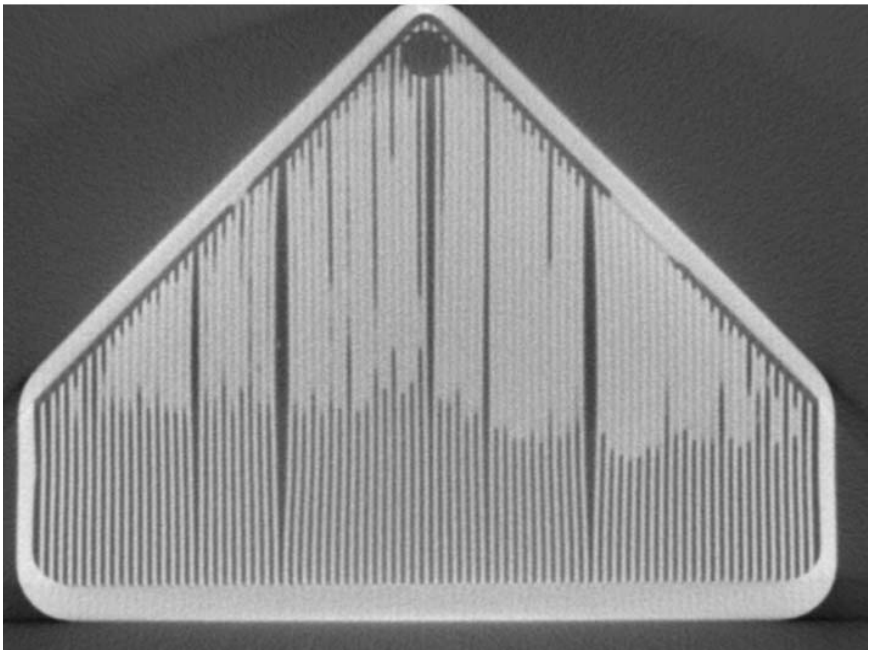

(b) Cut Plane B CT Scan

Figure 41. Solidworks vs. CT comparison of evaporator section.

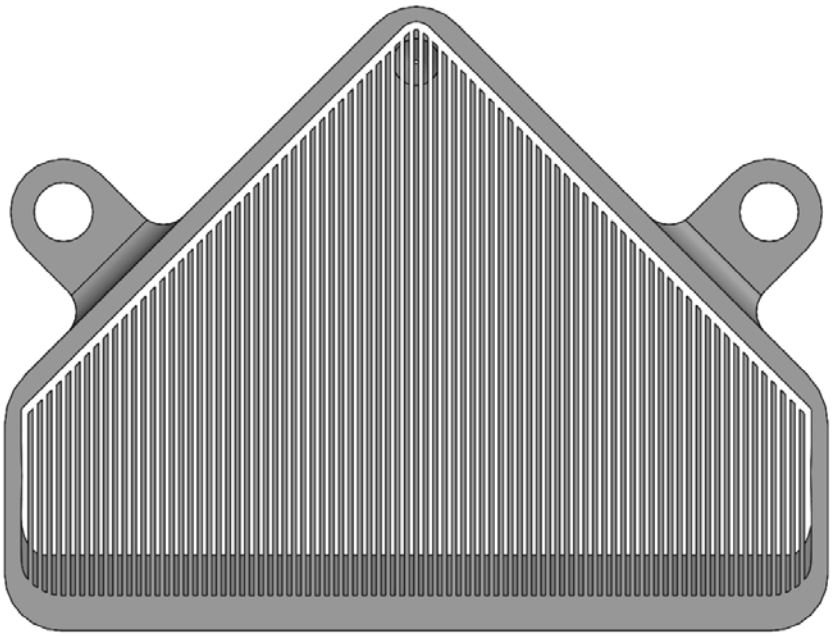

(a) Cut Plane C Expectations

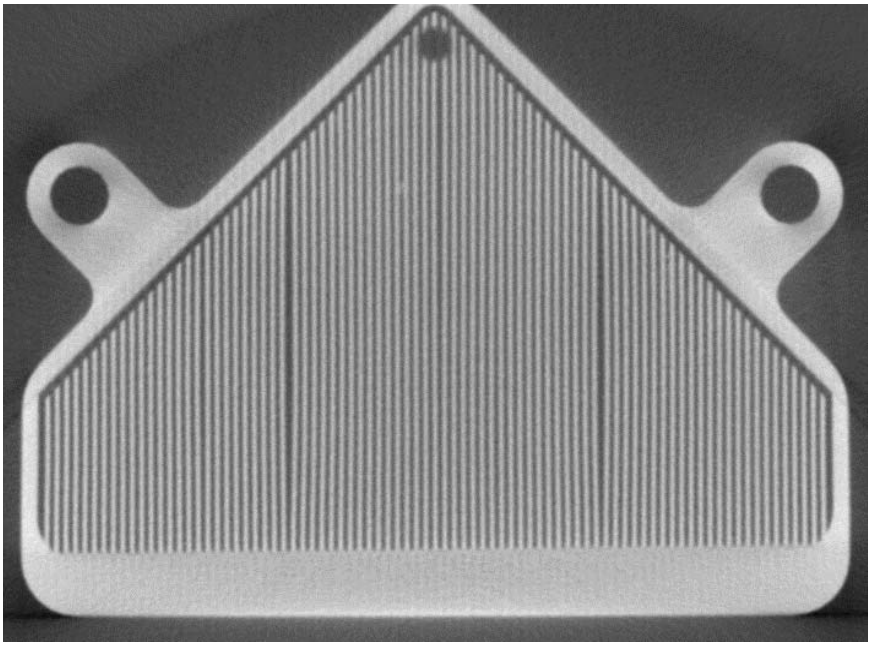

(b) Cut Plane C CT Scan

Figure 42. Solidworks vs. CT comparison of evaporator section.

These print issues by themselves do not discount the ability to additively manufacture a heat pipe but give several key aspects of the printing process that need to be taken into account when designing parts that will be additively manufactured. It is also important to note that if printing capabilities supported the manufacturing of an integrated lattice wick, distortion issues would be minimal since there would be supports in multiple directions.

At this point it is important to mention that the grooves in the evaporator were mainly included to support the top face of the evaporator section. There are numerous design techniques that could be employed to limit the aspect ratio and number of supports in this section that would alleviate the issues in printing this section. This includes printing "pillars" with 0.5 mm elements in a "tree" formation to support the top face while avoiding excessively long, thin walls.

Lastly, the trapped printing powder that can be seen in Figure 41 is also an issue with the design of this heat pipe. The access hole at the evaporator section was supposed to allow for post-manufacturing cleaning access to ensure that all the remaining powder can be extracted. However, this was not enough to ensure that the remaining powder was removed mainly due to the proximity of the evaporator grooves. This is another issue that would need to be addressed in future revisions of this design. Additionally, axial grooves allow for the best opportunity to remove excess powder. If another wick design was chosen (i.e. - porous material or lattice structure) then additional steps would need to be taken to ensure the remaining powder can be extracted or the system could deal with excess powder.

4.4 Conduction Testing

Shown below are the conduction results that were taken from one of the test articles under a conduction only setup. Figure 43 shows the transient response of

the system with an input of 11.08 W and Figure 44 shows the temperature difference between the upper and lower thermocouples for this case. Also shown in Figure 45 are the maximum temperatures at each of the thermocouple locations during this test.

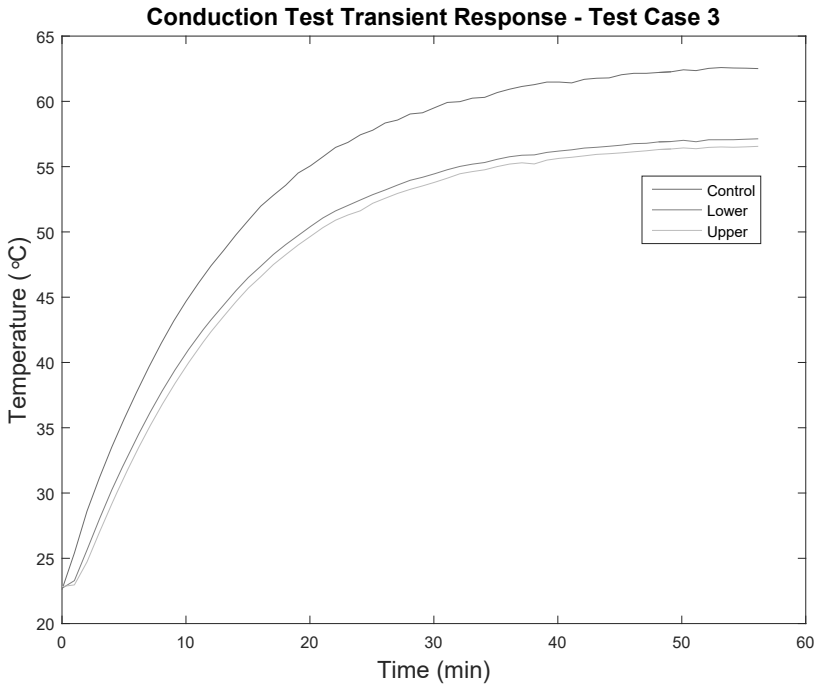

Figure 43. Transient response of conduction test case 3.

This single data set by itself does not provide much insight but when the four conduction tests are used to plot temperature difference as a function of power input, a trend can be seen (Figure 46). This trend is exactly what was expected when beginning this test and shows that the temperature difference between the thermocouples increases linearly as the input power is increased. However, the small $\triangle$T's observed in this test are worrisome because they fall well within the uncertainty of the thermocouples introducing uncertainty when discussing heat pipe functionality.

Figure 47 shows acetone's vapor pressure vs. temperature curve with the conduction results projected onto the curve to show what the maximum temperatures

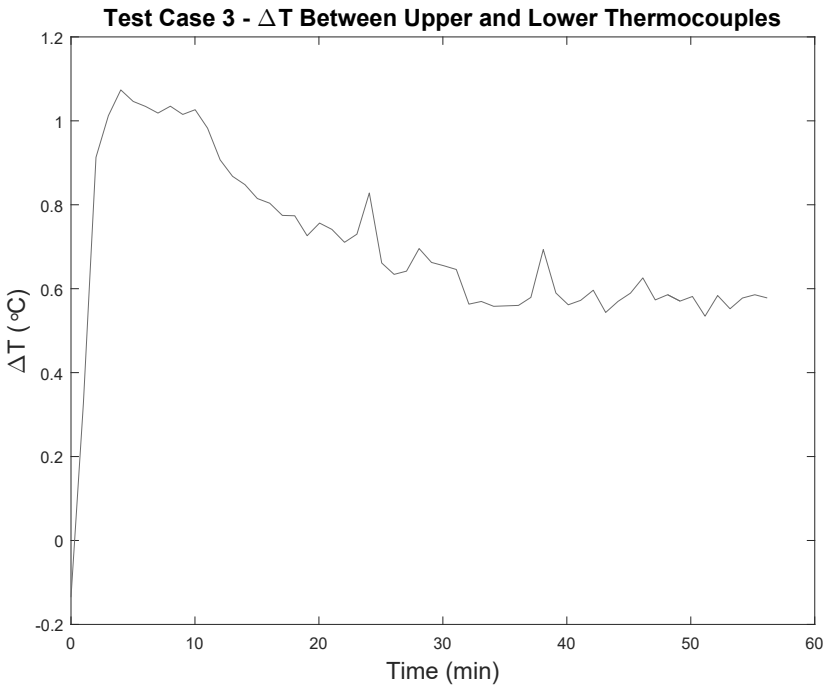

Figure 44. Temperature difference between upper and lower thermocouple results for case 3.

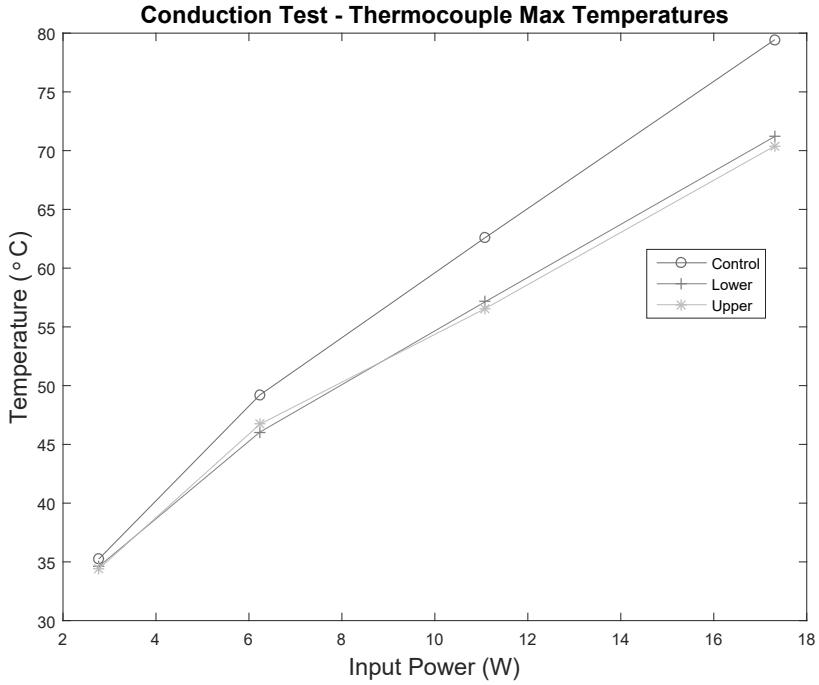

Figure 45. Maximum temperatures observed during conduction testing based on input.

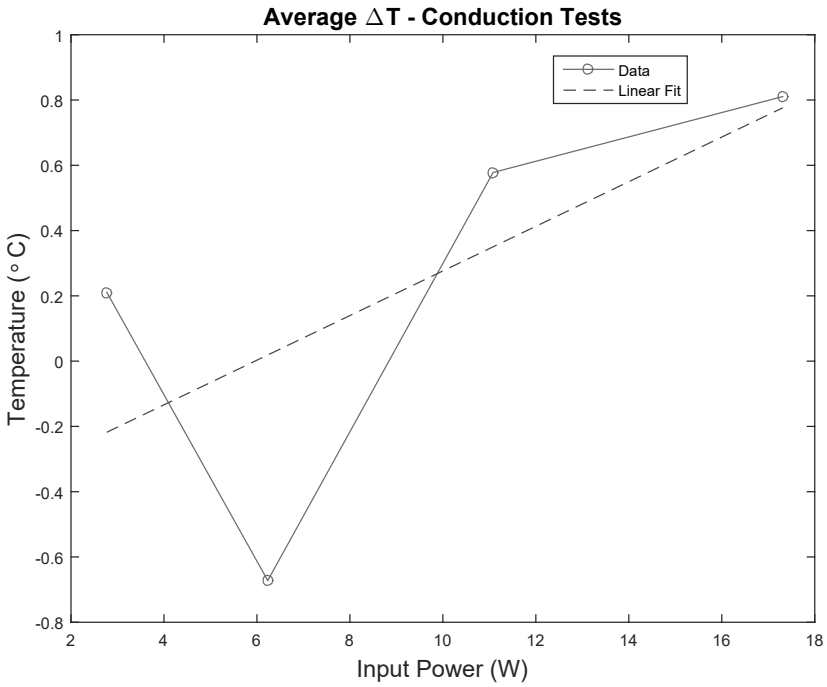

Figure 46. Average $\triangle$T between upper and lower thermocouples based on power input.

observed near the evaporator were. This give an understanding into at what power levels the transition from a nonfunctioning to functioning heat pipe should take place during the heat pipe tests.

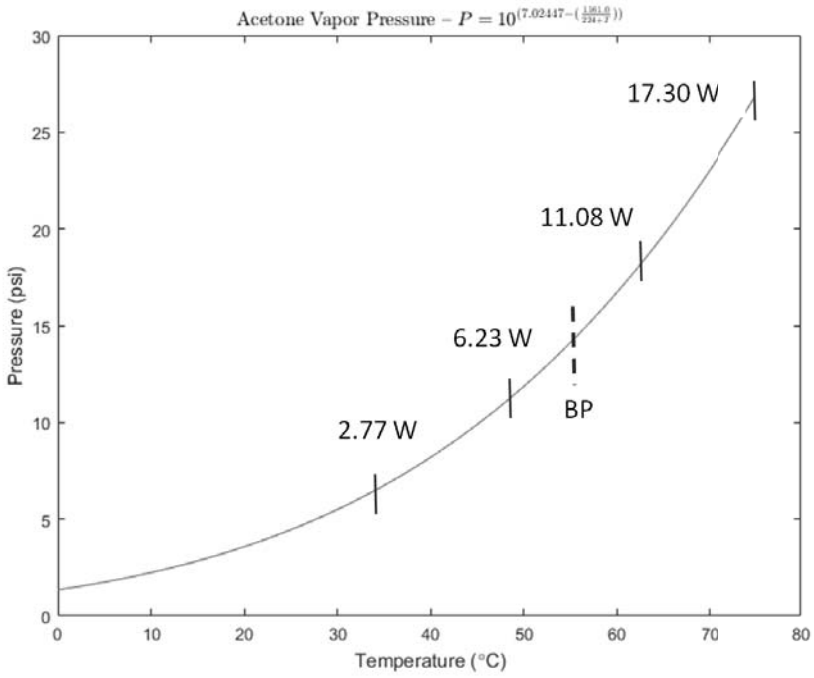

Figure 47. Conduction results mapped to acetone boiling point curve to determine when heat pipe should start functioning.

4.5 Heat Pipe Tests

4.5.1 Heat Pipe Test 1

Figures 48 & 49 show the first of ten test points conducted at various power levels to verify heat pipe functionality (Appendix 1 contains the rest of the test data). As mentioned in Chapter 3, HP1 is the conduction control test article and HP2 is the test article that should be functioning as a heat pipe once the boiling point of acetone is surpassed.

Looking at these plots, it is apparent that the heat pipe never went into a functioning state because the two test articles track each other very closely in terms of temperature. If test article 2 transitioned into a functioning heat pipe, this would have been reflected in the temperature data in the form of a lower temperature difference between the upper and lower thermocouples. Additionally, if the system was operat-

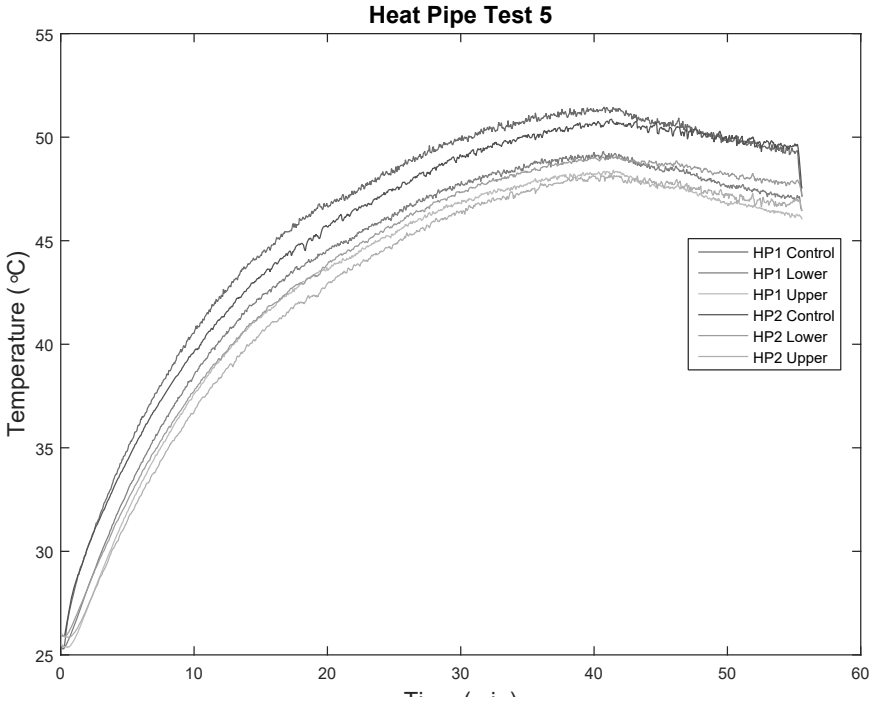

Figure 48. Test 1 transient response from 8.98 W input.

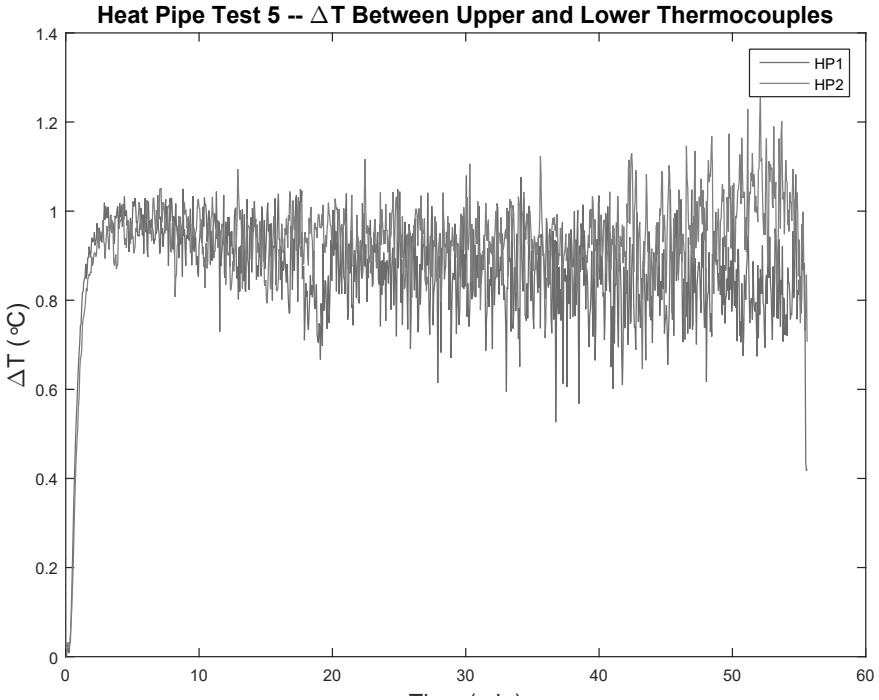

Figure 49. △T between upper and lower thermocouples at 8.98 W input.

ing as a heat pipe, there would be some power input range in which the temperature would remain fairly constant.

Although the previous figures give a good indication that the heat pipe was not functioning in any of the test cases, Figures 50 & 51 give a much clearer indication that this is the case. First, the maximum temperature observed (located at the condenser section) is plotted in Figure 51 for all test cases as a function of power input. Theoretically, if one test article was functioning as a heat pipe whereas the other was only an over designed thermal strap, there would be a diverging point near 55°C (input of 11 W) that would indicate the start of heat pipe operations, however, this is not the case.

The slope of the fitted lines also shows that a functioning heat pipe was not realized during this test. Specifically, re-arranging Equation 1, the equation becomes:

$$k_{eff} = -\frac{q_x}{A\frac{\partial T}{\partial x}} \tag{31}$$

From this, assuming the area (A) and length (∂x) are constant, the equation becomes a function of input power and temperature difference. Therefore, based on Fourier's Law, the slope of the fitted lines is the effective thermal conductivity of the tested system. If this is the case, the fact that there is an insignificant difference between the two test article slopes also indicates that a functioning heat pipe in not realized.

After the test, the working fluid was removed and it was discovered that some fluid leaked from the setup so an additional test was run to verify this wasn't the limiting factor in achieving a functioning heat pipe. These combine to clearly indicate that, at no point during this first heat pipe test, did the test article function as a heat pipe.

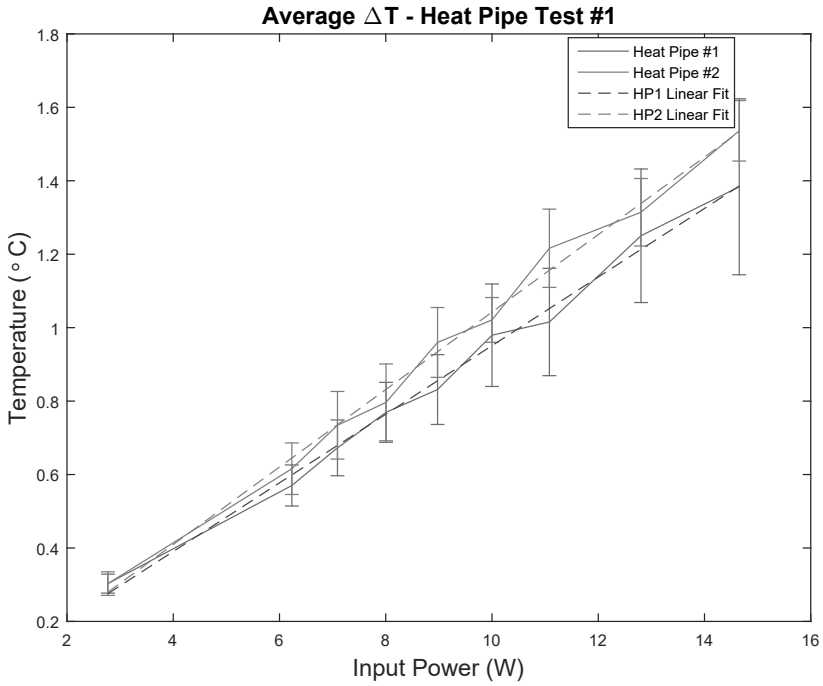

Figure 50. Average △T between upper and lower thermocouples in heat pipe tests for given power inputs.

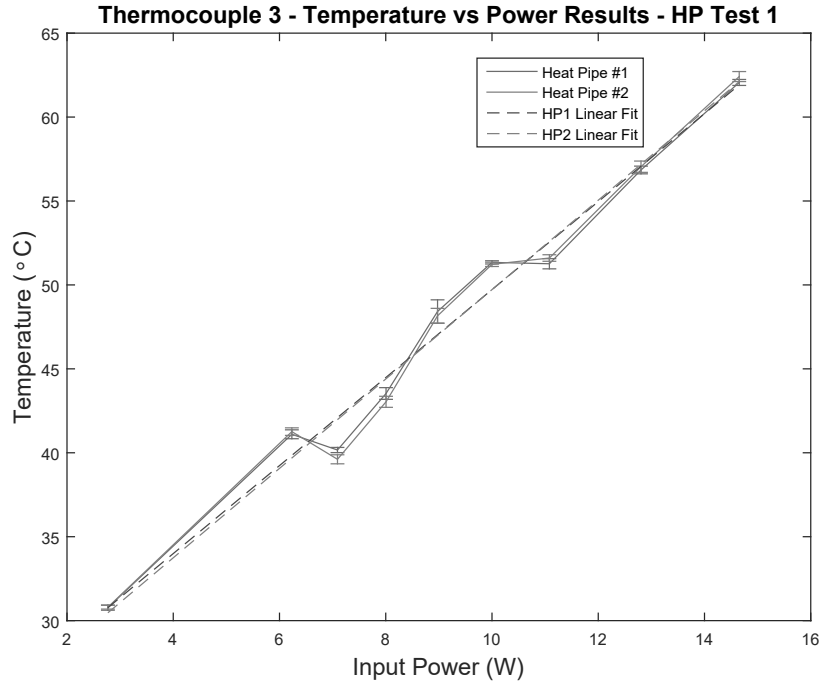

Figure 51. Average thermocouple 3 steady state temperature during heat pipe tests.

4.5.2 Heat Pipe Test 2

After the first heat pipe test failed to produce the desired results, the heat pipe was purged and re-filled since it seemed like some working fluid was lost during the first filling process. Care was taken to ensure that the correct amount of working fluid was added to the system and the test was re-run. In addition, data acquisition for this test was condensed to one single run at various power levels.

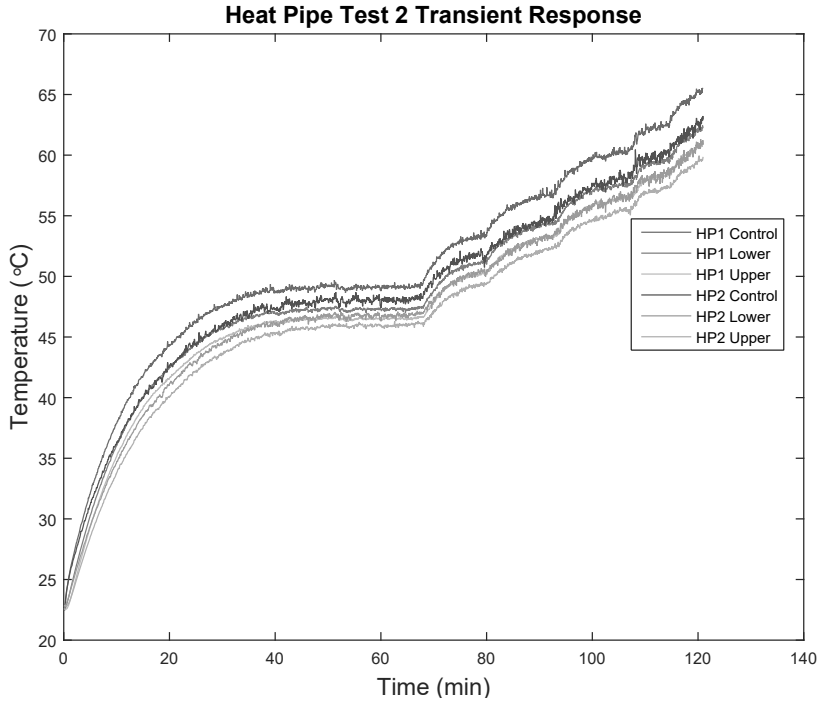

Figure 52. Transient response of test articles during heat pipe test 2.

Figure 52 shows the transient response for the second heat pipe test and, again, not many conclusions can be reached from this data alone. Figure 54 shows the temperature difference between the upper and lower thermocouples as a function of input power which gives much better insight into the success of this test.

Comparing results form this test (Figure 54) and the previous one (Figure 50) it is clear that there was a noticeable difference between the test data once temperatures reached levels near acetone's boiling point. This can be seen in the results as the

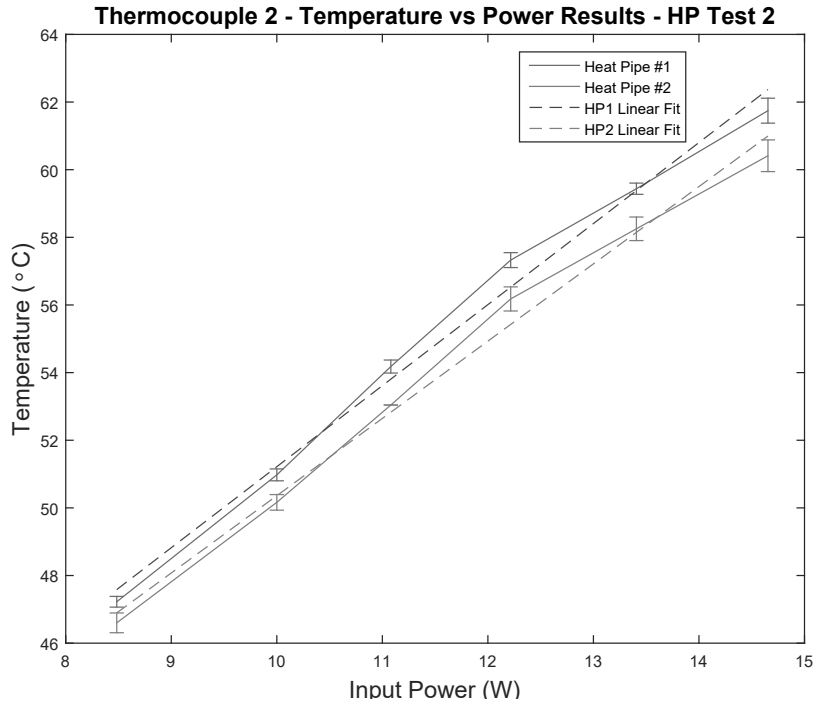

Figure 53. Average thermocouple 2 steady state temperature during heat pipe test 2.

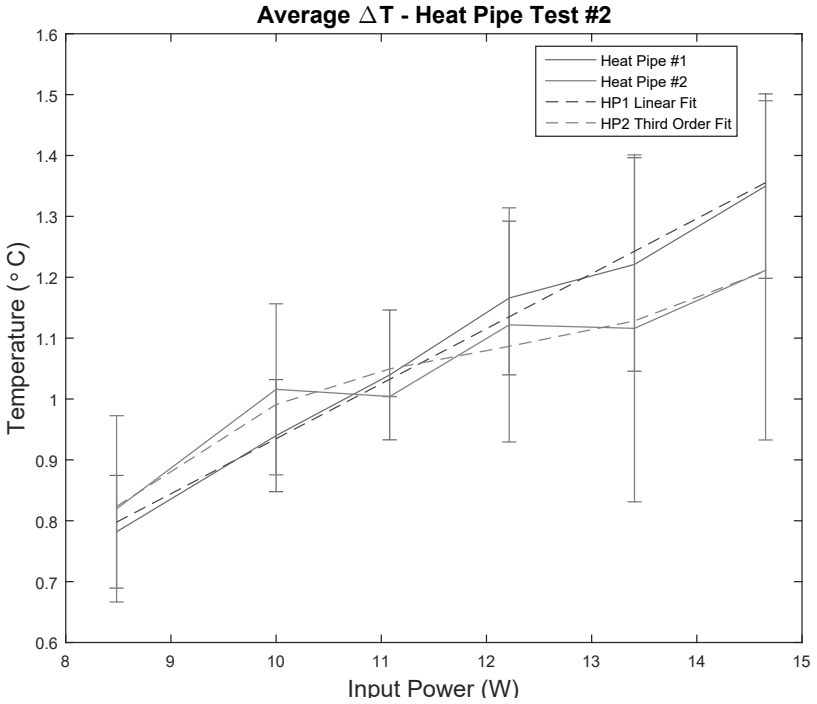

Figure 54. Average △T between upper and lower thermocouples in heat pipe tests for given power inputs.

"leveling" out that is observed in test article 2. The start of this trend change occurs at an input of 11.08 W which reached temperatures near 55 °C. This trend continues for the next two tests as well before returning to a linear trend between $\triangle$T and power input.

Overall, from the raw temperature plots, the data for test article 2 trends like a heat pipe would (i.e. - lower temperature gradients) between input powers of 11 & and 13.5 W, however, with the significant uncertainty associated with the measurements no definitive statements can be made. In addition, looking at Equation 31, the effective thermal conductivity for the intended heat pipe seems to increase between these input powers. However, it is important to note that a linear trendline could be fit within the error bars to the data based on the the error estimates for the data. This would then lead to effective thermal conductivities indicate a heat pipe was not functioning in this test. These combined uncertainties lead to the conclusion that a functioning heat pipe was not realized during this test.

4.5.3 Heat Pipe Test 3

The last heat pipe test that was run was done so in an increased convective heat dissipation environment. That is, a fan circulated air over the test articles as compared to a natural convection environment that the first two tests were tested in.

Figure 55 shows the transient response for this test and the effect of adding an increased convective heat dissipation environment is immediately evident. By adding a forced convective boundary condition on the system, a significant increase in convective heat transfer drives much larger temperature differences in the system. Despite this, Figure 57 depicts results extremely similar to the first test; the temperature difference between the upper and lower thermocouples increases linearly with the input and there is not an indication of a functioning heat pipe. Also, as in heat pipe test

1, the effective thermal conductivities obtained from this test support the fact that a functioning heat pipe was not realized during this test since the slopes observed in /freffig:ctdel are almost identical.

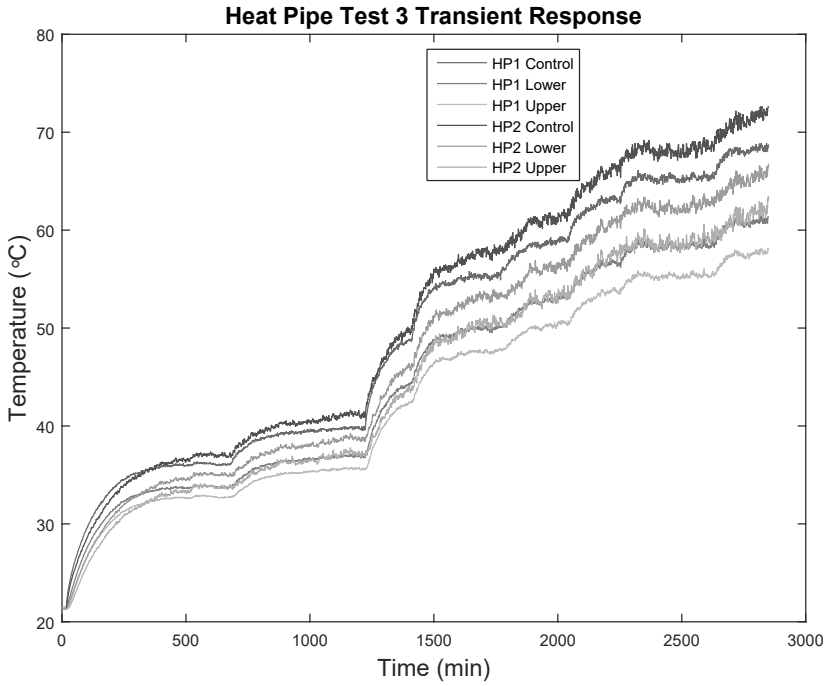

Figure 55. Transient response of test articles during heat pipe test 3.

4.5.4 Summary

From the three tests run there is no indication in the data that the heat pipe was functioning, not even as a thermosyphon. This fact, combined with the relative magnitude of error in these measurements, forces the conclusion that a functioning heat pipe was not realized during these experiments.

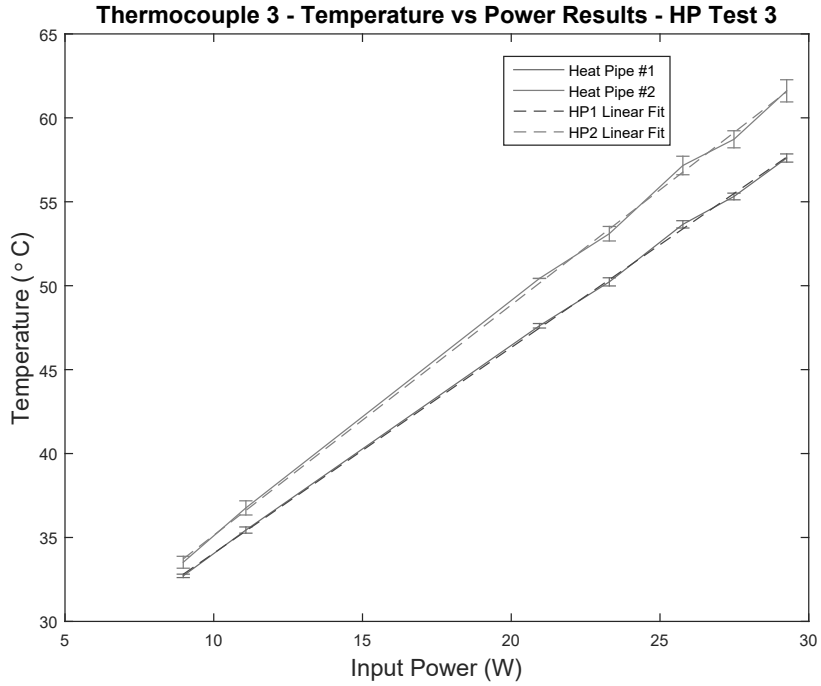

Figure 56. Average thermocouple 3 steady state temperature during heat pipe test 3.

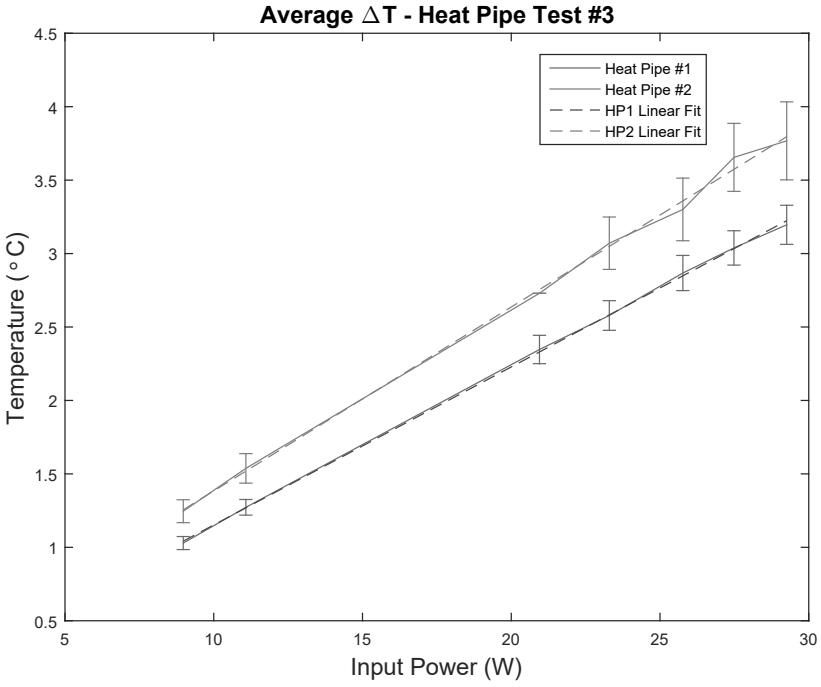

Figure 57. Average △T between upper and lower thermocouples in heat pipe tests for given power inputs.

4.6 Structural Testing

Finite element analysis and laser vibrometer testing results are given in Table 13. Actual vibe testing was not performed due to scheduling conflicts with the vibration table. Comparing the results below, significant differences between the analytical and experimental results are observed. Looking only at the first mode and assuming the laser vibrometer is detecting first bending as the first mode, there is a 500% difference between the expected and observed result.

The discrepancy between the detection of the first bending mode points to an issue in modeling approach. This could be the result of several differences between the model and test setup. First, the boundary conditions in the FE model could be inducing added stiffness from over constraining the base of the heat pipe. In the model, the entire bottom face of the part was constrained. However, in reality, the base is free to lose contact with the table since the bolt locations are the only physical constraints. Additionally, the laser vibrometer could be picking up a mode at 243 Hz that is not present in the FE model. This could be the result of environmental noise or rigid body modes, albeit unlikely. With the results given, further FE modeling revisions would need to be carried out to ensure the model is accurately predicting results that could be used in the design of future heat pipe models.

	Frequency (Hz)		
Mode	**FEA**	**Laser Vibrometer**	**Vibe Test**
1	1264.9	243	N/A
2	3291.3	1690	N/A
3	4533.3	2100	N/A

Table 13. Results from FE model and laser vibrometer test data.

5. Conclusions

5.1 Research Conclusions

Despite the obvious shortfalls in observing a functioning heat pipe, several crucial aspects of additively manufacturing an integrated heat pipe with structural functionality were determined from the work done for this research.

Looking specifically at wick designs, there are three prominent conclusions that can be made. First, with the current state of additive manufacturing techniques, manufacturing a porous metal wick that contains continuous channels with the required porosity for wicking ability is not feasible. That is, with the methods presented and decided upon in this research, the porosity levels achieved are $3\times$ lower than the minimum porosities used in functioning heat pipes with porous wicks. Second, a structured lattice or screen wick cannot be manufactured with the current state of additive manufacturing due to minimum wall thickness and tolerance limitations. If these limitations are expanded with decreases in minimum wall thicknesses and tolerance specifications, this option offers a robust and capable wick design. Specifically, if additive manufacturing allowed for mesh size 100 (openings/in^2) to be applied to a lattice structure, this would result in a wick that has lower frictional pressure drops than a porous wick while having a much larger capillary potential than a grooved design. Lastly, current additive manufacturing techniques allow for an axial grooved wick design to be integrated into a heat pipe. However, the grooves cannot be printed on the scale needed to generate enough capillary head to overcome the effects of gravity. Despite this, an axial grooved wick design can theoretically operate as a heat pipe in a terrestrial environment in certain orientations, as well as in a microgravity environment, or as a thermosyphon in a terrestrial application, although no wick is required to operate as a thermosyphon.

With the understanding of applicable wick designs, the ability to additively manufacture a functioning heat pipe was also investigated in this research. Despite running three heat pipe tests, the actual demonstration of a functioning heat pipe did not occur. Two of the three cases definitively did not operate in a manner consistent with heat pipe functionality. The second heat pipe test could be argued as a success but the results have significant uncertainty in them. These facts compound to force the conclusion that this research was not able to demonstrate a functioning additively manufactured heat pipe.

Despite the undesirable result obtained during testing, the ability to successfully additively manufacture a functioning heat pipe cannot be ruled out due to the limitations imposed on this research. These limitations included using nontraditional geometry to mimic Figure 2, test sections that could not exceed 8 in, and additive manufacturing limitations that forced an axial groove wick design that is suitable for space applications. If these limitations were lifted, several key design aspects could be changed to increase the probability of a successful heat pipe test.

Lastly, there are several issues when discussing the ability to create an integrated thermal management/structural component. The first of these is the ability to model the heat pipe design in a FE environment. A functioning heat pipe design will have wick features that are several orders of magnitude less than the case size. This poses the problem of modeling the wick which will drive a very dense mesh in the wick sections causing very large FE models that could be difficult to solve.

5.2 Impacts of Research

Although a functioning heat pipe was not demonstrated for this research, there are indications that one could be produced via additive manufacturing if print resolution increases and it would be fully functional despite the design limitations imposed by

additive manufacturing. Even with an axial groove wick design, a heat pipe provides significant increases in thermal conductivity over traditional thermal strap designs. Utilizing this technology in a spacecraft system would then allow for an increase in operating temperatures of the component being cooled by the heat pipe. For radio systems, the ability to operate at a higher temperatures correlate to an increase in available power resulting in a much more capable system in terms of increased range and/or data rate.

Utilizing the ability to integrate the manufactured heat pipe with structural members further allows for an increase in spacecraft capability due to weight savings from this dual purpose component. This ability allows for an increase in capability due to extra design space or system cost savings. The results provided in this research lay the groundwork and provide useful lessons learned for future revisions of additively manufacturing a heat pipe.

5.3 Recommendations for Future Research

Throughout the process of researching, testing, and defending this research, there were several areas that could be improved in future iterations of this problem.

After discussing the approach used in this research with a subject matter expert, it was determined that the first area that can be significantly improved is the overall test setup. The first major issue was the overall heat pipe design used in this research. A giant step was taken from concept to manufactured test article in using an "L" shaped design rather than a simple straight tube section. This design choice was made early in the planning for this research and severely impacted the ability to predict a solution and properly perform functionality testing. As discussed, this research used axial grooves that could not provide enough capillary head to work against gravity. This issue could have been resolved if a horizontal design was used

but, based on the "L" shape design, a horizontal configuration could not have been used since the condenser had to be above the evaporator due to the wick limitations. In addition, with an enlarged evaporator section, heat needed to be applied to the bottom of the design since that is where the working fluid will pool. Future revisions of this research should also increase the heat pipe length. During testing, very small temperature differences were observed across the effective length of the heat pipe. This led to results that were inconclusive. If a longer effective heat pipe length was used, the temperature differences observed would be significantly larger. Along the same lines, the evaporator and adiabatic sections of the heat pipe should be insulated and the condenser should not be insulated. This will reduce any heat losses that occur between the input and radiator driving lower uncertainty. A better approximation of heat input into the system could also be determined if insulation prevented unwanted losses. In addition, the heater thermocouple should be placed directly between the heater and heat pipe to get a more accurate temperature input. All of the modifications outlined above are aimed at reducing the uncertainties that were present in this research to support the ability to determine effective thermal conductivity. In the current test, the heat flux was not well known leading to issues in calculating an actual value versus using approximations from the power input vs. temperature plots. In addition, thermal vacuum testing could be performed to completely remove convective heat dissipation from the system. With the mentioned improvements, the effective thermal conductivity could be determined explicitly since the uncertainties that hindered this research would be removed.

In addition to the above modifications to the test setup, the filling technique used to fill the heat pipe with its working fluid needs to be changed. In this research it was decided that purging the system with nitrogen would be an acceptable option but Peterson offers that care should be taken to ensure that the only molecules present in

the heat pipe internals should be the working fluid [2]. Further testing of additively manufactured heat pipes should follow the steps outlined in the text to ensure no additional losses are impeding the ability of the heat pipe to function.

Another area for improvement is the additively manufactured wick design and analysis procedure. For the lattice design, research should continue in the lattice wick design process. For spacecraft applications, this design offers an ideal trade-off between capillary head and permeability; however, in order for this design to feasible, print resolution needs to see a 3x increase. For the axial grooved wick design, research should continue and be used for demonstrating the ability of additive manufacturing to create an integrated heat pipe wick design due to the ease of integration of this wick type and functionality in a spacecraft operating environment. Lastly, for the porous metal wick design, further research could be conducted in choosing appropriate spacing and layer thicknesses combined with a specific beam pattern to create a porous wick. The results provided from this research offer a good starting point but further refinement needs to be made in order to ensure pore sizes suitable for capillary action and continuous channels throughout the part are manufactured. Lastly, common to all three wick designs, improvements should be made to the wicking test of each article. Additive manufacturing introduces imperfections that could affect the wicking ability of the wick and this additional loss needs to be characterized. In addition, only testing the wicks can provide information on how small features can be made without affecting the wick design in a structural sense.

A thermal modeling tool that could predict heat pipe performance would be a very good investment for future work in the area of additively manufactured heat pipes. With a tool that could accurately predict the behavior of a heat pipe design, customization could occur allowing for the best design in terms of heat pipe performance while also ensuring the structural functions of the part are preserved.

Additionally, since the heat pipe designs are additively manufactured, very intricate and uncommon designs could be created necessitating a robust tool to ensure that the design functions properly.

Another area of the current design that should be redesigned is the support structure used in the evaporator section. As was discovered by NDI, there were significant warping issues along the length of the extended fins due to their high length to width aspect ratio. This design was an easy solution to ensure that the evaporator top face was supported during printing. From the print issues observed, a better design to support the upper evaporator face while limiting disruption in the evaporator section can be achieved.

The last recommendation is a longer term concept that should be incorporated after the above recommendations are implemented and the researcher is confident in being able to additively manufacture a functioning heat pipe. Since the ultimate goal of this research is to investigate the feasibility of incorporating a 3D printed heat pipe into a spacecraft structure, the actual integration should be carried out and testing should be completed for a 1U CubeSat design.

5.4 Conclusion

Additively manufacturing a functioning heat pipe that can be used as a spacecraft thermal management solution in addition to providing structural advantages offers significant opportunities in spacecraft design. By integrating these components, significant advantages in the operating envelope can be achieved resulting in a more capable system.

Appendix A. First Appendix - Conduction Test Results

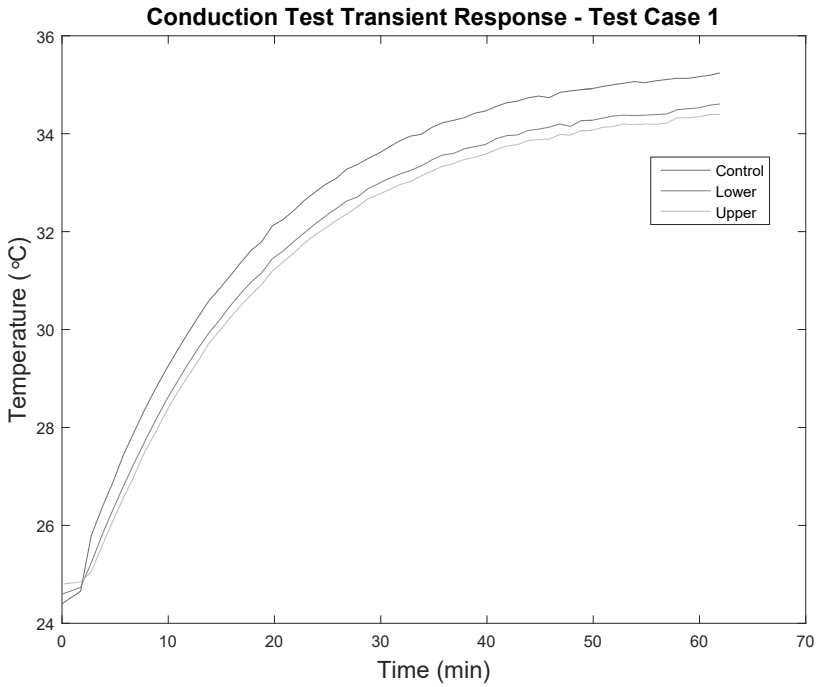

Figure 58. Transient response of conduction test case 1.

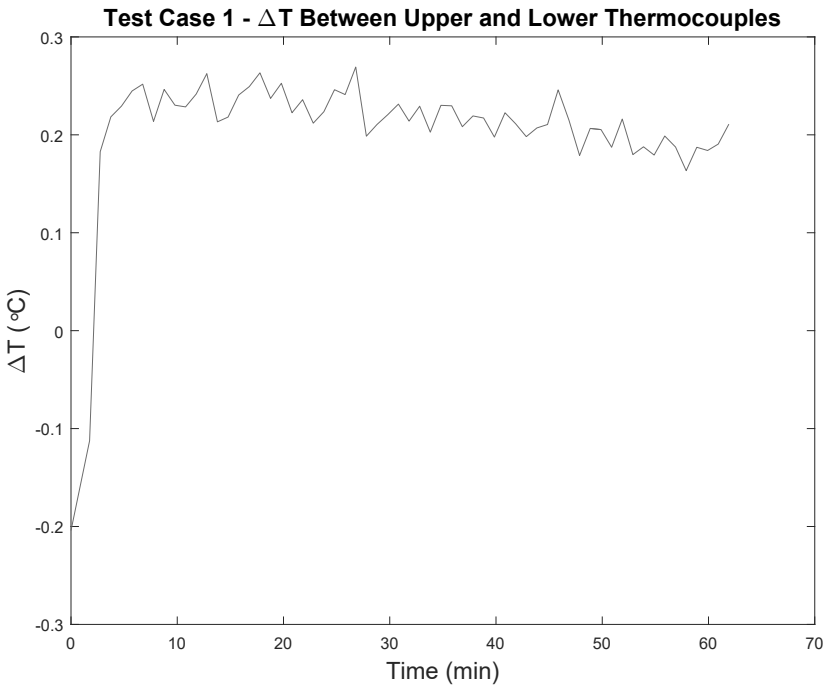

Figure 59. Temperature difference between upper and lower thermocouple results for case 1.

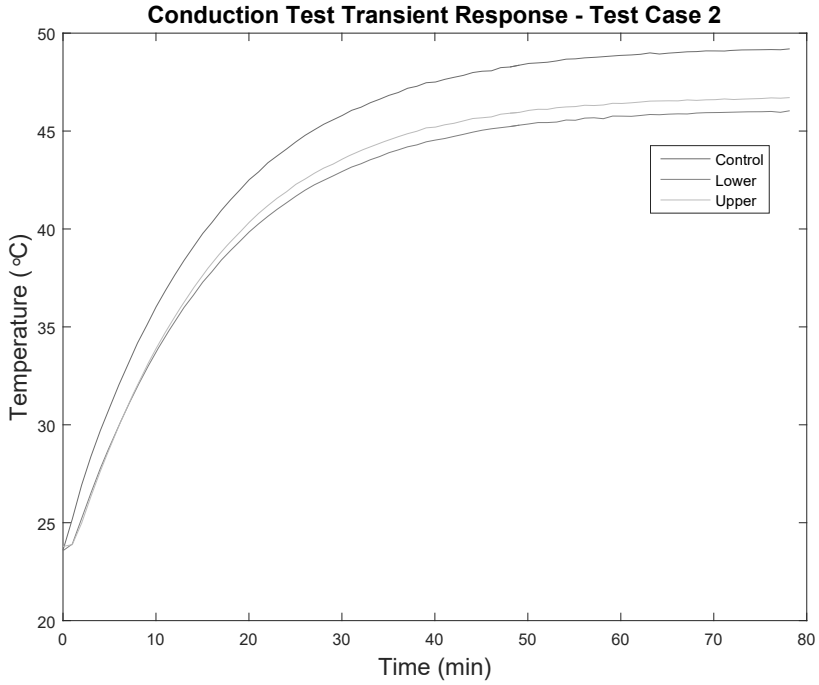

Figure 60. Transient response of conduction test case 2.

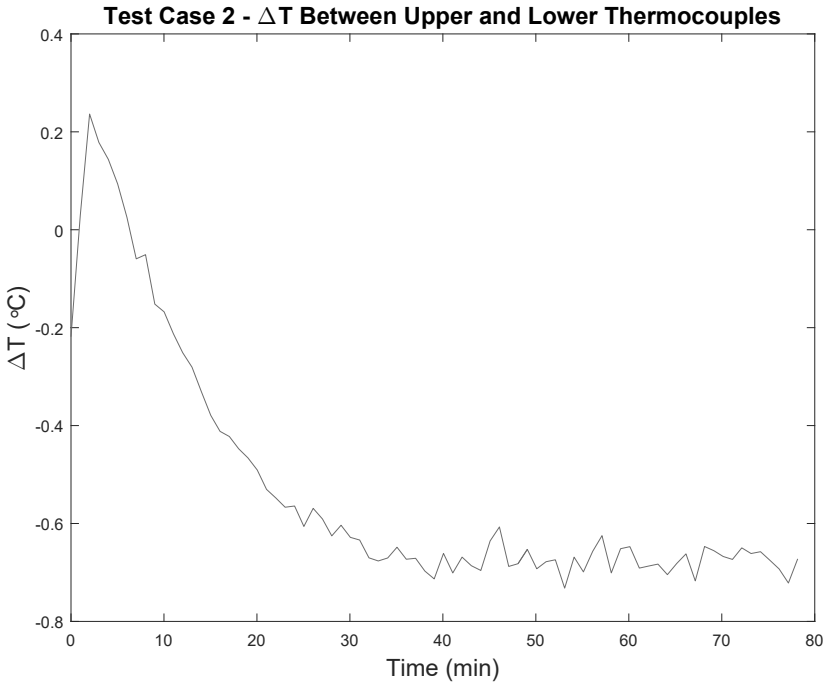

Figure 61. Temperature difference between upper and lower thermocouple results for case 2.

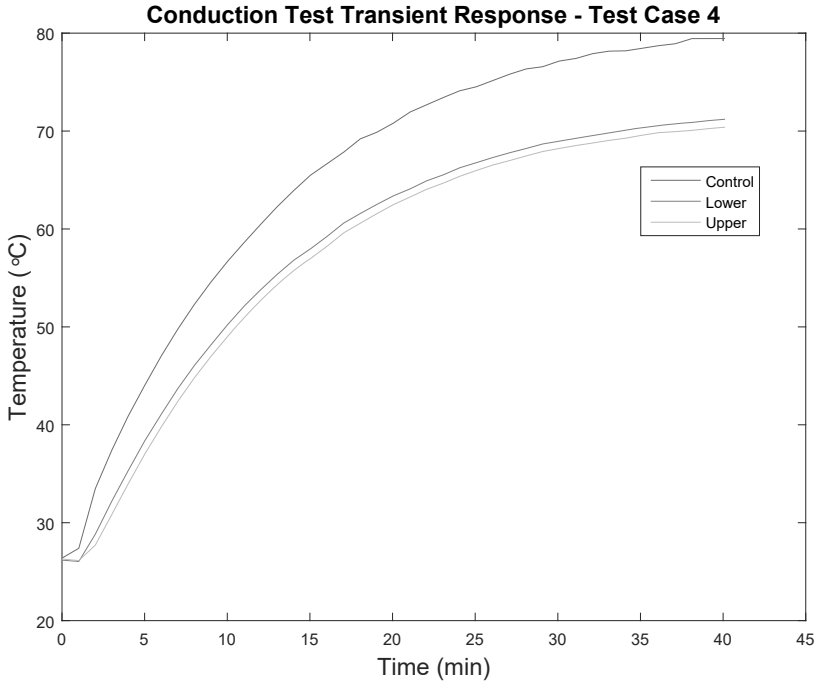

Figure 62. Transient response of conduction test case 4.

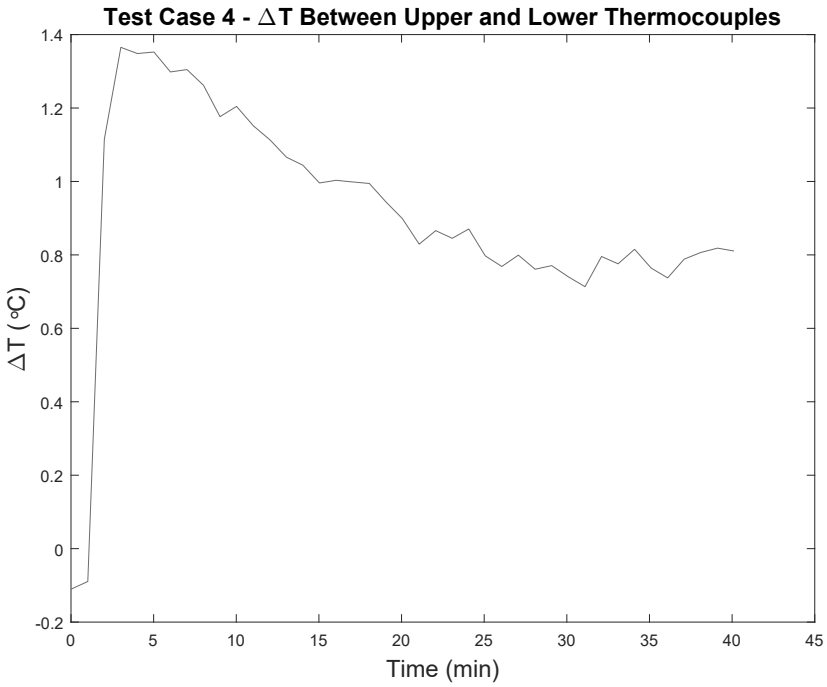

Figure 63. Temperature difference between upper and lower thermocouple results for case 4.

Appendix B. Second Appendix - Heat Pipe Test Results

B.1 Heat Pipe Test Case 1 – Additional Results

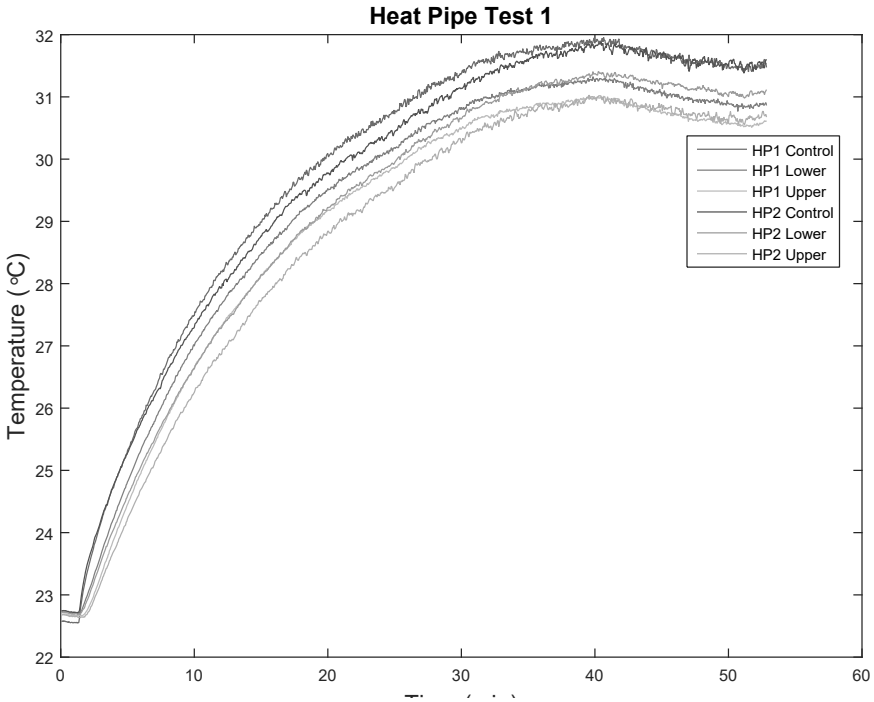

Figure 64. Test 1 transient response from 2.77 W input.

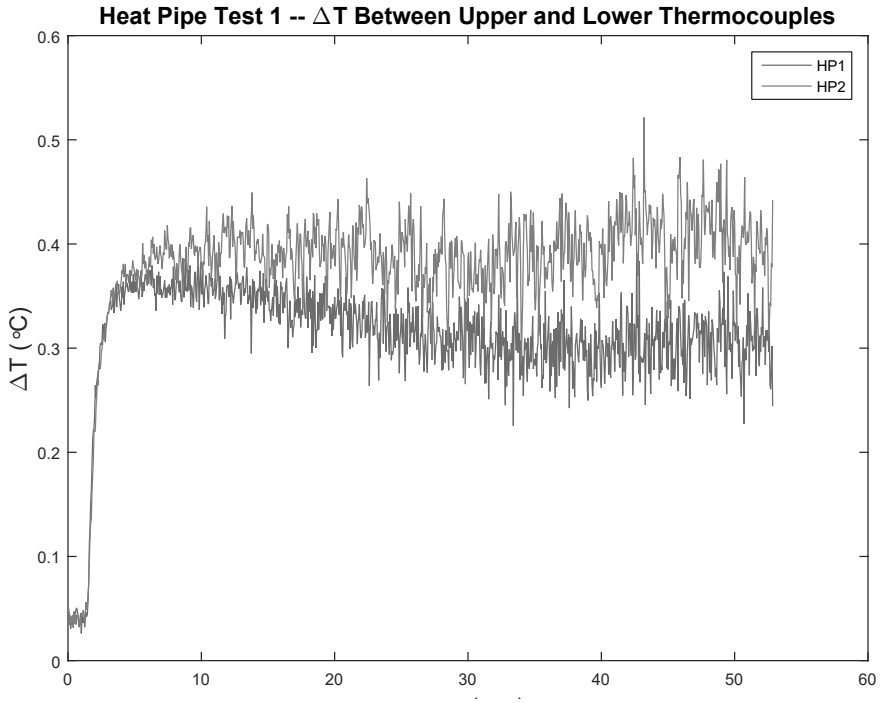

Figure 65. △T between upper and lower thermocouples at 2.77 W input.

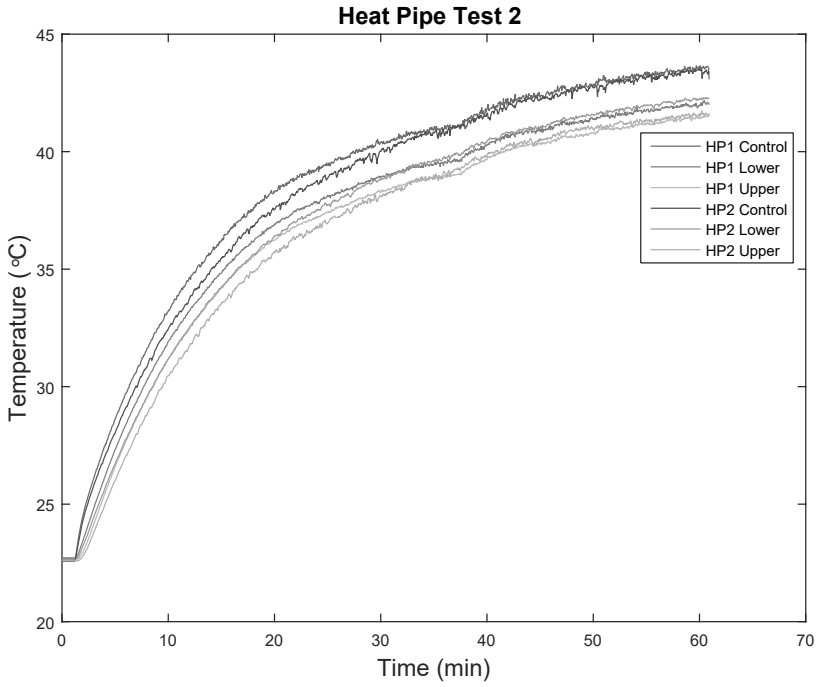

Figure 66. Test 1 transient response from 6.23 W input.

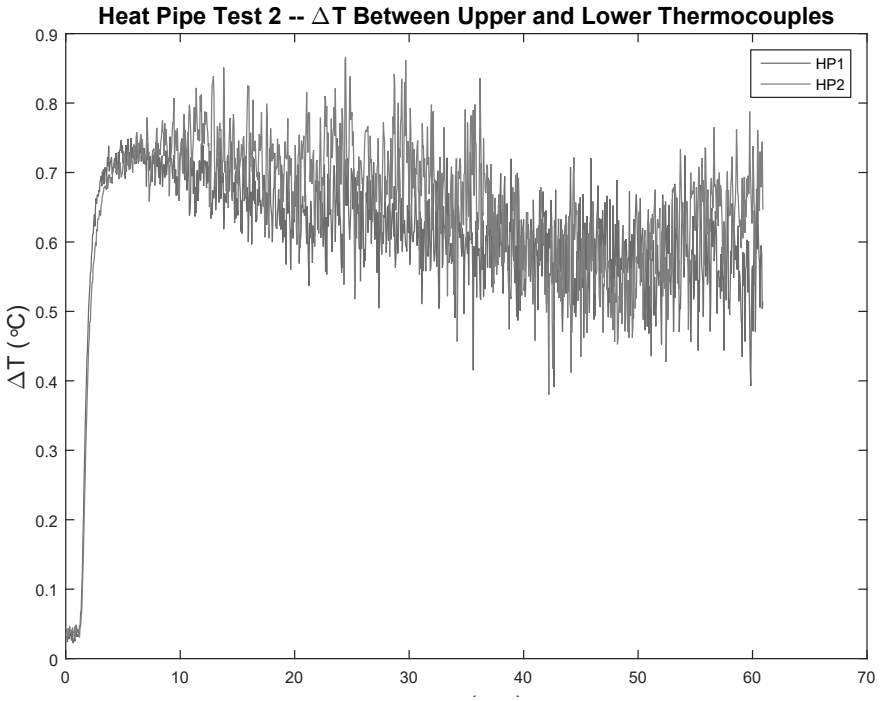

Figure 67. △T between upper and lower thermocouples at 6.23 W input.

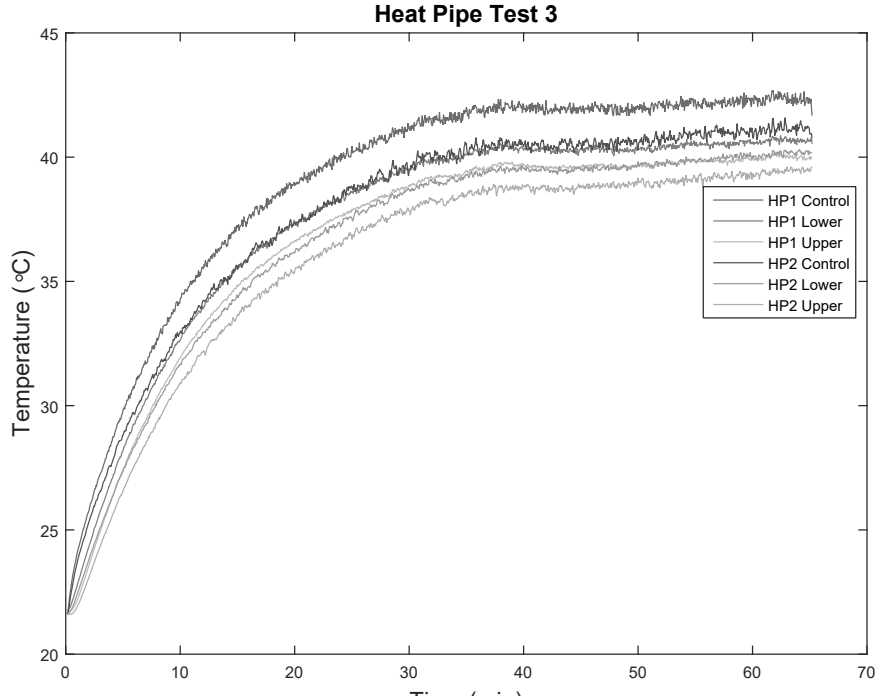

Figure 68. Test 1 transient response from 7.09 W input.

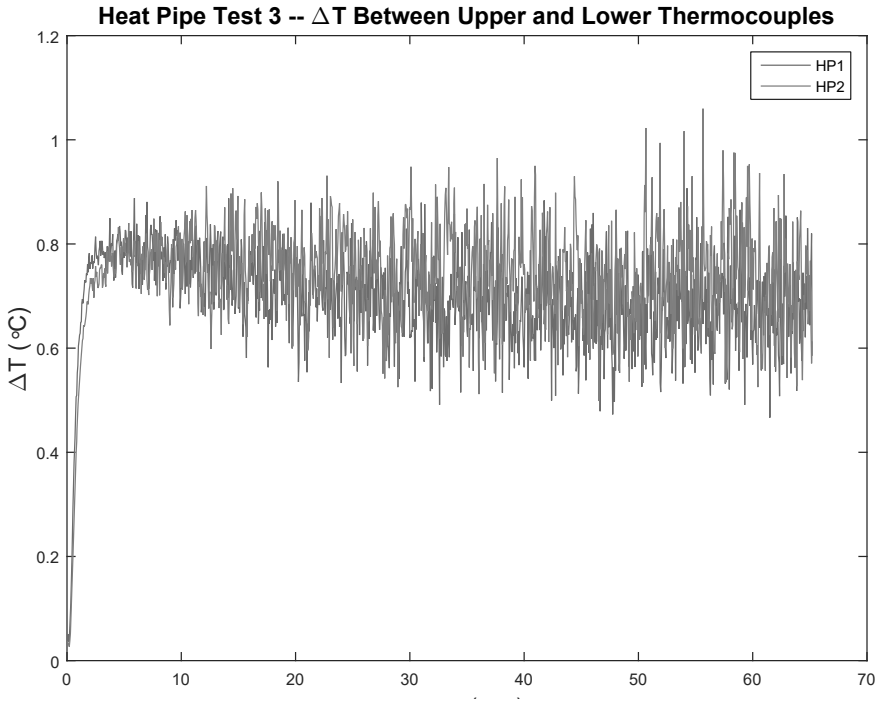

Figure 69. △T between upper and lower thermocouples at 7.09 W input.

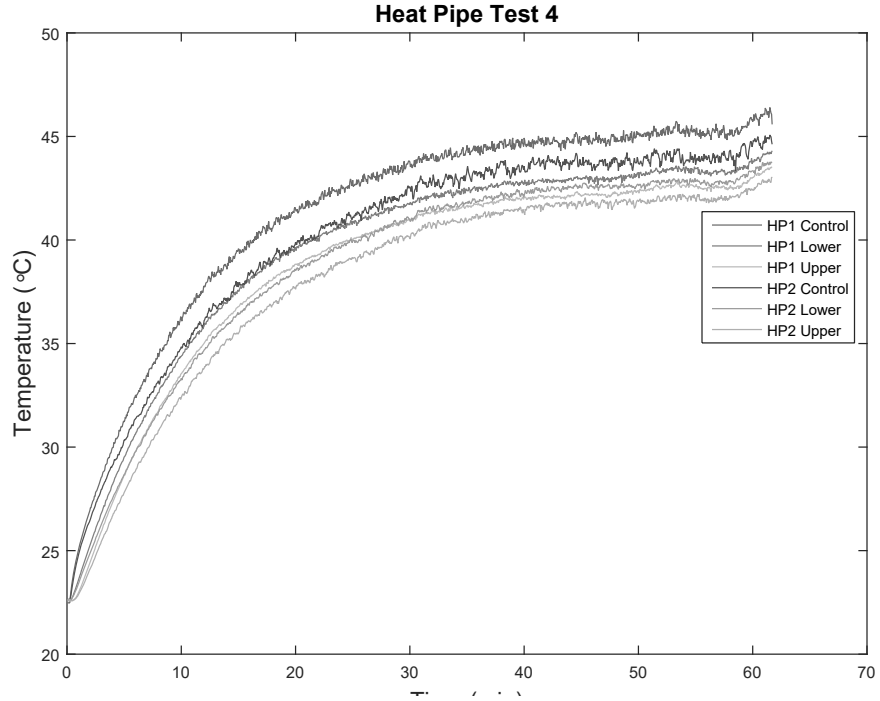

Figure 70. Test 1 transient response from 8.01 W input.

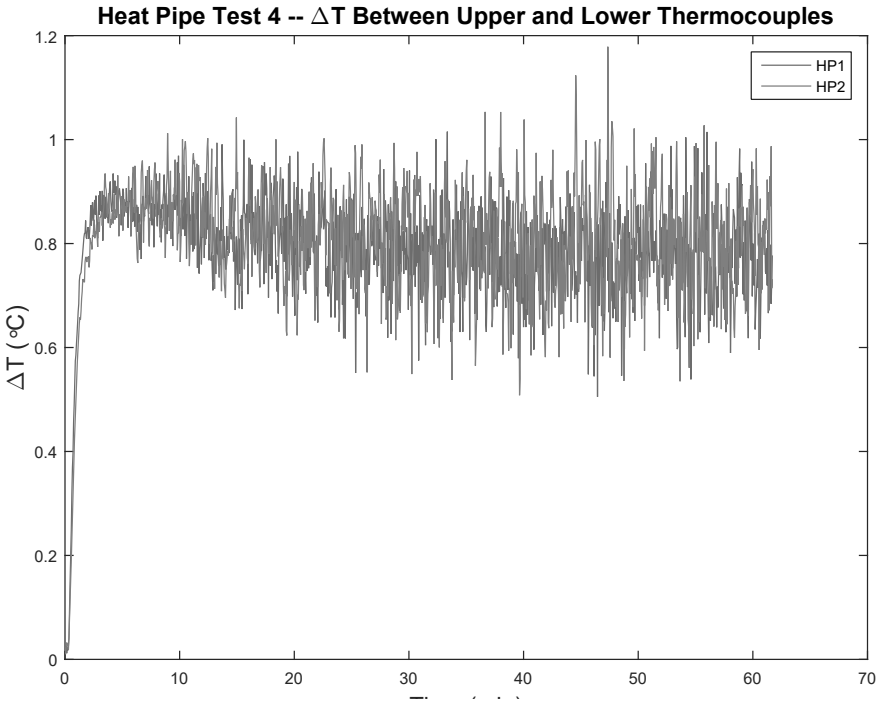

Figure 71. △T between upper and lower thermocouples at 8.01 W input.

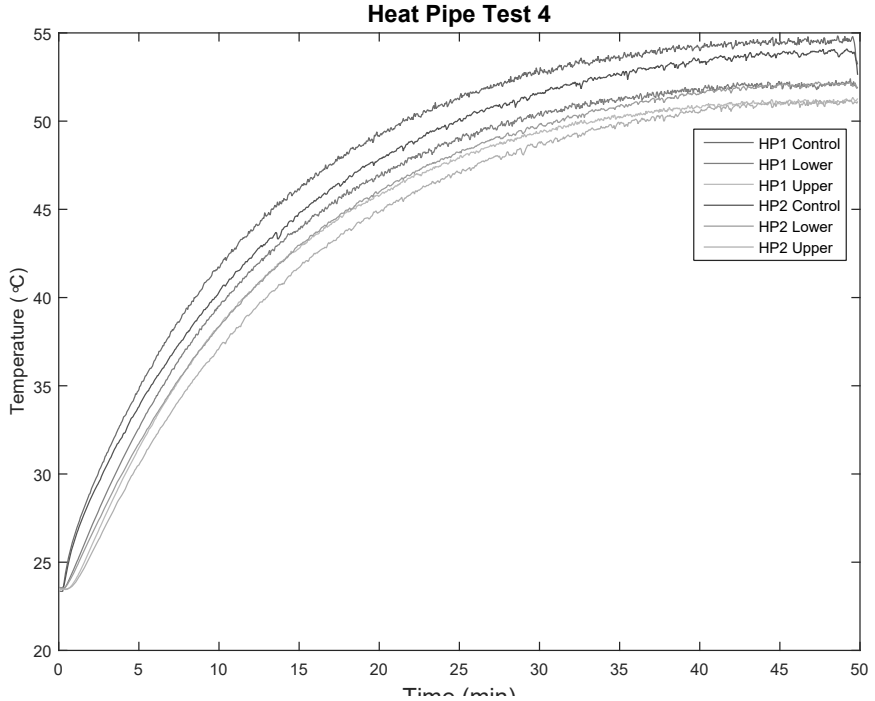

Figure 72. Test 1 transient response from 10.00 W input.

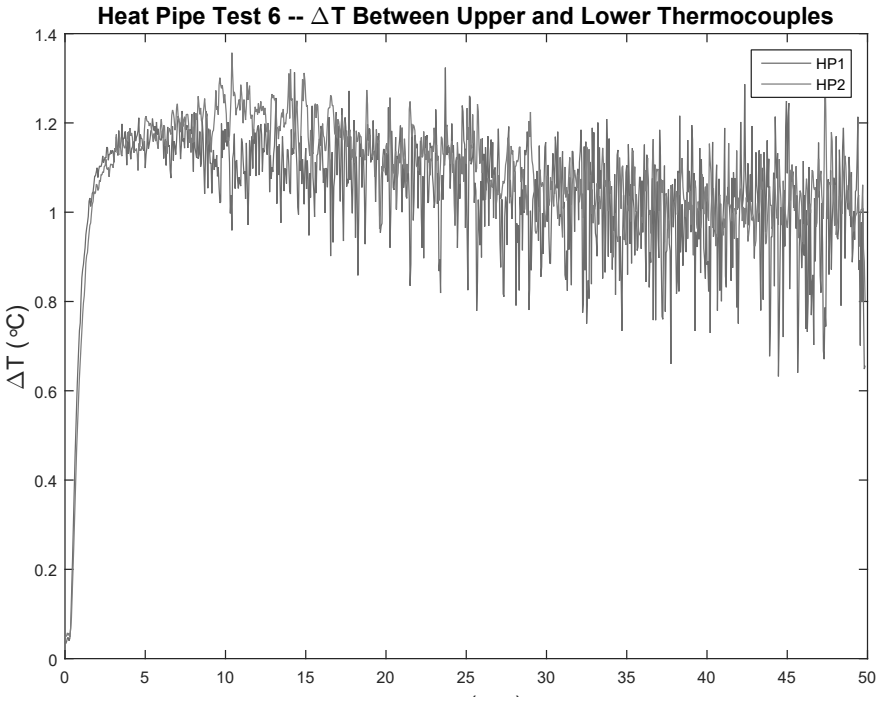

Figure 73. △T between upper and lower thermocouples at 10.00 W input.

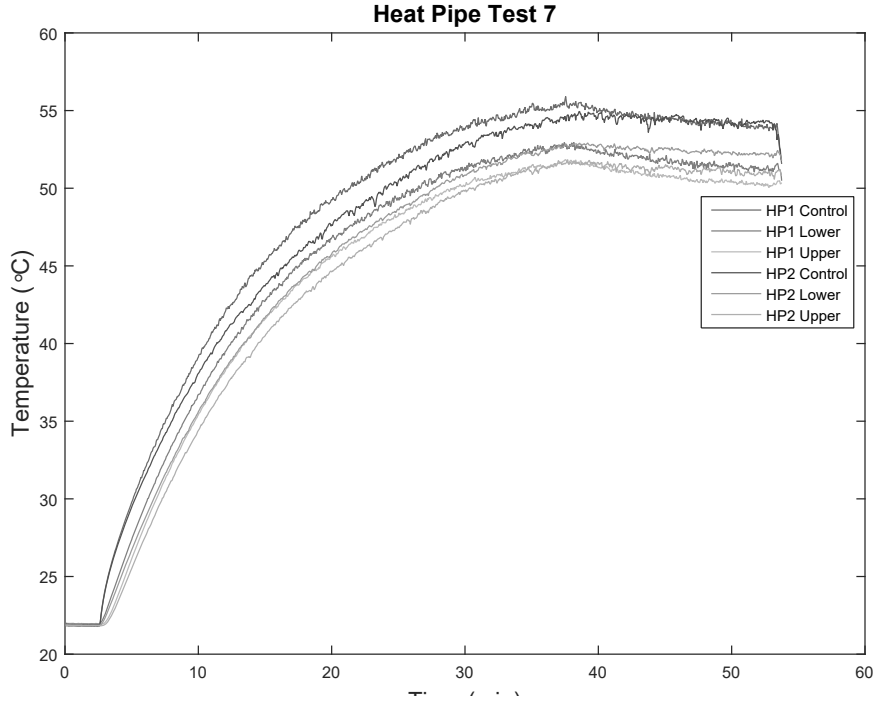

Figure 74. Test 1 transient response from 11.08 W input.

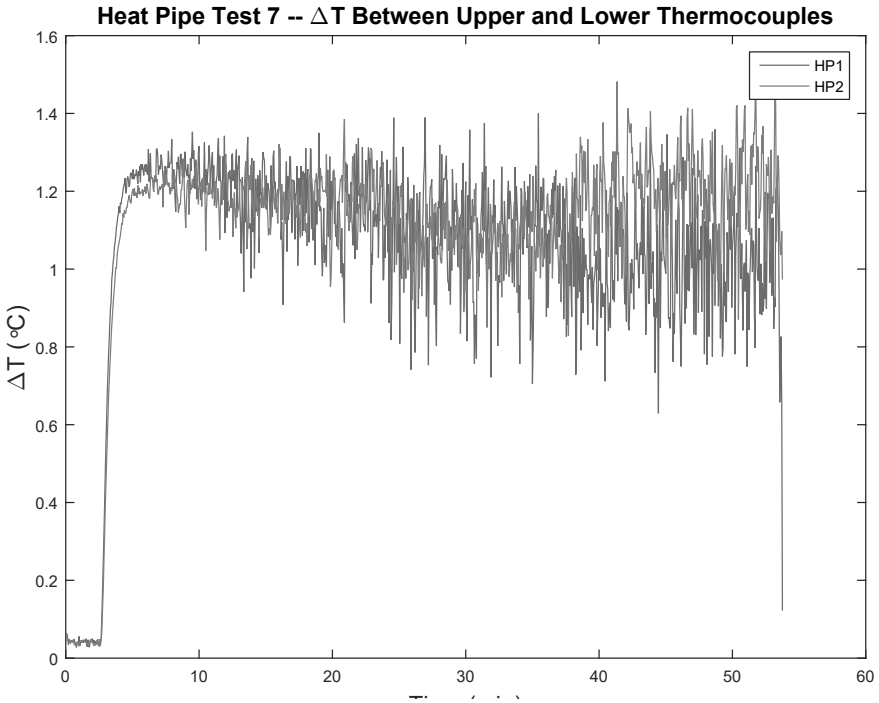

Figure 75. △T between upper and lower thermocouples at 11.08 W input.

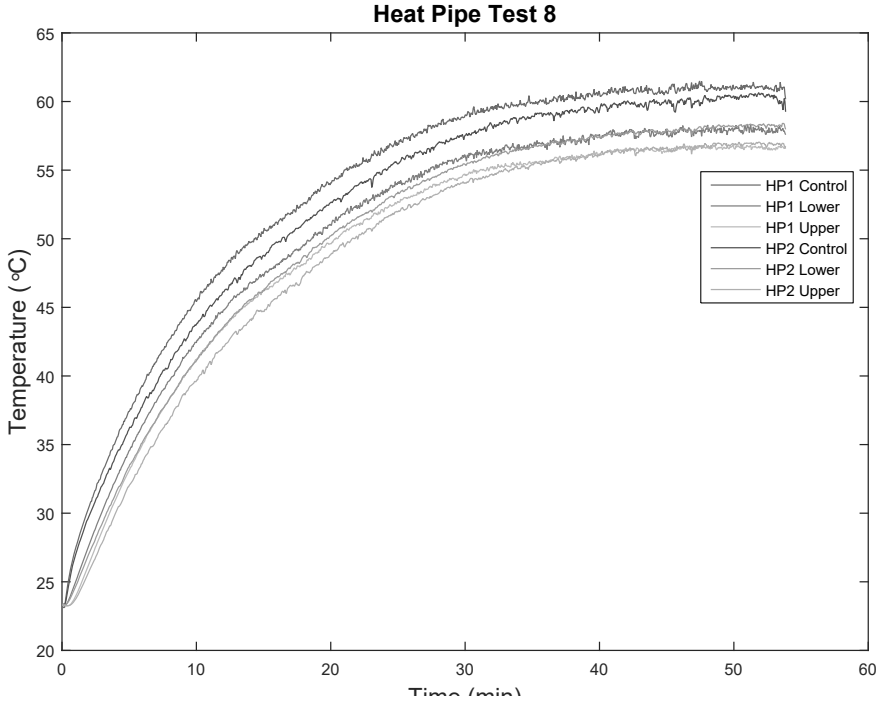

Figure 76. Test 1 transient response from 12.80 W input.

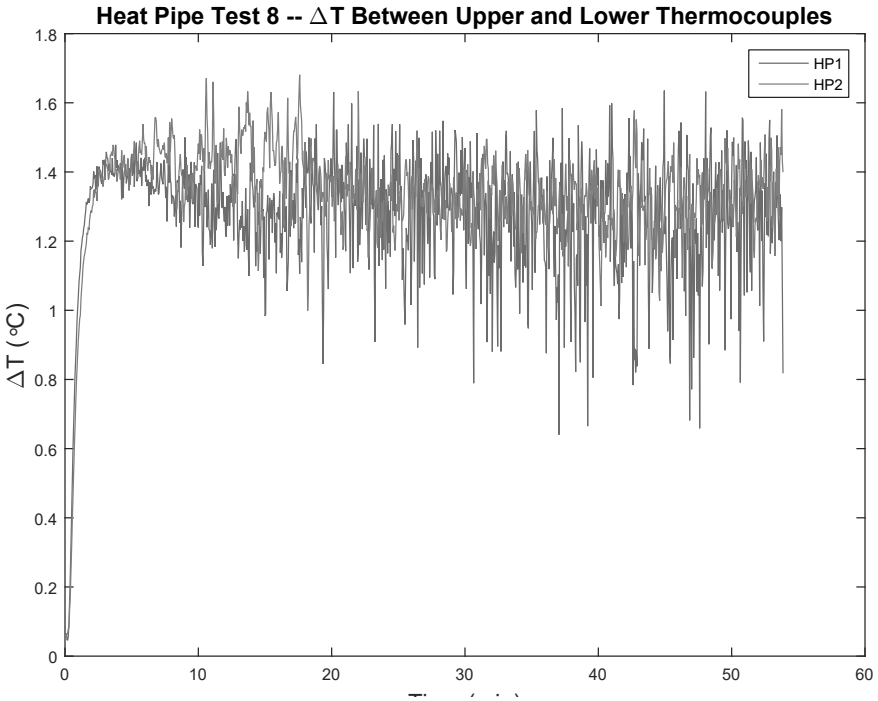

Figure 77. △T between upper and lower thermocouples at 12.80 W input.

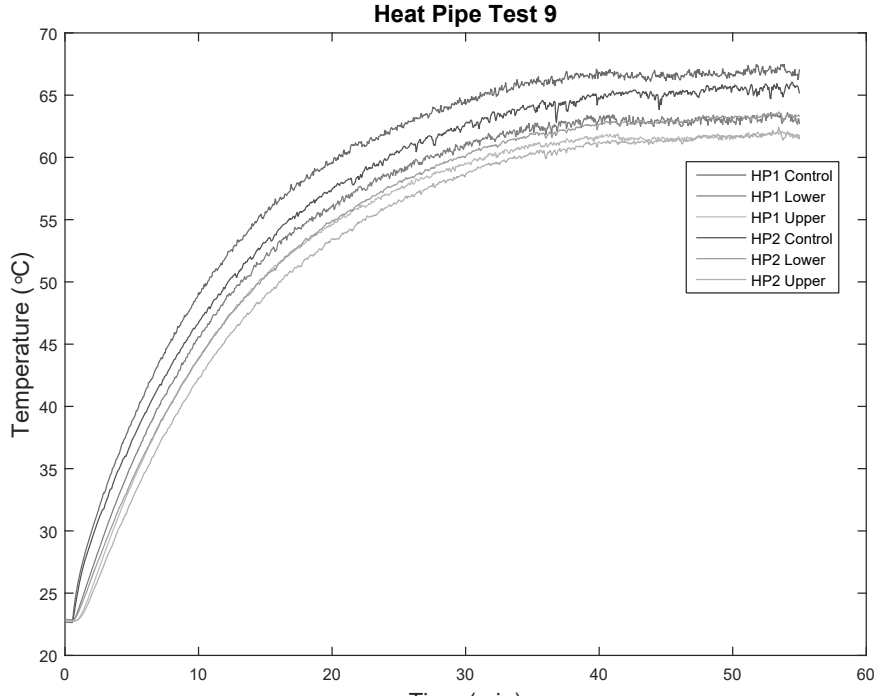

Figure 78. Test 1 transient response from 14.65 W input.

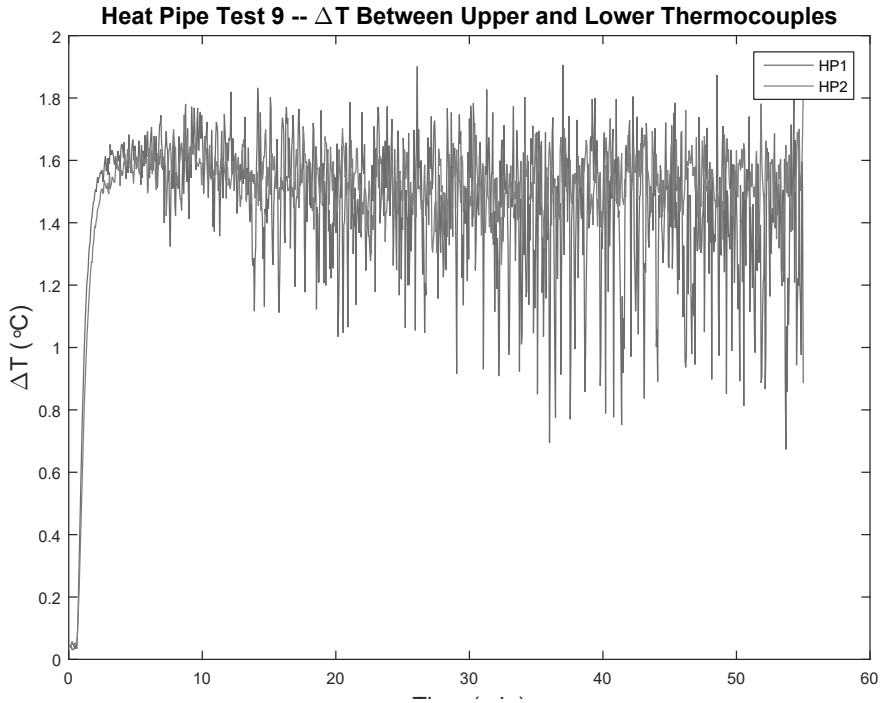

Figure 79. △T between upper and lower thermocouples at 14.65 W input.

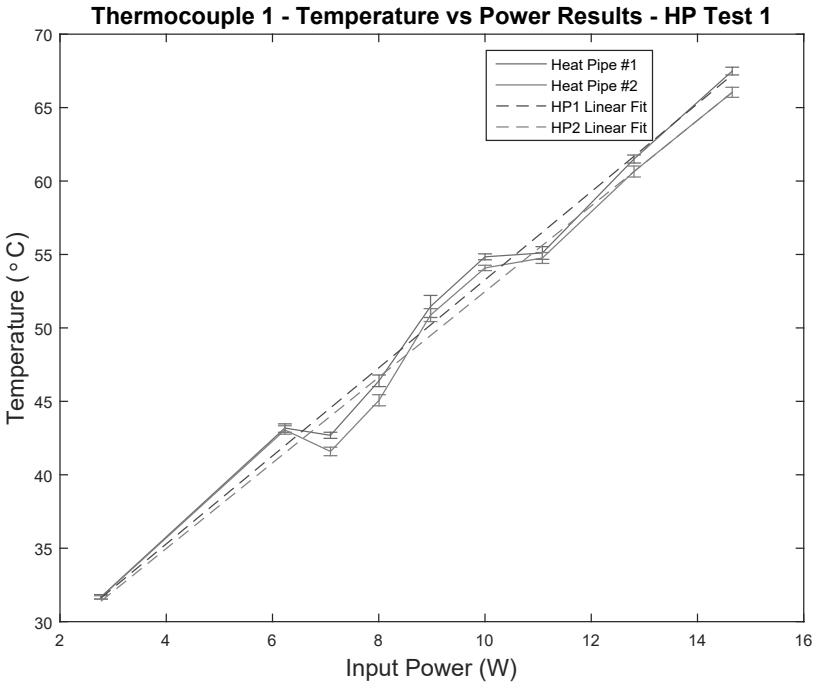

Figure 80. Average thermocouple 1 steady state temperature during heat pipe tests.

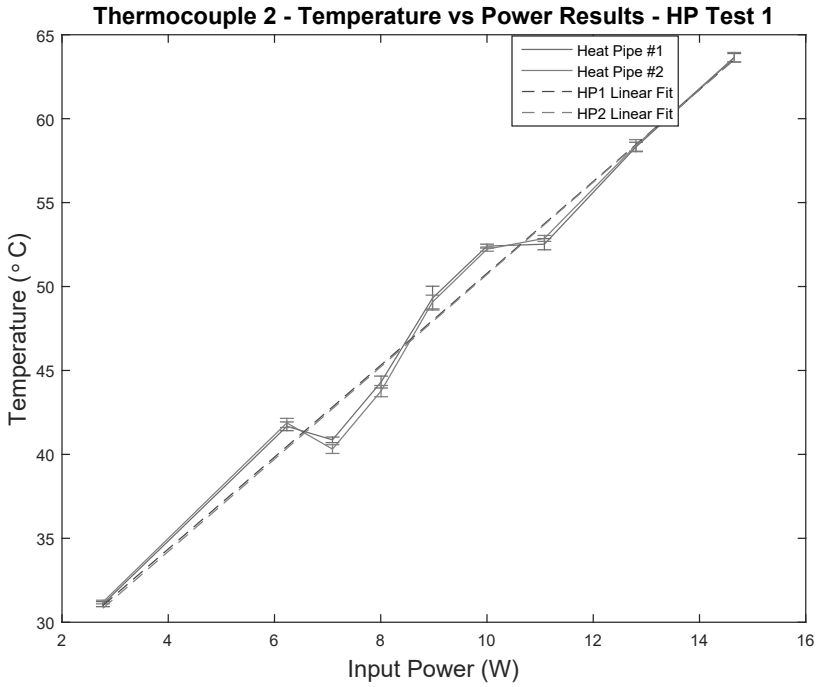

Figure 81. Average thermocouple 2 steady state temperature during heat pipe tests.

B.2 Heat Pipe Test Case 2 – Additional Results

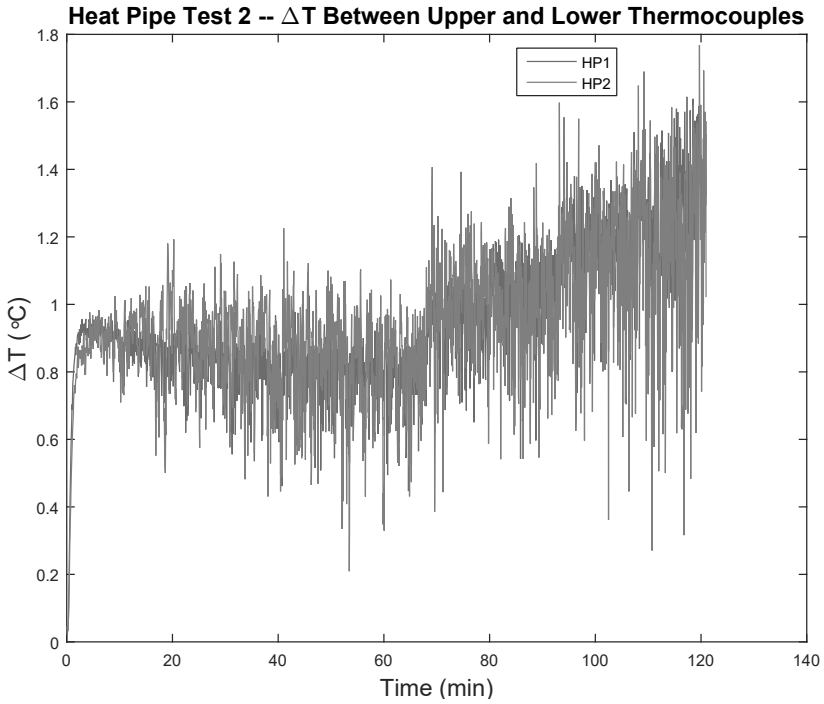

Figure 82. △T between upper and lower thermocouples during heat pipe test 2.

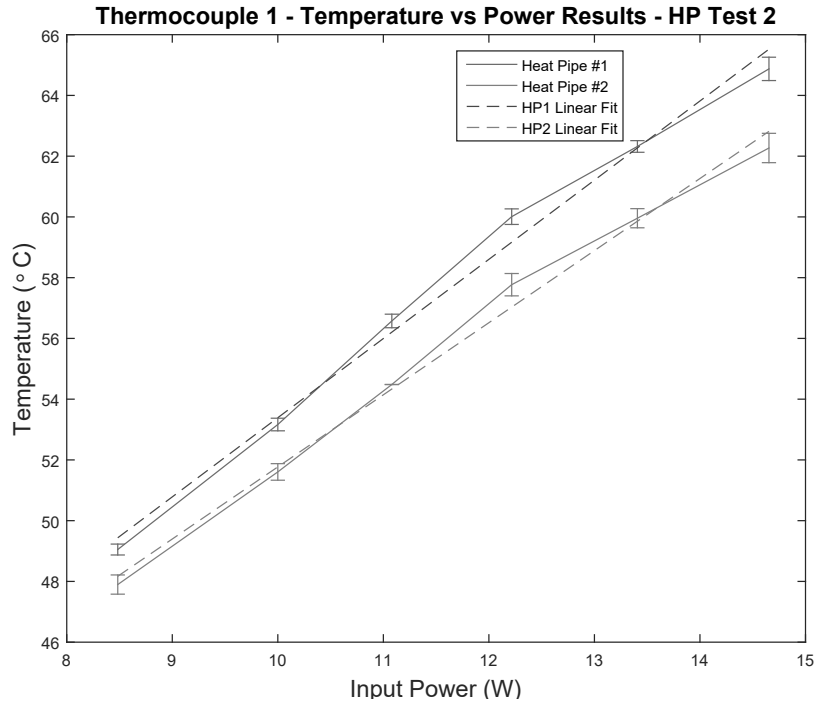

Figure 83. Average thermocouple 1 steady state temperature during heat pipe test 2.

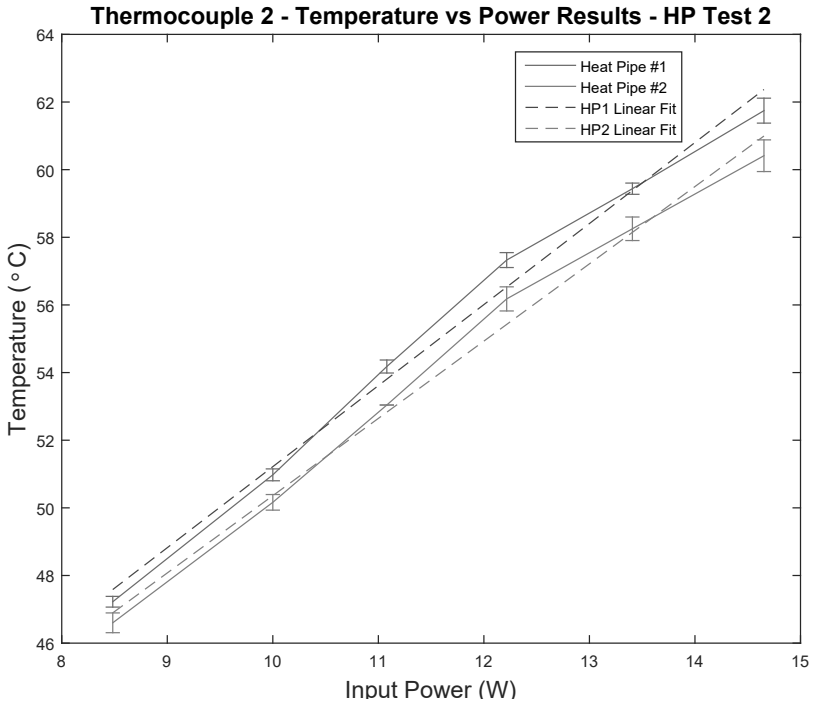

Figure 84. Average thermocouple 2 steady state temperature during heat pipe test 2.

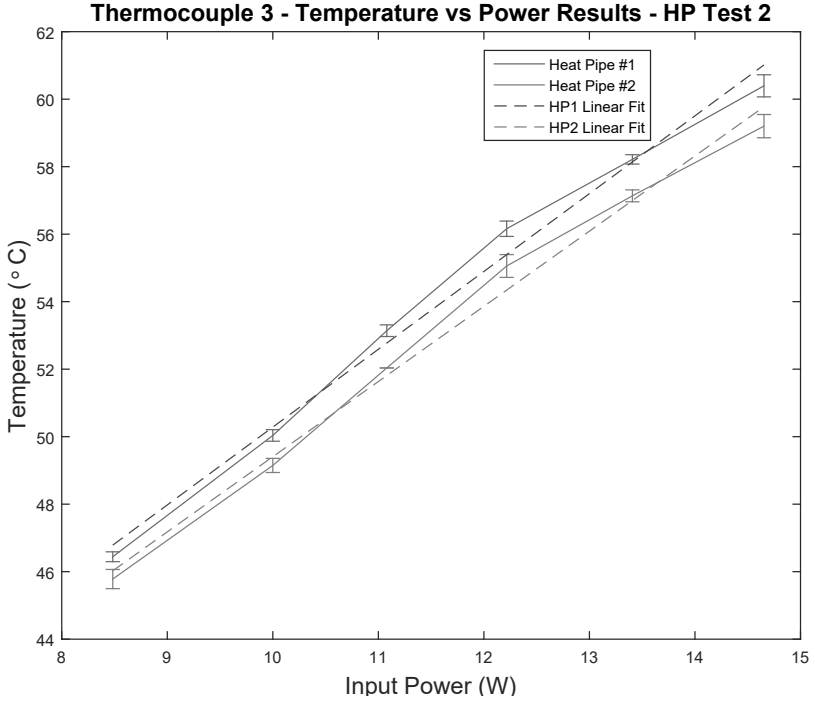

Figure 85. Average thermocouple 3 steady state temperature during heat pipe test 2.

B.3 Heat Pipe Test Case 3 – Additional Results

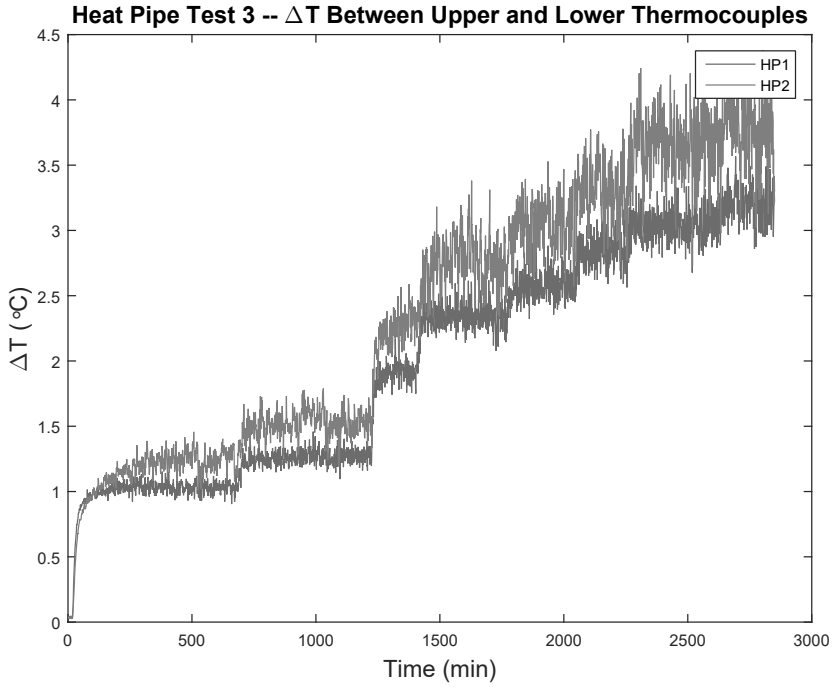

Figure 86. △T between upper and lower thermocouples during heat pipe test 3.

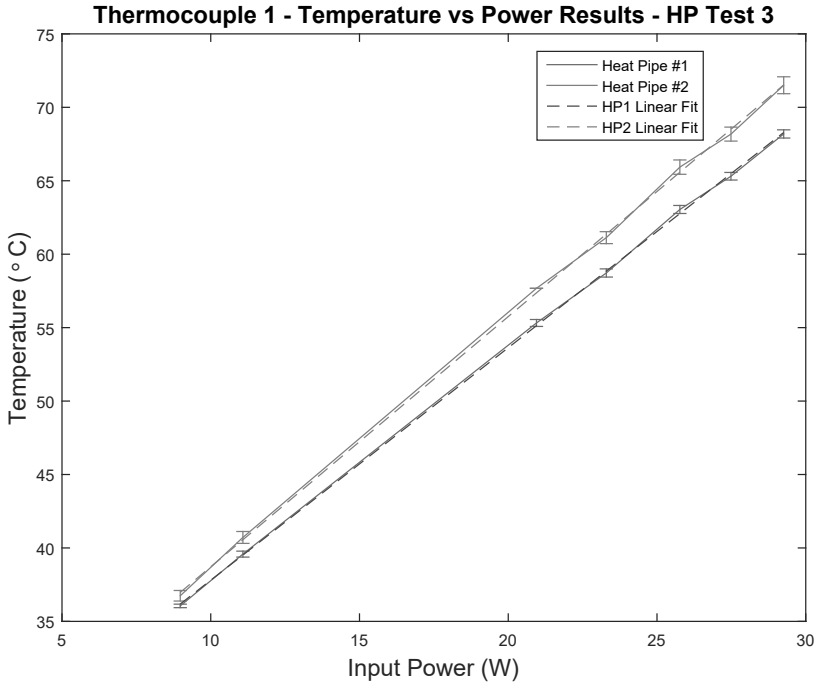

Figure 87. Average thermocouple 1 steady state temperature during heat pipe test 3.

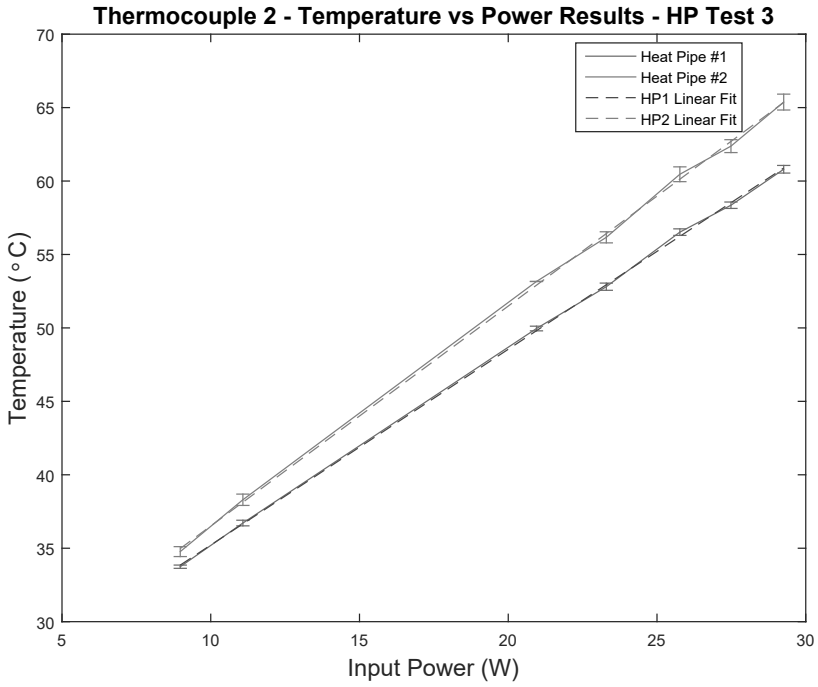

Figure 88. Average thermocouple 2 steady state temperature during heat pipe test 3.

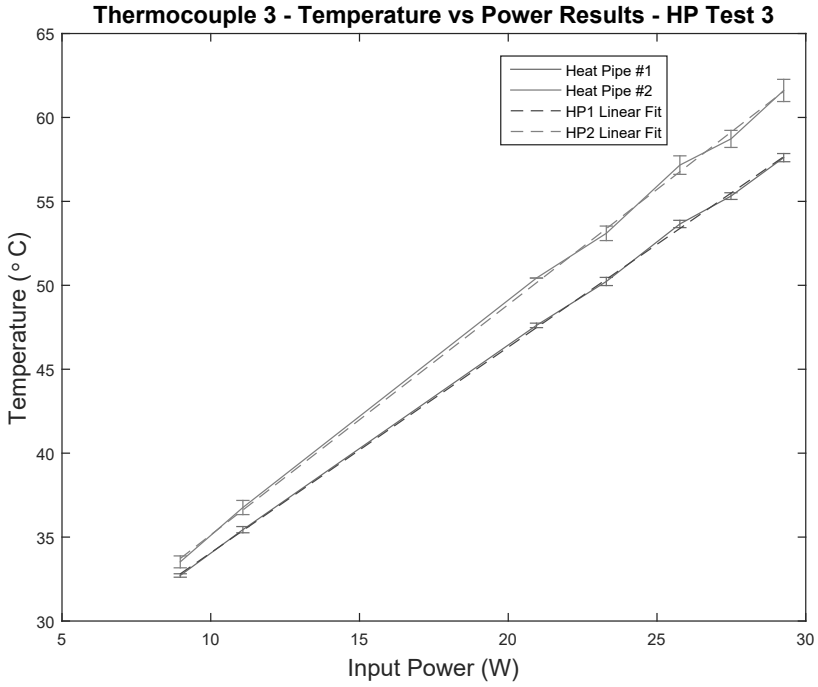

Figure 89. Average thermocouple 3 steady state temperature during heat pipe test 3.

Bibliography

1. L. Perkins and W. Buck, "Improvements in Devices for the Diffusion or Transference of Heat," UK Patent No. 22272, London, 1892.

2. G. P. Peterson, *An Introduction to Heat Pipes: Modeling, Testing, and Applications*. John Wiley & Sons, Inc, 1994.

3. University of Twente, "Two-phase heat transfer principles," 2017. [Online]. Available: https://home.ctw.utwente.nl/witsww/index.php/research/two-phase-principles

4. K. N. Shukla, "Heat Pipe for Aerospace Applications: An Overview," *Journal of Electronics Cooling and Thermal Control*, vol. 5, no. 5, pp. 1–14, 2015. [Online]. Available: http://www.scirp.org/journal/jectchttp://dx.doi.org/10.4236/jectc.2015.51001http://creativecommons.org/licenses/by/4.0/

5. K. V. Wong and A. Hernandez, "A Review of Additive Manufacturing," *ISRN Mechanical Engineering*, vol. 2012, pp. 1–10, 2012. [Online]. Available: http://www.hindawi.com/journals/isrn.mechanical.engineering/2012/208760/

6. G. K. Lewis and E. Schlienger, "Practical considerations and capabilities for laser assisted direct metal deposition," *Materials & Design*, vol. 21, no. 4, pp. 417–423, 2000.

7. M. Shellabear and O. Nyrhilä, "DMLS Development History and State of the Art," in *LANE Conference*, Erlangen, Germany, 2004, pp. 1–12. [Online]. Available: https://www.mendeley.com/catalog/dmls-development-history-state-art-3/?utm{_}source=desktop{\&}utm{_}medium=1.17.6{\&}utm{_}campaign=open{_}catalog{\&}userDocumentId={\%}7Bd0bd9921-4acf-4067-8dc4-82d427ceb291{\%}7D

8. L. E. Murr, "Metal Fabrication by Additive Manufacturing Using Laser and Electron Beam Melting Technologies," *Journal of Materials Science and Technology*, pp. 1997–2006, 2006.

9. F. P. Incropera, D. P. DeWitt, T. L. Bergman, and A. S. Lavine, *Fundamentals of Heat and Mass Transfer*, 2007.

10. A. Faghri, *Heat Pipe Science and Technology*. Taylor & Francis, 1995.

11. Thermal-Fluids Central, "Capillary Wick Designs and Structures in Heat Pipes," 2014. [Online]. Available: http://www.thermalfluidscentral.org/encyclopedia/index.php/Capillary{_}Wick{_}Designs{_}and{_}Structures{_}in{_}Heat{_}Pipes

12. H. J. Wang, H. C. Tsai, H. K. Chen, and T. K. Shing, "Capillarity of rectangular micro grooves and their application to heat pipes," *Tamkang Journal of Science and Engineering*, vol. 8, no. 3, pp. 249–255, 2005.

13. W. Gao, Y. Zhang, D. Ramanujan, K. Ramani, Y. Chen, C. B. Williams, C. C. Wang, Y. C. Shin, S. Zhang, and P. D. Zavattieri, "The Status, Challenges, and Future of Additive Manufacturing in Engineering," *Computer-Aided Design*, vol. 69, pp. 65–89, 2015. [Online]. Available: http://www.sciencedirect.com/science/article/pii/S0010448515000469

14. Design Engineering, "Study: 3D printing saves weight, fuel in aerospace design," 2015. [Online]. Available: http://www.design-engineering.com/study-3d-printing-saves-weight-fuel-in-aerospace-design-136069/

15. M. Molitch-Hou, "First Jet Engines with 3D-Printed Nozzles Delivered to Airbus," 2016. [Online]. Available: http://www.engineering.com/AdvancedManufacturing/ArticleID/11948/First-Jet-Engines-with-3D-Printed-Nozzles-Delivered-to-Airbus.aspx

16. T. Kellner, "The FAA Cleared the First 3D Printed Part to Fly in a Commercial Jet Engine from GE," GE, Tech. Rep., 2015. [Online]. Available: http://www.gereports.com/post/116402870270/the-faa-cleared-the-first-3d-printed-part-to-fly/

17. ASTM F42, "Additive Manufacturing Standards Structure," 2016. [Online]. Available: https://www.astm.org/COMMIT/F42{_}ISOASTM{_}AdditiveManuStandardsStructure.pdf

18. J. R. Wertz, D. F. Everett, and J. J. Puschell, *Space Mission Engineering: The New SMAD*. Microcosm Press, 2011.

19. NASA, "NASA-STD-7001," Tech. Rep., 2011. [Online]. Available: https://standards.nasa.gov/standard/nasa/nasa-std-7001

20. I3DMFG, "Manufacturing Best Practices," The Dalles, Oregon, 2015.

21. EOS, "M290 Specifications," 2014. [Online]. Available: https://www.eos.info/eos-m290

22. F. Dullen, *Porous Media*. San Diego, CA: Academic Press, Inc., 1991.

23. Kramer Industries Inc, "Mesh Size," 2016. [Online]. Available: http://www.kramerindustriesonline.com/finishing-guides/mesh-size.htm

24. North Star Imaging, "NSI Overview," Irvine, CA, Tech. Rep., 2016. [Online]. Available: http://4nsi.com/systems/x50

25. National Institute of Standards and Technology, "Acetone Data Sheet," 2016. [Online]. Available: http://webbook.nist.gov/cgi/cbook.cgi?ID=C67641&Mask=4

26. K. S. Udell, "Heat Transfer in Porous Media Considering Phase Change and Capillarity - The Heat Pipe Effect," *International Journal of Heat and Mass Transfer*, vol. 28, no. 2, pp. 485–495, 1985.

27. G. P. Peterson, L. S. Fletcher, S. R. Raghunathan, M. a. Gillan, and R. D. Mitchell, "Effective thermal conductivity of sintered heat pipe wicks," *Journal of Thermophysics and Heat Transfer*, vol. 1, no. 4, pp. 343–347, 1987.

28. EOS, "Material Data Sheet: AlSi10Mg," 2014. [Online]. Available: https://www.eos.info/material-m

REPORT DOCUMENTATION PAGE

Form Approved
OMB No. 0704–0188

1. REPORT DATE *(DD–MM–YYYY)*	2. REPORT TYPE	3. DATES COVERED *(From — To)*
03–03–2017	Master's Thesis	August 2015 - March 2017

4. TITLE AND SUBTITLE

Additively Manufactured Spacecraft Thermal Control System

5a. CONTRACT NUMBER

5b. GRANT NUMBER

5c. PROGRAM ELEMENT NUMBER

6. AUTHOR(S)

Lanzo, Daniel T., Capt, USAF

5d. PROJECT NUMBER

5e. TASK NUMBER

5f. WORK UNIT NUMBER

7. PERFORMING ORGANIZATION NAME(S) AND ADDRESS(ES)

Air Force Institute of Technology
Graduate School of Engineering and Management (AFIT/EN)
2950 Hobson Way
WPAFB OH 45433-7765

8. PERFORMING ORGANIZATION REPORT NUMBER

AFIT-ENY-MS-17-M-271

9. SPONSORING / MONITORING AGENCY NAME(S) AND ADDRESS(ES)

Sponsor Witheld

10. SPONSOR/MONITOR'S ACRONYM(S)

11. SPONSOR/MONITOR'S REPORT NUMBER(S)

12. DISTRIBUTION / AVAILABILITY STATEMENT

Distribution Statement A. Approved for public release; Distribution Unlimited.

13. SUPPLEMENTARY NOTES

This material is declared work of the U.S. Government and is not subject to copyright protection in the United States.

14. ABSTRACT

Heat pipes offer a very effective thermal management solution when dealing with high powered spacecraft electronics. However, current technologies dictate that these solutions be manufactured via different processes with several integration steps. Additive manufacturing offers unique opportunities to manufacture integrated parts that cannot be realized via traditional means; heat pipes are no exception. This thesis explores three key areas of additively manufacturing heat pipes for spacecraft thermal control. First, the ability to print different wick types is explored and test samples are printed and tested for wicking potential. Second, the functionality of an additively manufactured heat pipe design is tested by performing a side-by-side comparison between a heat pipe and conduction only setup. Lastly, the ability to create dual purpose components is explored by analyzing the structural capabilities of the heat pipe design and its impact on weight and complexity of spacecraft systems. Although conclusive test results were not obtained during this design revision, additive manufacturing offers viable and unique solutions for integrated heat management and structural solutions.

15. SUBJECT TERMS

spacecraft, thermal, heat pipe, additive manufacturing, AM, lattice, wick

16. SECURITY CLASSIFICATION OF:			17. LIMITATION OF ABSTRACT	18. NUMBER OF PAGES	19a. NAME OF RESPONSIBLE PERSON
a. REPORT	b. ABSTRACT	c. THIS PAGE			Carl R. Hartsfield, AFIT/ENY
U	U	U	U	128	19b. TELEPHONE NUMBER *(include area code)* (937)255-3636 x.4667; carl.hartsfield@afit.edu